Estudos em Ciências Exatas e da Terra

Desafios, Avanços e Possibilidades

Alireza Mohebi Ashtiani
(organizador)

VOL III

EDITORA ARTEMIS
2025

Estudos em Ciências Exatas e da Terra

Desafios, Avanços e Possibilidades

Alireza Mohebi Ashtiani
(organizador)

VOL III

EDITORA ARTEMIS
2025

2025 *by Editora Artemis*
Copyright © Editora Artemis
Copyright do Texto © 2025 Os autores
Copyright da Edição © 2025 Editora Artemis

O conteúdo deste livro está licenciado sob uma Licença de Atribuição Creative Commons Atribuição-Não-Comercial NãoDerivativos 4.0 Internacional (CC BY-NC-ND 4.0). Direitos para esta edição cedidos à Editora Artemis pelos autores. Permitido o download da obra e o compartilhamento, desde que sejam atribuídos créditos aos autores, e sem a possibilidade de alterá-la de nenhuma forma ou utilizá-la para fins comerciais.

A responsabilidade pelo conteúdo dos artigos e seus dados, em sua forma, correção e confiabilidade é exclusiva dos autores. A Editora Artemis, em seu compromisso de manter e aperfeiçoar a qualidade e confiabilidade dos trabalhos que publica, conduz a avaliação cega pelos pares de todos manuscritos publicados, com base em critérios de neutralidade e imparcialidade acadêmica.

Editora Chefe	Profª Drª Antonella Carvalho de Oliveira
Editora Executiva	M.ª Viviane Carvalho Mocellin
Direção de Arte	M.ª Bruna Bejarano
Diagramação	Elisangela Abreu
Organizador	Prof. Dr. Alireza Mohebi Ashtiani
Imagem da Capa	Abstract Style Landscapes /123RF
Bibliotecário	Maurício Amormino Júnior – CRB6/2422

Conselho Editorial

Prof.ª Dr.ª Ada Esther Portero Ricol, *Universidad Tecnológica de La Habana "José Antonio Echeverría"*, Cuba
Prof. Dr. Adalberto de Paula Paranhos, Universidade Federal de Uberlândia, Brasil
Prof. Dr. Agustín Olmos Cruz, *Universidad Autónoma del Estado de México*, México
Prof.ª Dr.ª Amanda Ramalho de Freitas Brito, Universidade Federal da Paraíba, Brasil
Prof.ª Dr.ª Ana Clara Monteverde, *Universidad de Buenos Aires*, Argentina
Prof.ª Dr.ª Ana Júlia Viamonte, Instituto Superior de Engenharia do Porto (ISEP), Portugal
Prof. Dr. Ángel Mujica Sánchez, *Universidad Nacional del Altiplano*, Peru
Prof.ª Dr.ª Angela Ester Mallmann Centenaro, Universidade do Estado de Mato Grosso, Brasil
Prof.ª Dr.ª Begoña Blandón González, *Universidad de Sevilla*, Espanha
Prof.ª Dr.ª Carmen Pimentel, Universidade Federal Rural do Rio de Janeiro, Brasil
Prof.ª Dr.ª Catarina Castro, Universidade Nova de Lisboa, Portugal
Prof.ª Dr.ª Cirila Cervera Delgado, *Universidad de Guanajuat*o, México
Prof.ª Dr.ª Cláudia Neves, Universidade Aberta de Portugal
Prof.ª Dr.ª Cláudia Padovesi Fonseca, Universidade de Brasília-DF, Brasil
Prof. Dr. Cleberton Correia Santos, Universidade Federal da Grande Dourados, Brasil
Dr. Cristo Ernesto Yáñez León – New Jersey Institute of Technology, Newark, NJ, Estados Unidos
Prof. Dr. David García-Martul, *Universidad Rey Juan Carlos de Madrid*, Espanha
Prof.ª Dr.ª Deuzimar Costa Serra, Universidade Estadual do Maranhão, Brasil
Prof.ª Dr.ª Dina Maria Martins Ferreira, Universidade Estadual do Ceará, Brasil
Prof.ª Dr.ª Edith Luévano-Hipólito, *Universidad Autónoma de Nuevo León*, México
Prof.ª Dr.ª Eduarda Maria Rocha Teles de Castro Coelho, Universidade de Trás-os-Montes e Alto Douro, Portugal
Prof. Dr. Eduardo Eugênio Spers, Universidade de São Paulo (USP), Brasil
Prof. Dr. Eloi Martins Senhoras, Universidade Federal de Roraima, Brasil
Prof.ª Dr.ª Elvira Laura Hernández Carballido, *Universidad Autónoma del Estado de Hidalgo*, México

Editora Artemis
Curitiba-PR Brasil
www.editoraartemis.com.br
e-mail:publicar@editoraartemis.com.br

Prof.ª Dr.ª Emilas Darlene Carmen Lebus, *Universidad Nacional del Nordeste/ Universidad Tecnológica Nacional*, Argentina
Prof.ª Dr.ª Erla Mariela Morales Morgado, *Universidad de Salamanca*, Espanha
Prof. Dr. Ernesto Cristina, *Universidad de la República*, Uruguay
Prof. Dr. Ernesto Ramírez-Briones, *Universidad de Guadalajara*, México
Prof. Dr. Fernando Hitt, *Université du Québec à Montréal*, Canadá
Prof. Dr. Gabriel Díaz Cobos, *Universitat de Barcelona,* Espanha
Prof.ª Dr.ª Gabriela Gonçalves, Instituto Superior de Engenharia do Porto (ISEP), Portugal
Prof.ª Dr.ª Galina Gumovskaya – Higher School of Economics, Moscow, Russia
Prof. Dr. Geoffroy Roger Pointer Malpass, Universidade Federal do Triângulo Mineiro, Brasil
Prof.ª Dr.ª Gladys Esther Leoz, *Universidad Nacional de San Luis,* Argentina
Prof.ª Dr.ª Glória Beatriz Álvarez, *Universidad de Buenos Aires,* Argentina
Prof. Dr. Gonçalo Poeta Fernandes, Instituto Politécnido da Guarda, Portugal
Prof. Dr. Gustavo Adolfo Juarez, *Universidad Nacional de Catamarca*, Argentina
Prof. Dr. Guillermo Julián González-Pérez, *Universidad de Guadalajara, México*
Prof. Dr. Håkan Karlsson, *University of Gothenburg*, Suécia
Prof.ª Dr.ª Iara Lúcia Tescarollo Dias, Universidade São Francisco, Brasil
Prof.ª Dr.ª Isabel del Rosario Chiyon Carrasco, *Universidad de Piura*, Peru
Prof.ª Dr.ª Isabel Yohena, *Universidad de Buenos Aires,* Argentina
Prof. Dr. Ivan Amaro, Universidade do Estado do Rio de Janeiro, Brasil
Prof. Dr. Iván Ramon Sánchez Soto, *Universidad del Bío-Bío*, Chile
Prof.ª Dr.ª Ivânia Maria Carneiro Vieira, Universidade Federal do Amazonas, Brasil
Prof. Me. Javier Antonio Albornoz, *University of Miami and Miami Dade College*, Estados Unidos
Prof. Dr. Jesús Montero Martínez, *Universidad de Castilla - La Mancha*, Espanha
Prof. Dr. João Manuel Pereira Ramalho Serrano, Universidade de Évora, Portugal
Prof. Dr. Joaquim Júlio Almeida Júnior, UniFIMES - Centro Universitário de Mineiros, Brasil
Prof. Dr. Jorge Ernesto Bartolucci, *Universidad Nacional Autónoma de México*, México
Prof. Dr. José Cortez Godinez, Universidad Autónoma de Baja California, México
Prof. Dr. Juan Carlos Cancino Diaz, Instituto Politécnico Nacional, México
Prof. Dr. Juan Carlos Mosquera Feijoo, *Universidad Politécnica de Madrid*, Espanha
Prof. Dr. Juan Diego Parra Valencia, *Instituto Tecnológico Metropolitano de Medellín*, Colômbia
Prof. Dr. Juan Manuel Sánchez-Yáñez, *Universidad Michoacana de San Nicolás de Hidalgo,* México
Prof. Dr. Juan Porras Pulido, *Universidad Nacional Autónoma de México*, México
Prof. Dr. Júlio César Ribeiro, Universidade Federal Rural do Rio de Janeiro, Brasil
Prof. Dr. Leinig Antonio Perazolli, Universidade Estadual Paulista (UNESP), Brasil
Prof.ª Dr.ª Lívia do Carmo, Universidade Federal de Goiás, Brasil
Prof.ª Dr.ª Luciane Spanhol Bordignon, Universidade de Passo Fundo, Brasil
Prof. Dr. Luis Fernando González Beltrán, *Universidad Nacional Autónoma de México*, México
Prof. Dr. Luis Vicente Amador Muñoz, *Universidad Pablo de Olavide*, Espanha
Prof.ª Dr.ª Macarena Esteban Ibáñez, *Universidad Pablo de Olavide*, Espanha
Prof. Dr. Manuel Ramiro Rodriguez, *Universidad Santiago de Compostela*, Espanha
Prof. Dr. Manuel Simões, Faculdade de Engenharia da Universidade do Porto, Portugal
Prof.ª Dr.ª Márcia de Souza Luz Freitas, Universidade Federal de Itajubá, Brasil
Prof. Dr. Marcos Augusto de Lima Nobre, Universidade Estadual Paulista (UNESP), Brasil
Prof. Dr. Marcos Vinicius Meiado, Universidade Federal de Sergipe, Brasil
Prof.ª Dr.ª Mar Garrido Román, *Universidad de Granada*, Espanha
Prof.ª Dr.ª Margarida Márcia Fernandes Lima, Universidade Federal de Ouro Preto, Brasil
Prof.ª Dr.ª María Alejandra Arecco, *Universidad de Buenos Aires*, Argentina
Prof.ª Dr.ª Maria Aparecida José de Oliveira, Universidade Federal da Bahia, Brasil
Prof.ª Dr.ª Maria Carmen Pastor, *Universitat Jaume I*, Espanha
Prof.ª Dr.ª Maria da Luz Vale Dias – Universidade de Coimbra, Portugal

Editora Artemis
Curitiba-PR Brasil
www.editoraartemis.com.br
e-mail:publicar@editoraartemis.com.br

Prof.ª Dr.ª Maria do Céu Caetano, Universidade Nova de Lisboa, Portugal
Prof.ª Dr.ª Maria do Socorro Saraiva Pinheiro, Universidade Federal do Maranhão, Brasil
Prof.ª Dr.ª MªGraça Pereira, Universidade do Minho, Portugal
Prof.ª Dr.ª Maria Gracinda Carvalho Teixeira, Universidade Federal Rural do Rio de Janeiro, Brasil
Prof.ª Dr.ª María Guadalupe Vega-López, *Universidad de Guadalajara, México*
Prof.ª Dr.ª Maria Lúcia Pato, Instituto Politécnico de Viseu, Portugal
Prof.ª Dr.ª Maritza González Moreno, *Universidad Tecnológica de La Habana*, Cuba
Prof.ª Dr.ª Mauriceia Silva de Paula Vieira, Universidade Federal de Lavras, Brasil
Prof. Dr. Melchor Gómez Pérez, Universidad del Pais Vasco, Espanha
Prof.ª Dr.ª Ninfa María Rosas-García, Centro de Biotecnología Genómica-Instituto Politécnico Nacional, México
Prof.ª Dr.ª Odara Horta Boscolo, Universidade Federal Fluminense, Brasil
Prof. Dr. Osbaldo Turpo-Gebera, *Universidad Nacional de San Agustín de Arequipa*, Peru
Prof.ª Dr.ª Patrícia Vasconcelos Almeida, Universidade Federal de Lavras, Brasil
Prof.ª Dr.ª Paula Arcoverde Cavalcanti, Universidade do Estado da Bahia, Brasil
Prof. Dr. Rodrigo Marques de Almeida Guerra, Universidade Federal do Pará, Brasil
Prof. Dr. Saulo Cerqueira de Aguiar Soares, Universidade Federal do Piauí, Brasil
Prof. Dr. Sergio Bitencourt Araújo Barros, Universidade Federal do Piauí, Brasil
Prof. Dr. Sérgio Luiz do Amaral Moretti, Universidade Federal de Uberlândia, Brasil
Prof.ª Dr.ª Silvia Inés del Valle Navarro, *Universidad Nacional de Catamarca*, Argentina
Prof.ª Dr.ª Solange Kazumi Sakata, Instituto de Pesquisas Energéticas e Nucleares (IPEN)- USP, Brasil
Prof.ª Dr.ª Stanislava Kashtanova, *Saint Petersburg State University,* Russia
Prof.ª Dr.ª Susana Álvarez Otero – Universidad de Oviedo, Espanha
Prof.ª Dr.ª Teresa Cardoso, Universidade Aberta de Portugal
Prof.ª Dr.ª Teresa Monteiro Seixas, Universidade do Porto, Portugal
Prof. Dr. Valter Machado da Fonseca, Universidade Federal de Viçosa, Brasil
Prof.ª Dr.ª Vanessa Bordin Viera, Universidade Federal de Campina Grande, Brasil
Prof.ª Dr.ª Vera Lúcia Vasilévski dos Santos Araújo, Universidade Tecnológica Federal do Paraná, Brasil
Prof. Dr. Wilson Noé Garcés Aguilar, *Corporación Universitaria Autónoma del Cauca*, Colômbia
Prof. Dr. Xosé Somoza Medina, *Universidad de León*, Espanha

Dados Internacionais de Catalogação na Publicação (CIP)
(eDOC BRASIL, Belo Horizonte/MG)

E82 Estudos em Ciências Exatas e da Terra: Desafios, Avanços e Possibilidades III / Organizador Alireza Mohebi Ashtiani. – Curitiba, PR: Artemis, 2025.

Formato: PDF
Requisitos de sistema: Adobe Acrobat Reader
Modo de acesso: World Wide Web
Inclui bibliografia
Edição bilíngue
ISBN 978-65-81701-75-8
DOI 10.37572/EdArt_101225758

1. Ciências exatas e da terra – Pesquisa – Brasil. I. Ashtiani, Alireza Mohebi.

CDD 509

Elaborado por Maurício Amormino Júnior – CRB6/2422

EDITORA ARTEMIS
2025

Editora Artemis
Curitiba-PR Brasil
www.editoraartemis.com.br
e-mail:publicar@editoraartemis.com.br

PRÓLOGO

O volume III de **Estudos em Ciências Exatas e da Terra: Desafios, Avanços e Possibilidades** reúne um conjunto plural de pesquisas que refletem a vitalidade, a complexidade e o caráter interdisciplinar das ciências contemporâneas. Os dez capítulos aqui apresentados, provenientes de diversos países e contextos institucionais, oferecem um panorama abrangente dos desafios científicos atuais e das soluções inovadoras que emergem do diálogo entre matemática, física, química, engenharia, geociências, sustentabilidade ambiental e desenvolvimento territorial, reafirmando a amplitude teórica e aplicada dessas áreas.

Para favorecer a leitura e destacar as afinidades conceituais entre os temas, a obra foi organizada em três eixos temáticos que evidenciam os diferentes modos pelos quais o conhecimento científico se articula com problemas reais e necessidades sociais urgentes, propondo uma aproximação integradora e contemporânea das Ciências Exatas e da Terra.

1. Modelagem Matemática, Simulação, Processos Físicos e Engenharia Aplicada

O primeiro eixo reúne estudos orientados pela lógica da modelagem, da caracterização de materiais e da investigação de sistemas físico-químicos complexos. Aqui, a matemática desempenha um papel central, seja na descrição do crescimento populacional, na interpretação de curvas de relações molares ou na análise termoestrutural de concretos refratários usados na indústria siderúrgica. A ênfase comum está na busca por métodos rigorosos de análise, na construção de modelos interpretativos e na compreensão dos comportamentos materiais sob diferentes condições. Esses capítulos mostram como a formulação matemática e a experimentação se complementam, de forma decisiva, na explicação de fenômenos fundamentais para a ciência e a engenharia, evidenciando a potência dos métodos quantitativos na resolução de problemas complexos.

2. Sustentabilidade, Meio Ambiente, Tecnologias de Remediação e Ecodesign

O segundo eixo destaca pesquisas alinhadas aos desafios ambientais contemporâneos, trazendo propostas inovadoras para o desenvolvimento de tecnologias limpas, novos materiais sustentáveis e soluções de remediação ecológica. Os capítulos abordam desde práticas de ecodesign em produtos plásticos, passando pela criação de adsorventes de origem agroindustrial, até aplicações de biomassa vegetal para remoção de contaminantes e estratégias que ampliam o desempenho energético de sistemas fotovoltaicos, articulando ciência de materiais e preocupações ambientais. O núcleo

unificador deste eixo é o compromisso com a sustentabilidade, com a valorização de resíduos, com a mitigação de impactos ambientais e com a promoção de alternativas tecnológicas responsáveis e acessíveis que dialogam diretamente com demandas sociais emergentes.

3. Território, Geociências e Desenvolvimento Agrário-Industrial

O terceiro eixo aborda temas relacionados à organização do espaço, à história das indústrias de base e às dinâmicas socioeconômicas ligadas ao uso da terra. Os capítulos discutem a trajetória de figuras marcantes das geociências, analisam políticas e práticas de consolidação fundiária em escala nacional e refletem sobre as transformações industriais que moldam setores-chave como o agrícola e o petrolífero. Ao articular perspectivas históricas, econômicas e territoriais, este eixo evidencia como as ciências exatas e da terra também se expressam na compreensão dos processos sociais e produtivos que estruturam países e regiões, demonstrando que a pesquisa científica contribui igualmente para interpretações críticas sobre o desenvolvimento nacional.

A estrutura temática proposta pretende, portanto, facilitar a leitura e realçar o alcance multidisciplinar das pesquisas reunidas. Cada eixo demonstra, a seu modo, como o rigor científico pode contribuir para o entendimento de problemas concretos e para o desenvolvimento de soluções inovadoras, sejam elas de caráter teórico, tecnológico ou socioambiental, reforçando o papel estratégico da ciência na construção de futuros possíveis.

Esperamos que esta obra inspire pesquisadores, estudantes e profissionais a aprofundar o diálogo entre diferentes áreas do conhecimento e a reconhecer, na diversidade temática aqui apresentada, novas possibilidades de investigação e ação.

Desejo a todos uma excelente leitura!

Alireza Mohebi Ashtiani

SUMÁRIO

MODELAGEM MATEMÁTICA, SIMULAÇÃO, PROCESSOS FÍSICOS E ENGENHARIA APLICADA

SUSTENTABILIDADE, MEIO AMBIENTE, TECNOLOGIAS DE REMEDIAÇÃO E ECODESIGN

TERRITÓRIO, GEOCIÊNCIAS E DESENVOLVIMENTO AGRÁRIO-INDUSTRIAL

CAPÍTULO 1

THERMOSTRUCTURAL BEHAVIOR OF A REFRACTORY CONCRETE FOR LADLE FURNACE[1]

Data de submissão: 24/11/2025
Data de aceite: 08/12/2025

Edgardo Benavidez
Universidad Tecnológica Nacional
Facultad Regional San Nicolás
San Nicolás de los Arroyos
Buenos Aires, Argentina
https://orcid.org/0000-0003-1524-4203

ABSTRACT: The structural development of an alumina (Al_2O_3) and spinel ($MgO{\cdot}Al_2O_3$) refractory concrete was evaluated at service temperatures (1000–1600 °C). This material, used in the steel industry, is part of the refractory lining of ladle furnaces. For the study, concrete specimens were cast and cured under ambient temperature and humidity conditions, then dried (105 °C – 24 h) and heat-treated (500 °C – 3 h). Structural variation was analyzed through dilatometry at a constant heating rate (5 °C/min up to 1600 °C) and isothermal dilatometry (4 hours) in the range of 1000–1500 °C. Specimens treated between 1000 °C and 1200 °C showed Al_2O_3 and $MgAl_2O_4$ as the main phases, while the formation of calcium hexaluminate (CA_6) was observed starting at 1400 °C. Dilatometry indicates that the refractory expands linearly up to around 1100 °C, then accelerates its expansion until approximately 1325 °C, a phenomenon associated with the formation of calcium dialuminate (CA_2). A contraction stage of the concrete occurs between 1330–1460 °C due to the sintering of ceramic grains; this densification behavior is slowed around 1460 °C by the increasing kinetics of calcium hexaluminate (CA_6) formation. From 1540 °C onward, the ceramic sintering process becomes dominant, leading to densification (contraction) of the material. Considering its specific use on the bottom or sidewall of a ladle furnace, and taking into account the different dimensional variations obtained in the isothermal dilatometry tests, the presence of compressive stresses is estimated in regions at temperatures between 1200 °C and 1300 °C, relative to zones at 1000 °C (considered neutral), and tensile stresses in refractory regions exposed to 1500 °C.
KEYWORDS: alumina; spinel; refractory; dilatometry; XRD.

1. INTRODUCTION

Conventional steel products are mainly manufactured through the integrated Blast Furnace process, followed by the primary metallurgy stage, which is commonly carried out in a vessel known as LD converter or Basic Oxygen Furnace (BOF). The steel is

[1] The author acknowledges the financial support provided by the National Technological University (Argentina) and the technical collaboration of Eng. Ricardo Ponte and Eng. Ailén Ponte. There are no conflicts of interes.

then transferred to ladle furnaces (LF) during the so-called secondary metallurgy stage, where the obtained steel undergoes an additional refining process (**Ghosh, 2001**). At this stage, the final adjustment of impurities in the liquid steel (sulfur, phosphorus, carbon, oxygen, nitrogen, and hydrogen) is performed, achieving a very low level of inclusions. This steel refining operation generally consists of deoxidation, desulfurization, and dephosphorization processes, through which controlled additions of alloying elements are made along with simultaneous modification of inclusions. These operations determine the type of refractory lining for the vessel.

The ladle lining uses carbon-containing refractory bricks, such as MgO-C (magnesia-carbon), Al_2O_3-MgO-C (alumina-magnesia-carbon), and CaO-MgO-C (dolomite-carbon). However, the need to produce ultra-low carbon content (ULCC) steels for automotive quality led to the use of carbon-free refractories to prevent carbon absorption from the lining (**Biswas & Sarkar, 2020**). Thus, alumina-spinel refractories (Al_2O_3-MgO·Al_2O_3) began to be used in ladle furnaces, particularly in wall areas in contact with molten metal (metal line) and in the bottom zone. At the ladle bottom (Fig. 1), the liquid metal directly impacts the refractory when steel is transferred from the converter to the ladle furnace, subjecting this type of castable to severe thermal and mechanical stresses.

The thickness of these refractories placed on the ladle bottom is around 300 mm. Therefore, during operation, this material is in direct contact with liquid steel, enduring temperatures of approximately 1600°C on its hot face and below 1000°C on its cold face. Consequently, the temperature gradient imposed on this material during service can generate different crystallographic phases throughout its thickness, considering that it is applied at low temperature and achieves consolidation upon being put into service. The formation of these phases is associated with volume changes, leading to the generation of mechanical stresses, mainly during the first hours of operation.

Fig. 1: Ladle furnace scheme.

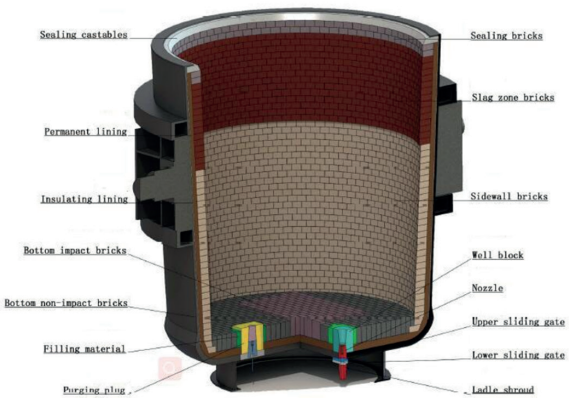

Alumina-spinel refractories are manufactured using synthetic aggregates of very high-purity alumina, such as white tabular alumina and white fused alumina, in addition to magnesium spinel (MA: $MgO{\cdot}Al_2O_3$), magnesia (MgO), and calcined alumina in fine fractions. High-alumina refractories with spinel addition offer advantages such as lower thermal conductivity and lower thermal expansion coefficient compared to MgO-C or Al_2O_3-MgO-C (AMC) bricks, resulting in reduced heat loss through the ladle wall, lower shell temperature, and high thermal shock resistance. Spinel (MA) can be added as "preformed" or can develop "in situ" in high-alumina castables during heating at high temperatures (**Zhang & Lee, 2004**). Refractories with preformed spinel exhibit high volumetric stability, while those with in-situ spinel have the advantage of gradual volumetric expansion with increasing temperature and high corrosion resistance against steel slags containing FeO and MnO (**Braulio et al., 2011**). Thus, preformed spinel is added to high-alumina castables for the following purposes: (i) to increase slag corrosion resistance and (ii) to improve high-temperature mechanical strength.

Moreover, MA spinel presents a stoichiometric range where the solid solubility of alumina in MA is greater than that of magnesia at the same temperature; therefore, alumina-rich MA spinels are commonly used in refractory manufacturing. In these cases, the notation $MgO{\cdot}nAl_2O_3$ is used, where n is the number of moles of alumina and can reach a value of n = 7.3 (**Jing et al., 2000**). The use of preformed spinel improves the mechanical strength of Al_2O_3–MA castables (**MacZura et al., 1995; Ko et al., 1994; Ko & Chan, 1999**). This improvement has been attributed to the reaction of CaO with alumina from alumina-rich MA, forming calcium hexaluminate (CA_6), which enhances bonding between spinel, alumina, and CA_6 grains in the matrix. The addition of alumina-rich spinel has also been shown to improve creep resistance in low- and ultra-low-cement alumina-spinel castables (**McConnell et al., 2002**). Thermo-mechanical properties of castables, such as hot modulus of rupture (HMOR) and refractoriness under load (RUL) of high-alumina refractories, are significantly improved by adding high-purity preformed spinel (**Sako et al., 2010**). Refractories with preformed spinel exhibit good thermal shock resistance and erosion resistance in applications such as purging plugs and well blocks used in steelmaking ladles (**Biswas & Sarkar, 2020**).

2. MATERIALS AND METODOLOGY

The material studied is an alumina-spinel castable that contains "preformed" spinel. The composition, as oxide percentages, is shown in Table 1.

Table 1: Composition (wt% of oxides) of the starting castable.

Oxide	Al_2O_3	SiO_2	Fe_2O_3	Na_2O	MgO	CaO
Wt.%	91.7	0.1	0.1	0.2	5.4	2.5

The castable used as the study material consists mainly of Al_2O_3, MgO, and CaO, with impurities (less than 0.2%) of SiO_2, Fe_2O_3, and Na_2O. Based on its CaO content (2.5 wt%), it can be classified as a low-cement castable. Considering the alumina percentage in ideal spinel (71.7% Al_2O_3 – 28.3% MgO), the material should have an alumina/spinel ratio of approximately 3. As shown later, the spinel incorporated in the starting material is an alumina-rich spinel. It is important to note that spinel is predominantly added to the fine fraction of the refractory castable.

Before shaping, the material was sieved to select particle sizes smaller than 6.35 mm (passing ASTM 1/4" mesh) to properly prepare the specimens for dilatometry. Prismatic castable specimens measuring 10 mm × 10 mm × 40 mm were shaped by casting in acrylic molds, with an addition of 6 wt% water. Curing was carried out under ambient temperature and humidity conditions for 72 hours. The specimens were then demolded and dried at 100°C for 24 hours. Subsequently, they were heat-treated at a rate of 20°C/h up to 350°C (3 hours) and then at 30°C/h up to 500°C (3 hours) to complete hydration reactions (Fig. 2.a). The specimens obtained in this way are referred to as HC and are shown in the image in Fig. 2.b.

Fig. 2: (a) Heat treatment and (b) specimens obtained prior to dilatometry tests.

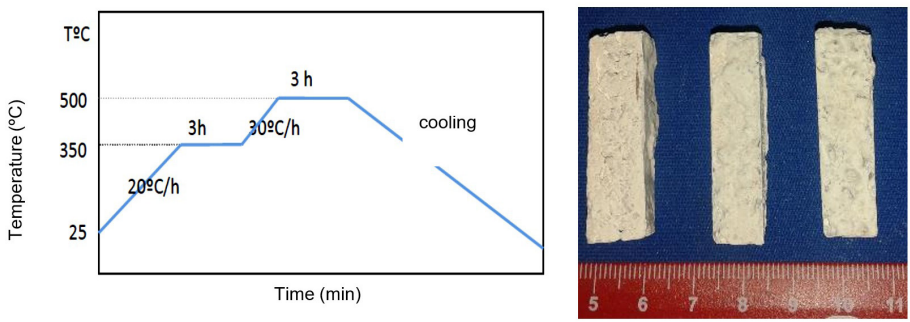

The HC specimens were subjected to different cycles in a horizontal dilatometer (Theta, Dilatronic II) at a heating rate of 5°C/min. A first HC sample was monitored up to 1600°C without holding time (designated HS-1600), and then five dilatometry tests were performed up to defined temperatures (TD) of 1000°C, 1200°C, 1300°C, 1400°C, and 1500°C, with a holding time of 4 hours at each T_D; these specimens were designated as HS-1000, HS-1200, HS-1300, HS-1400, and HS-1500, respectively.

The specimens tested in the dilatometry cycles were sectioned into three parts. One part was selected to determine apparent density and porosity using the Archimedes method with distilled water as the immersion liquid. Another part was embedded in resin, ground with SiC papers, and polished with diamond paste (6, 3, and 1 μm), then examined by scanning electron microscopy and energy-dispersive spectroscopy (SEM-EDS) using a FEG-SEM Quanta 200 microscope. A third part was ground into powder for crystallographic analysis by X-ray diffraction (XRD) using a Philips X'Pert Pro instrument.

3. RESULTS AND ANALYSIS

The XRD patterns obtained from the samples dried at 100°C (HC) show peaks corresponding to alumina and spinel phases (Fig. 3).

Fig. 3: X-ray diffraction pattern of the sample HC (100 °C-24 h).

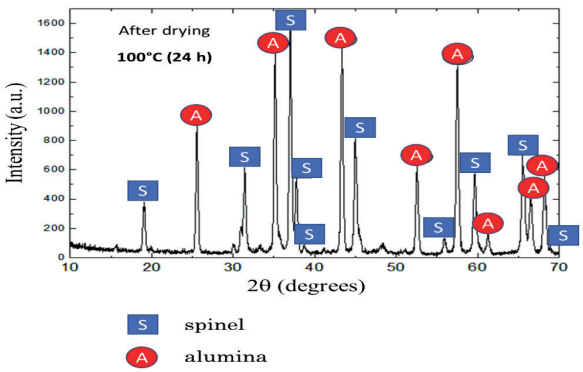

Table 2 lists the experimentally measured diffraction angles (2θ) for alumina and spinel and compares them with the theoretical values for both phases.

Table 2: Intensities of alumina and spinel peaks measured in the HC diffractogram.

Alumina

2θ (measured)	2θ (theoretical)	Δ (2θ)
25.53	25.576	- 0.046
35.15	35.150	0.000
37.75	37.767	- 0.017
43.37	43.340	+ 0.030
52.53	52.548	- 0.018
57.51	57.498	+ 0.012
61.29	61.303	- 0.013
66.55	66.514	+ 0.036
68.25	68.202	+ 0.048
		+ 0.004°

MA spinel

2θ (measured)	2θ (theoretical)	Δ (2θ)
19.11	19.028	+ 0.082
31.43	31.270	+ 0.160
37.03	36.850	+ 0.180
38.73	38.522	+ 0.208
44.99	44.830	+ 0.160
55.91	55.656	+ 0.254
59.61	59.367	+ 0.243
65.53	65.238	+ 0.292
68.93	68.637	+ 0.293
		+ 0.208°

It can be observed that the spinel peaks shift toward positive (2θ) values compared to those of stoichiometric spinel, whereas the alumina peaks do not. Considering Bragg's law:

$$\lambda = 2.d_{hkl}.sen\theta \quad (1)$$

where: λ = 1,54056 nm and d_{hkl} is the interplanar spacing, and considering that magnesium spinel (MA) has a cubic structure, it is possible determine the lattice parameter (*a*) of MA spinel using the following expression:

$$d_{hkl} = \frac{a}{\sqrt{h^2 + k^2 + l^2}} \quad (2)$$

The lattice parameter of spinel reported in the literature (theoretical) and that obtained in this work (measured) are shown in Table 3.

Table 3: Calculation of the lattice parameter of MA from theoretical and experimental data.

h	*k*	*l*	sin θ (theoretical)	*a* (Å) (theoretical)	sin θ (measured)	*a* (Å) (measured)
1	1	1	0.165288596	8.0714	0.165994296	8.0374
2	2	0	0.269508133	8.0836	0.270852469	8.0438
3	1	1	0.316063032	8.0827	0.317552916	8.0451
2	2	2	0.329871891	8.0887	0.331584888	8.0472
4	0	0	0.381312409	8.0800	0.382602807	8.0531
4	2	2	0.466818872	8.0833	0.468777953	8.0498
5	1	1	0.4952085	8.0821	0.497049686	8.0525
4	4	0	0.539050123	8.0831	0.541194636	8.0514
5	3	1	0.563792755	8.0825	0.565902701	8.0527
				0.8082 nm		**0.8048 nm**

Thus, the lattice parameter determined for the spinel in the material under study is a = 0.805 nm, which is smaller than that calculated for stoichiometric spinel (0.808 nm). According to a previous study (**Jing et al., 2000**), where the variation of the spinel lattice parameter (a) was analyzed as a function of stoichiometry (n) for $MgO{\cdot}nAl_2O_3$, the value obtained is n = 1.4 (Fig. 4.a).

Fig. 4: (a) Spinel lattice parameter as a function of the number of alumina moles (n) in the MA stoichiometry and (b) its position in the $MgO\text{-}Al_2O_3$ diagram.

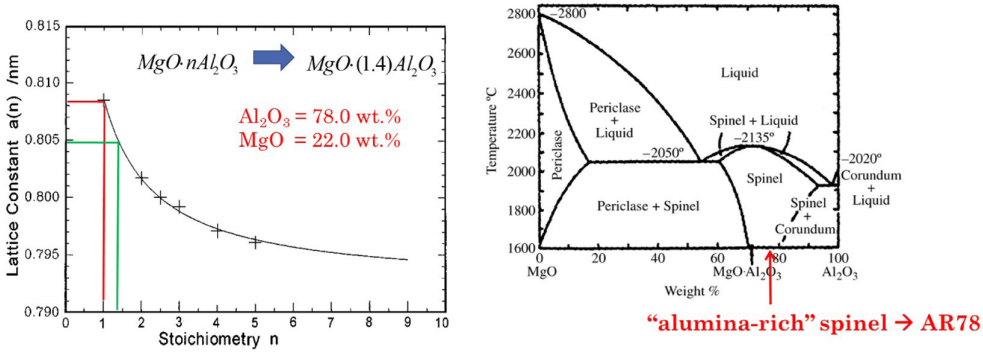

This MA stoichiometry corresponds to an alumina content of approximately 78 wt%, considering the $MgO\text{-}Al_2O_3$ phase equilibrium diagram (Fig. 4.b). Based on this result, it can be estimated that the spinel used as the raw material in the castable under study is an MA of the AR78 type.

The different crystalline phases detected in the HC specimens after the dilatometry tests are presented in Table 4.

Table 4: Crystalline phases observed in HS specimens at different temperatures.

Temperature	**1000°C** (4 h)	**1200°C** (4 h)	**1300°C** (4 h)	**1400°C** (4 h)	**1500°C** (4 h)	**1600°C** (0 h)
Crystalline phases	A MA CA $C_{12}A_7$	A MA CA_2	A MA CA_2	A MA CA_6 CA_2	A MA CA_6	A MA CA_6

A = Al_2O_3
MA = $MgO \cdot Al_2O_3$
CA = $CaO \cdot Al_2O_3$
CA_2 = $CaO \cdot 2Al_2O_3$
$C_{12}A_7$ = $12CaO \cdot 7Al_2O_3$
CA_6 = $CaO \cdot 6Al_2O_3$

The diffractograms of HS specimens treated at 1400°C, 1500°C, and 1600°C are shown in Fig. 5.

Fig. 5: X-ray diffractograms of HS samples and percentages of phases present.

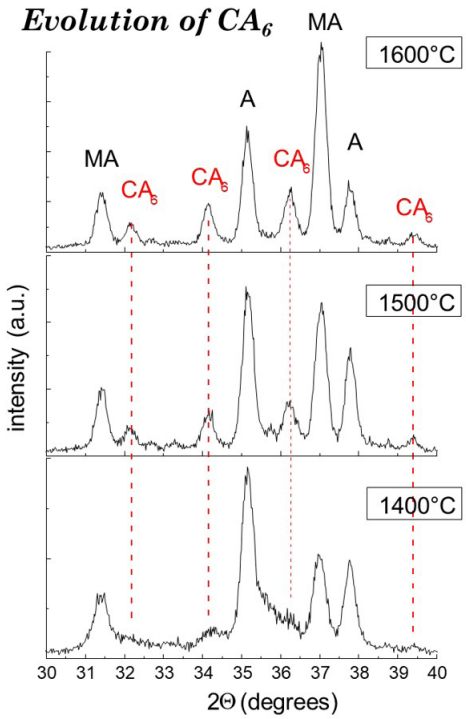

Temp (°C)	% Al_2O_3	% MA	A:MA
1000	76	24	≈ 3,2
1200	74	26	≈ 2,8
1300	75	25	≈ 3,0
1400	77	23	≈ 3,3
1500	59	41	≈ 1,4
1600	53	47	≈ 1,1

Temp (°C)	% Al_2O_3	% MA	% CA_6
1500	53	33	14
1600	37	44	19

These diffractograms show the development of calcium hexaluminate (CA_6), which begins to appear at around 1400°C and then exhibits increasing peak intensity at 1500°C and 1600°C. The percentages calculated from the peak intensities of alumina (A), spinel (MA), and calcium hexaluminate (see tables to the right of the diffractograms) indicate the highest CA_6 content in the specimen treated at 1600°C. The reaction kinetics for CA_6 formation from CA_2 and Al_2O_3 is very slow at temperatures below 1350°C but increases significantly above 1450°C (**Pieta et al., 2015**).

On the other hand, performing a similar analysis on the alumina-to-spinel ratio (A:MA) reveals a decrease in the alumina percentage, which is associated with the consumption of Al_2O_3 due to the increased formation of CA_6.

Figure 6 shows micrographs (left) and EDS analyses (right) of different specimens.

Fig. 6: Micrographs of specimens and EDS analysis of the HC (top), HS-1200 (center), and HS-1400 (bottom) specimens.

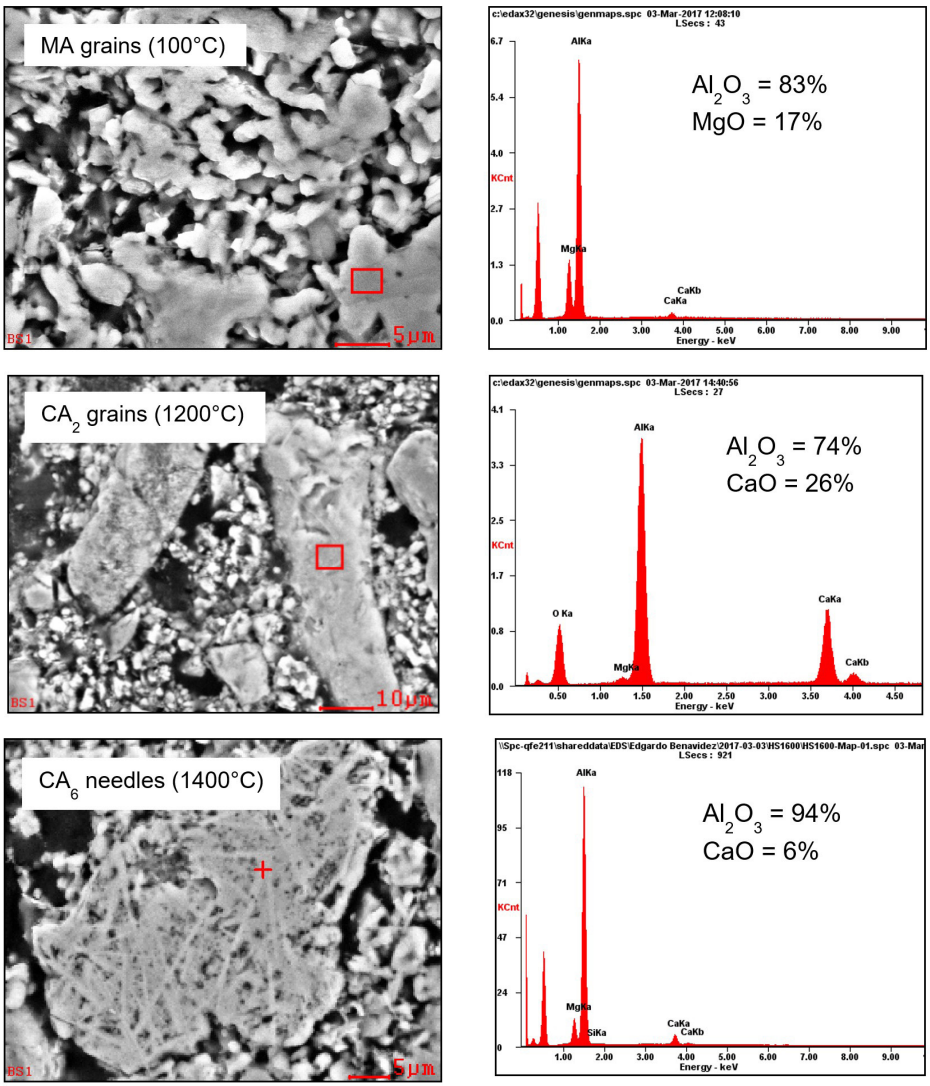

The top micrograph corresponds to the HC specimen (100°C – 24h), where MA spinel grains (red square) stand out, with a content of ≈83% Al_2O_3. Thus, through EDS analysis, it is established, consistent with the XRD peaks of this sample, that the MA spinel grains are rich in alumina. The center micrograph corresponds to the HS-1200 specimen, where calcium dialuminate (CA_2) grains (red square) are highlighted (see EDS spectrum). According to the values in Table 4, this phase is present at 1200, 1300, and 1400°C, later reacting with alumina (A) to form calcium hexaluminate (CA_6). In the bottom micrograph corresponding to the HS-1400 specimen, CA_6 “needles” (red cross) are highlighted.

The apparent porosity values determined for these specimens are shown in Fig. 7. The open porosity remains constant between 1000–1200°C (≈16 vol %), showing a significant increase at 1300°C, where the highest porosity is observed (≈ 25 vol %). The porosity values then decrease smoothly and continuously for HS-1400 (≈ 23 vol %) and HS-1500 (≈ 21 vol %).

Fig. 7: Open porosity values at different temperaturas.

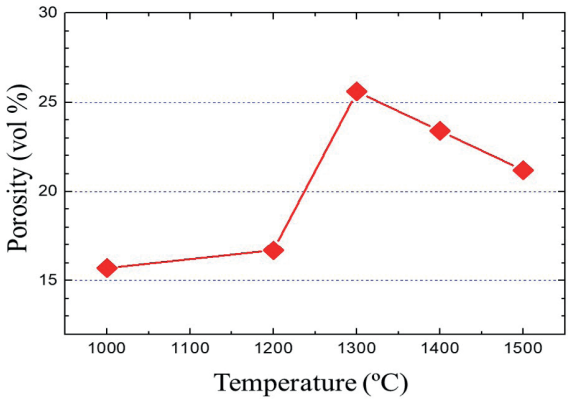

The lower porosity measured from 1400 °C onward may be associated with the formation of calcium hexaluminate (CA_6) at that temperature. According to some authors, CA_6 grains are detected inside the pores, preventing the formation of interconnected pores (**Wang et al., 2018**), which are directly linked to apparent porosity. In addition, the expansion of CA_6 grains tends to reduce pore size.

For the volumetric changes of the calcium–alumina (CA) phases, the values presented in Table 5 are considered, where the weight percentages of lime and alumina, melting temperature (T_{melt}), density (ρ), molar mass (M_m), and molar volume (V_m) of the different phases are listed, as considered in this work.

Table 5. Properties of CA phases.

Mineral	T_{melt} (°C)	CaO (%)	Al_2O_3 (%)	ρ (g/cm³)	M_m (g/mol)	V_m (cm³/mol)
C	2570	100	-	3,32	56,08	16,89
$C_{12}A_7$	1415-1495	48,6	51,4	2,69	1386,64	515,48
CA	1600	35,5	64,5	2,98	158,04	53,03
CA_2	1750-1765	21,6	78,4	2,91	260,00	89,35
CA_6	1830	8,4	91,6	3,38	667,84	197,59
A	2051	-	100	3,98	101,96	25,62

The general thermal behavior of the concrete up to 1600 °C is shown in Fig. 8 (**Benavidez et al., 2018**). It can be observed that the concrete expands linearly up to around 1100 °C; from that point, the curve accelerates its expansion until reaching 1325 °C. Then, the concrete begins to contract slowly until reaching 1385 °C. From this temperature onward, the contraction rate increases and stops around 1480 °C. At approximately 1530 °C, the contraction accelerates again until reaching 1620 °C, which is the maximum temperature recorded in the test.

Fig. 8: Dilatometric curve of concrete up to 1600 °C (HS-1600 specimen).

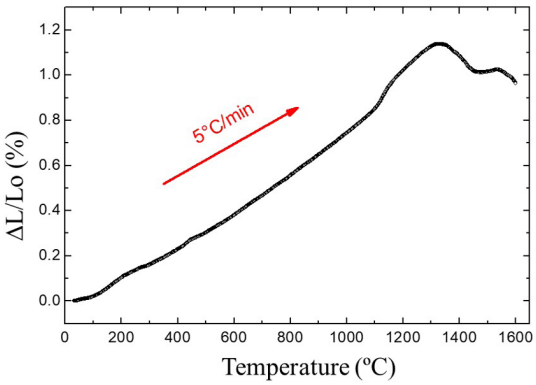

The area of interest in the dilatometric curve focuses on the region between 1000–1600 °C. Fig. 9 shows this region, where the material exhibits expansions and contractions within this temperature range, and four zones are identified. In zone (1), between 1110 °C and 1325 °C, an expansion is observed, which is attributed to the formation of calcium dialuminate through the reaction in Eq. 3, representing a volume increase of ≈ 13.5 % (**Wang et al., 2016**), according to the M_m and V_m values given in Table 5.

$$CA + A = CA_2 \quad (3)$$

Expansions due to the formation of CA_2 from CA and alumina have previously been reported (**Criado et al., 1976**). Zone (2), between 1330 °C and 1460 °C, shows a contraction attributed to the sintering of ceramic grains, which produces densification of the material. Zone (3), starting at 1460 °C, shows a slight expansion associated with the formation of CA_6, according to Eq. 4.:

$$CA_2 + 4A = CA_6 \quad (4)$$

This small volumetric expansion of ≈ 3 % (**Wang et al., 2016**) slows down the densification of the concrete in the range of 1480–1530 °C. In some cases, this expansion

has been attributed to the bonding between CA_6 grains and spinel grains in the matrix (**Ko and Lay, 2000**) or to the formation of hexagonal CA_6 platelets (**Auvray et al., 2008**). However, other authors have associated the reaction in Eq. (4) with a volume contraction (**Xu et al., 2015**).

Finally, from 1540 °C onward, zone (4), the sintering of ceramic grains once again dominates the densification of the material. At this stage, the presence of a small amount of liquid phase could also be expected, due to impurities in the raw materials, which may accelerate the sintering/densification of the refractory (**Ko and Lay, 2000**).

Fig. 9: Identification of the different zones of the HS-1600 dilatometric curve.

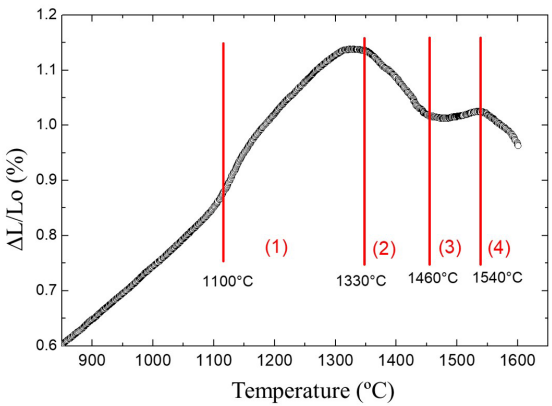

Fig. 10 shows, as an example, the isothermal dilatometry of HS-1300, where a constant heating rate of 5 °C/min is applied up to 1300 °C, maintaining that temperature for 4 hours.

Fig. 10: Dilatometric behavior of the sample HS-1300.

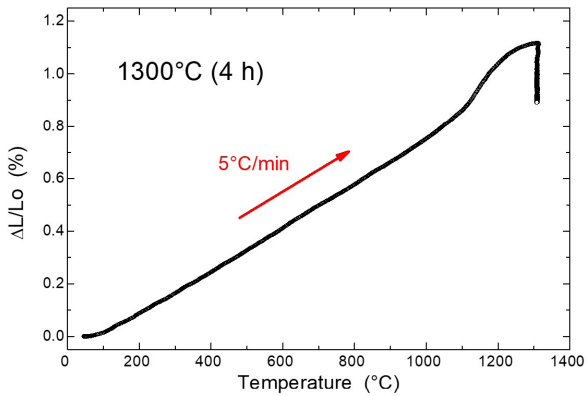

The isothermal dilatometries (4 hours) at the different T_D are shown in Fig. 11. In these curves, L_0 is considered as the length of the specimen at temperature T_D.

The dilatometries show that at 1000 °C there is a slight expansion behavior of the specimen ($\Delta L/L_0 > 0$), while for the remaining TD, the behavior is contraction. The contraction values, starting from TD = 1200 °C, increase as the temperature rises.

Fig. 11: Isothermal behavior at different temperatures T_D.

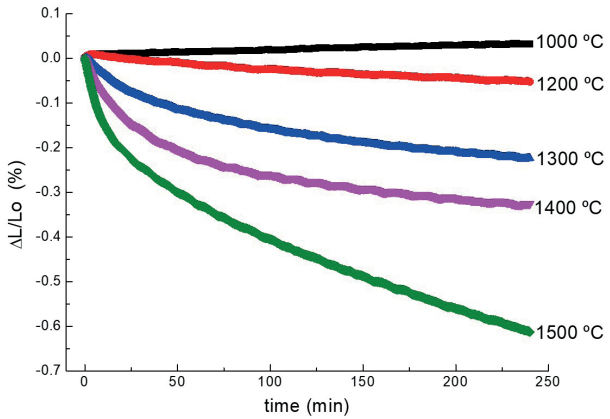

Table 6 lists the expansion and contraction values obtained at the different temperatures.

Tabla 6: Expansion and contraction values in isothermal dilatometry at different T_D.

Temp (°C)	$\Delta L/L_o$ (%)	Behavior
1000	+ 0.025	expansion
1200	- 0.062	contraction
1300	- 0.224	contraction
1400	- 0.310	contraction
1500	- 0.613	contraction

Considering a temperature gradient such as the one present in concrete located on a ladle floor, the dilatometry data indicate the presence of stresses resulting from the different dimensional changes. As mentioned, the refractory located at the bottom of the ladle is subjected to a temperature gradient ranging from 1600 °C on the hot face (in contact with the molten steel) to temperatures below 1000 °C on the cold face.

Analyzing the profile of contractions and expansions after 4 hours (Table 6), and considering a neutral stress at 1000 °C, a mechanical stress profile such as the one shown in Fig. 12 may be present in the alumina–spinel concrete analyzed in this work. The temperature of 1000 °C was selected as the point of neutral stress because, below this temperature, no significant dimensional variations are recorded. The $\Delta L/L_0$ (%) values

indicated on the dilatometric curve in Fig. 12 refer to the initial length (L_0) recorded at room temperature. This means that, relative to this initial L_0, the concrete will have an expansion of ≈ 0.77 % at 1000 °C (after 4 h), while it will have expanded ≈ 0.96 % at 1200 °C (4 h), ≈ 0.90 % at 1300 °C (4 h), ≈ 0.77 % at 1400 °C (4 h), and finally ≈ 0.40 % at 1500 °C (4 h).

Fig. 12: Compressive and tensile stresses developed at different temperature levels.

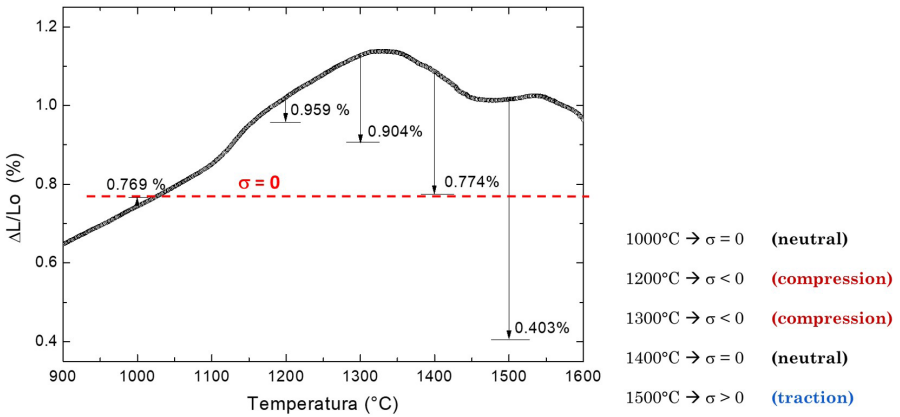

Thus, if applied stresses are not considered (as in dilatometry tests), the zones at 1200 °C and 1300 °C, after 4 hours, will reach greater expansions (0.959 % and 0.904 %, respectively) relative to the initial length (L_0) measured at room temperature. Therefore, the layers of concrete in service that register these temperatures tend to have a greater length than the zone at 1000 °C (taken as neutral), meaning that, in service, they would be subjected to compressive stresses ($\sigma < 0$).

Conversely, the region located at 1500 °C (4 h) shows an expansion value (0.403 %) lower than that at 1000 °C (0.769 %). Therefore, after 4 hours in service, the concrete zones situated at 1400 °C (near the hot face) will be subjected to tensile stresses ($\sigma > 0$) relative to the zone at 1000 °C (farther from the hot face). These zones under tensile stress can be considered prone to thermomechanical failure.

Finally, the region located at 1400 °C shows a linear expansion (0.774 %) of the same order as that obtained at 1000 °C (0.769 %), so mechanical stresses can be considered negligible ($\sigma = 0$) relative to the zone at 1000 °C.

4. CONCLUSIONS

Some key points to highlight in this study were: (i) the evolution of the crystalline phases of a commercial alumina–spinel concrete between 1000 °C and 1600 °C was determined; (ii) the dimensional changes associated with the formation of calcium

dialuminate and calcium hexaluminate were confirmed through porosity and dilatometry data; (iii) a profile of dimensional variations based on isothermal dilatometry data was presented. At this point, it is important to emphasize the generation of thermomechanical stresses due to the dimensional changes experienced by this material in a steel ladle, where a significant temperature gradient occurs under service conditions.

REFERENCES

Auvray. J-M., Gault, C. y Huger, M. (2008). Microstructural changes and evolutions of elastic properties versus temperatura of alumina and alumina-magnesia refractory castables. *J. Eur. Ceram. Soc.*, *28*, 1953-1960.

Benavidez, E., Ponte, A. y Ponte R. (2018). Comportamiento térmico de un hormigón refractario para aplicaciones en horno cuchara. *Libro de resúmenes extendidos del 18° Congreso Internacional de Metalurgia y Materiales*. Bariloche, Argentina. 336-338.

Biswas, S. y Sarkar, D. (2020). Introduction to Refractories for Iron- and Steelmaking. Springer Nature. https://doi.org/10.1007/978-3-030-43807-4.

Braulio, M. A. L., Rigaud, M., Buhr, A. Parr, C. y Pandolfelli, V. C. (2011). Spinel-containing alumina-based refractory castables. *Ceram. Int.*, *37*, 1705-1724.

Criado, E., Estrada, D.A. y de Aza, S. (1976). Estudio dilatométrico sobre la formación de dialuminato y hexaluminato de calcio en cementos y hormigones refractarios. *Bol. Soc. Esp. Cerám. Vidr.*, *15*(5). 319-321.

Ghosh, A. (2000). *Secondary Steel Making – Principle and Applications*, CRC Press. DOI: 10.1201/9781420042313.

Jing, S.Y., Lin, L.B., Huang, N.K., Zhang, J. y Lu, Y (2000). Investigation on lattice constants of Mg-Al spinels. *J. Mater. Sci. Lett.*, *19*, 225–227.

Ko, Y-C. y Lay, J. T. (2000). Thermal expansion characteristics of alumina-magnesia and alumina-spinel castables in the temperature range 800-1650°C. *J. Am. Ceram. Soc. 83*, 2872-2874.

Ko, Y-C. y Chan, C. F. (1999). Effect of spinel content on hot strength of alumina-spinel castables in the temperature range 1000–1500°C. *J. Eur. Ceram Soc*, *19*, 2633–2639.

MacZura, G., Madono, M., Kriechbaum, G. W. y Sewell, B. (1995). Low moisture regular corundum/spinel castables with superior properties. Proc. Unified Intl. Tech. Conf. On Refractories, Kyoto, Japan, 179-186.

McConnell, R.W., Marra, R.A. y Fullington, F.A. (2002). Benefits of sintered magnesium aluminate spinels in high purity castable refractories. *Refractories Applications and News 7*(2), 23–28.

Pieta, A., Bucko, M. M., Janus, M., Lis, J. y Jonas, S. (2015). Calcium hexaluminate synthesis and its influence on the properties of CA_2-Al_2O_3-based refractories. *J. Eur. Ceram. Soc.*, *35*, 4567-4571.

Sako, E.Y., Braulio, M. A. L., Brant, P. O. y Pandolfelli, V. C. (2010). The impact of pre-formed and in-situ spinel formation on the physical properties of cement bonded high alumina refractory castables. *Ceram. Int.*, *36*, 2079–2085.

Vance, M.W., Kriechbaum, G.W., Henrichsen, R.A., MacZura, G., Moody, K.J. y Munding, S. (1994). Influence of spinel additives on high-alumina/spinel castables. *Bull. Am. Ceram. Soc.*, *73*, 70–74.

Wang, Q., Li, Y., Xu, N., Xiang, R. y Li, S. (2018). Microstructure and phase evolution of cement-bonded high-alumina refractory castables for porous purging plugs. *J. Ceram. Sci. Technol., 9*, 1-6.

Wang, Y., Li, X., Zhu, B. y Chen, P. (2016). Microstructure evolution during the heating process and its effect on the elastic properties of CAC-bonded alumina castables. *Ceram. Int*., *42*, 11355-11362.

Xu, L., Chen, M., Huang, W-J., Wang, N., Dong, J-H y Ying, X-L. (2015). Effects of CaO content on sintering and lightweight of Al_2O_3-MgO-CaO refractories. *Materials Research Innovations*, *19*, 212-217.

Zhang, S. y Lee, W. E. (2004). Spinel-Containing Refractories en C.A Schacht, (Ed.). *Refractories Handbook*. (pp. 215-257) Marcel Dekker Inc.

CAPÍTULO 2

HOJAS DE CÁLCULO PARA PREDECIR CURVAS DE RELACIONES MOLARES EN SISTEMAS DONDE SE FORMAN COMPLEJOS DE INCLUSIÓN ENTRE FÁRMACOS (Far) Y CICLODEXTRINAS (CD)[1]

Data de submissão: 15/11/2025
Data de aceite: 02/12/2025

Alberto Rojas-Hernández
Universidad Autónoma
Metropolitana-Iztapalapa
Departamento de Química
Área de Química Analítica
Av. Ferrocarril San Rafael Atlixco 186
Col. Reyes de Reforma 1era Sección
09310. Alcaldía Iztapalapa
CDMX. México
https://orcid.org/0000-0001-9716-4762

Daniel Alejandro Ramos-Hernández
Universidad Autónoma
Metropolitana-Iztapalapa
Departamento de Química
Área de Química Analítica
https://orcid.org/0009-0000-8246-9272

Linda Alzucena Luna-Ortega
Universidad Autónoma
Metropolitana-Iztapalapa
Departamento de Química
Área de Química Analítica
https://orcid.org/0009-0006-9613-9585

Lucero Hernández-García
Universidad Autónoma
Metropolitana-Iztapalapa
Departamento de Química
Área de Química Analítica
https://orcid.org/0009-0008-9059-4338

María Teresa Ramírez-Silva
Universidad Autónoma
Metropolitana-Iztapalapa
Departamento de Química
Área de Química Analítica
https://orcid.org/0000-0003-1370-1466

Jorge Martínez-Guerra
Universidad Autónoma
Metropolitana-Iztapalapa
Departamento de Química
Área de Química Analítica
https://orcid.org/0000-0002-7615-1003

Manuel Eduardo Palomar-Pardavé
Universidad Autónoma
Metropolitana-Azcapotzalco
Departamento de Materiales
Área de Ingeniería de Materiales
https://orcid.org/0000-0002-2944-3599

Giaan Arturo Álvarez-Romero
Universidad Autónoma del
Estado de Hidalgo
División de Ciencias
Básicas e Ingenierías
Área de Académica de Química
https://orcid.org/0000-0002-9525-3937

[1] Partes de este trabajo se presentaron en memorias en extenso de la Asociación Mexicana de Química Analítica y de la Sociedad Química de México en el año de 2017.

RESUMEN: Hace algunas décadas se estudiaba el método de relaciones molares (*molar ratio*) en los libros de texto de Química Analítica y de Química Inorgánica, como una metodología para conocer la estequiometría de especies y sus constantes de equilibrio de formación. En las presentaciones de esos libros se encuentra el desarrollo para predecir dicha curva bajo tres supuestos: 1) Se forma sólo un complejo de estequiometría M_mL_n, 2) la reacción de formación de ese complejo es cuantitativa y 3) se mide una respuesta (*R*) que depende linealmente de la concentración del complejo formado. El método de relaciones molares se puede aplicar al estudio de las especies que se forman en sistemas del tipo fármaco (Far)-ciclodextrina (CD). En este trabajo se presentan hojas de cálculo para el estudio de este tipo de sistemas en donde se forman varias especies simultáneamente que contribuyen a la respuesta medida, sin que se requiera que su formación sea cuantitativa. Como ejemplos se presentan los casos de la curcumina con la β-ciclodextrina a pH = 3.6, de la curcumina con la 2-hidroxipropil-β-ciclodextrina a pH = 12.0 y del diclofenaco con la 2-hidroxipropil-β-ciclodextrina.
PALABRAS CLAVE: hojas de cálculo; método de relaciones molares; curcumina; diclofenaco; ciclodextrinas.

SPREADSHEETS TO PREDICT MOLAR RATIO CURVES FOR SYSTEMS WHERE INCLUSION COMPLEXES ARE FORMED BETWEEN DRUGS (Far) AND CYCLODEXTRINS (CD)

ABSTRACT: A few decades ago, the molar ratio method was studied in Analytical Chemistry and Inorganic Chemistry textbooks as a methodology to determine the stoichiometry of species and their formation equilibrium constants. The presentations in those books contain the development to predict this curve under three assumptions: 1) Only one complex of stoichiometry M_mL_n is formed, 2) the formation reaction of that complex is quantitative, and 3) a response (*R*) is measured that depends linearly on the concentration of the complex formed. The molar ratio method can be applied to the study of species that are formed in drug (Far)-cyclodextrin (CD) type systems. This work presents spreadsheets for the study of this type of system where several species are formed simultaneously that contribute to the measured response, without requiring that their formation be quantitative. Examples include curcumin with β-cyclodextrin at pH = 3.6, curcumin with 2-hydroxypropyl-β-cyclodextrin at pH = 12.0, and diclofenac with 2-hydroxypropyl-β-cyclodextrin.
KEYWORDS: spreadsheets, molar ratio method, curcumin, diclofenac, cyclodextrins

1. INTRODUCCIÓN

Hace décadas, el método de las relaciones molares se estudiaba en libros de texto de Química Analítica y Química Inorgánica para elucidar la estequiometría de especies del tipo M_mL_n. Sin embargo, el tratamiento clásico consideraba sólo la formación cuantitativa del complejo M_mL_n, midiendo una respuesta (*R*) que es directamente proporcional a la concentración de M_mL_n (Rojas-Hernández, 2013).

En sistemas del tipo anfitrión-huésped, como es el caso de las ciclodextrinas con moléculas orgánicas (que son sistemas de interés en la industria alimentaria y en la farmacéutica) es muy común considerar que la interacción de un anfitrión (como las ciclodextrinas, CD) con un huésped (como colorantes o fármacos, Far) forma un único complejo de inclusión de estequiometría 1:1. Sin embargo, cada vez se cuestiona más esta hipótesis y se encuentran más trabajos en la literatura científica en donde no se cumple (Escandar, 1999; Mucci, 1999; Martínez-Guerra, 2021).

Por otra parte, las constantes de equilibrio involucradas en estos sistemas no siempre permiten considerar que el proceso de formación asociado corresponde a una reacción cuantitativa, en las condiciones en donde el proceso ocurre. Y por el tipo de propiedades que se miden, casi nunca se puede considerar que la respuesta medida (*R*) se debe a un solo complejo de inclusión.

El objetivo de este trabajo es establecer modelos para predecir curvas de relaciones molares que pueden formar complejos del tipo Far(CD) y $Far(CD)_2$ (que tienen la forma de un sistema polidonador de la partícula CD, como se explica en Rojas-Hernández, 1995); para luego extender el modelo a la formación adicional del complejo $Far_2(CD)$ (necesario para poder predecir e interpretar casos como el descrito por Mucci, 1999). Se muestran algunos ejemplos para ver la bondad de la aplicación del método a la determinación de constantes de equilibrio de inclusión y a la interpretación de estos sistemas.

2. TEORÍA

2.1. MODELO PARA SISTEMAS $FAR(CD)_2$/FAR(CD)/FAR/CD

Como hay reportes de sistemas en donde se forman complejos de inclusión con estas estequiometrías (Escandar, 1999; Martínez-Guerra, 2021), se va a considerar un sistema en el que ocurra la formación de estos dos compuestos de inclusión.

Este modelo permite determinar las fracciones de las especies $Far(CD)_2$, Far(CD) y Far como función del pCD ($\equiv -\log[CD]$), siendo log el logaritmo base diez y [CD] la molaridad de la ciclodextrina en condiciones de equilibrio.

En un sistema del tipo $Far(CD)_2$/Far(CD)/Far/CD, en donde CD es la partícula intercambiable, se sabe que las fracciones molares de las especies que contienen Far **sólo dependen del valor de** pCD (Rojas-Hernández, 1995), de acuerdo con el conjunto de ecuaciones (1) a (3)

$$f_{10} \equiv f_{Far} = \frac{[Far]}{[Far]_{total}} = \frac{1}{1 + \beta_{11}[CD] + \beta_{12}[CD]^2} \quad (1)$$

$$f_{11} \equiv f_{Far(CD)} = \frac{[Far(CD)]}{[Far]_{total}} = f_{10}\beta_{11}[CD] \quad (2)$$

$$f_{12} \equiv f_{Far(CD)_2} = \frac{[Far(CD)_2]}{[Far]_{total}} = f_{10}\beta_{12}[CD]^2 \quad (3)$$

En las ecuaciones (1) a (3), $[Far]_{total} = [Far] + [Far(CD)] + [Far(CD)_2]$, en tanto que β_1 y β_2 representan las constantes de formación global de las especies Far(CD) y $Far(CD)_2$, respectivamente. Esto es:

$$Far + CD \rightleftarrows Far(CD) \quad con \quad \beta_{11} = \frac{[Far(CD)]}{[Far][CD]} \quad (4)$$

$$Far + 2CD \rightleftarrows Far(CD)_2 \quad con \quad \beta_{12} = \frac{[Far(CD)_2]}{[Far][CD]^2} \quad (5)$$

Ahora bien, si la respuesta *R* que se va a medir depende linealmente de las concentraciones de todas las especies presentes en el sistema, puede escribirse la ecuación (6):

$$R = k_{CD}[CD] + k_{Far}[Far] + k_{Far(CD)}[Far(CD)] + k_{Far(CD)_2}[Far(CD)_2] \quad (6)$$

Siendo k_{CD}, k_{Far}, $k_{Far(CD)}$ y $k_{Far(CD)_2}$, los factores de respuesta de las especies correspondientes.

Sustituyendo ahora las ecuaciones (1) a (3) en la ecuación (6) se obtiene la ecuación (7).

$$R = k_{CD}[CD] + \{k_{Far}f_{10} + k_{Far(CD)}f_{11} + k_{Far(CD)_2}f_{12}\}[Far]_{total} \quad (7)$$

Por otro lado, la concentración total de CD se puede escribir de acuerdo con la ecuación 8.

$$[CD]_{total} = [CD] + [Far(CD)] + 2[Far(CD)_2] = [CD] + [Far]_{total}(f_{11} + 2f_{12}) \quad (8)$$

Finalmente, por definición la relación (o cociente) molar se define como se muestra en la ecuación (9).

$$r_{CD} \equiv \frac{n_{CD_{total}}}{n_{Far_{total}}} = \frac{[CD]_{total}}{[Far]_{total}} = \frac{[CD] + [Far]_{total}(f_{11} + 2f_{12})}{[Far]_{total}} = \frac{[CD]}{[Far]_{total}} + (f_{11} + 2f_{12}) \quad (9)$$

Como se puede ver fácilmente, las ecuaciones (1) a (3) sólo dependen de la [CD] como variable y tienen a las constantes globales de formación de los complejos de inclusión como parámetros; en tanto que las ecuaciones (8) a (9) incluyen a la $[Far]_{total}$ como parámetro; finalmente, la ecuación (7) también tiene como parámetros a los factores de respuesta de las especies.

Así, en una hoja de cálculo se pueden dar valores a la [CD] para los parámetros dados de $[Far]_{total}$, las constantes globales de formación, los factores de respuesta y las ecuaciones (1) a (9). Con ello se pueden obtener curvas de relaciones molares R = f(r_{CD}) o R = g(pCD_{total})

2.2. MODELO PARA SISTEMAS $FAR(CD)_2$/FAR(CD)/FAR_2(CD)/FAR/CD

Aunque puede parecer extraño el considerar una especie que se forme enlazando dos moléculas de fármaco a una molécula de ciclodextrina, hay reportes de estos casos (Mucci, 1999). Es por eso que se decidió hacer una hoja de cálculo que pueda considerar la especie $Far_2(CD)$.

En este sistema, además de las especies consideradas en la subsección anterior (en los equilibrios de las ecuaciones (4) y (5)), se forma la especie $Far_2(CD)$, por lo que hay que considerar también su equilibrio de formación.

$$2Far + CD \rightleftarrows Far_2(CD) \quad con \quad \beta_{21} = \frac{[Far_2(CD)]}{[Far]^2[CD]} \quad (10)$$

Por lo tanto, la concentración total del fármaco es entonces:

$$[Far]_{total} = [Far] + [Far(CD)] + [Far(CD)_2] + 2[Far_2(CD)] \quad (11)$$

Esto hace que cambie la dependencia de las fracciones molares de las especies del sistema, pues ahora dependen no sólo de la [CD], sino también de la $[Far]_{total}$, como se muestra en las ecuaciones (12) a (15).

$$\phi_{10} \equiv \phi_{Far} = \frac{[Far]}{[Far]_{total}} = \frac{1}{1 + \beta_{11}[CD] + \beta_{12}[CD]^2 + 2\beta_{21}[CD][Far]} = \frac{1}{1 + \beta_{11}[CD] + \beta_{12}[CD]^2 + 2\beta_{21}[CD]\phi_{10}[Far]_{total}} \quad (12)$$

$$\phi_{11} \equiv \phi_{Far(CD)} = \frac{[Far(CD)]}{[Far]_{total}} = \phi_{10}\beta_{11}[CD] \quad (13)$$

$$\phi_{12} \equiv \phi_{Far(CD)_2} = \frac{[Far(CD)_2]}{[Far]_{total}} = \phi_{10}\beta_{12}[CD]^2 \quad (14)$$

$$\phi_{21} \equiv \phi_{Far_2(CD)} = \frac{2[Far_2(CD)]}{[Far]_{total}} = 2\phi_{10}^2\beta_{21}[CD][Far]_{total} \quad (15)$$

El factor 2 en la definición de la ecuación (15) es necesario para que las fracciones del componente estén bien definidas, por lo que su suma da el valor de 1.

La ecuación (12) permite despejar la fracción de Far de una ecuación cuadrática:

$$\phi_{10}{}^2(2\beta_{21}[Far]_{Total}[CD]) + \phi_{10}\left(1 + \beta_{11}[CD] + \beta_{12}[CD]^2\right) - 1 = 0 \quad (16)$$

de manera que:

$$\phi_{10} = \frac{-\left(1 + \beta_{11}[CD] + \beta_{12}[CD]^2\right) + \sqrt{(1 + \beta_{11}[CD] + \beta_{12}[CD]^2)^2 + 8\beta_{21}[Far]_{Total}[CD]}}{4\beta_{21}[Far]_{Total}[CD]} \quad (17)$$

Así, el conjunto de ecuaciones (17) y (13) a (15) puede ser evaluado en forma analítica para cada [CD], con valores fijos de $[Far]_{total}$ y las constantes de formación globales.

Las ecuaciones (7) a (9) también deben ser reescritas, de manera que:

$$R = k_{CD}[CD] + \left\{k_{Far}\phi_{10} + k_{Far(CD)}\phi_{11} + k_{Far(CD)_2}\phi_{12} + k_{Far_2(CD)}\frac{\phi_{21}}{2}\right\}[Far]_{total} \quad (18)$$

$$[CD]_{total} = [CD] + [Far(CD)] + [Far_2(CD)] + 2[Far(CD)_2] = [CD] + [Far]_{total}\left(\phi_{11} + 2\phi_{12} + \frac{\phi_{21}}{2}\right) \quad (19)$$

$$r_{CD} \equiv \frac{n_{CD_{total}}}{n_{Far_{total}}} = \frac{[CD]_{total}}{[Far]_{total}} = \frac{[CD] + [Far]_{total}\left(\phi_{11} + 2\phi_{12} + \frac{\phi_{21}}{2}\right)}{[Far]_{total}} = \frac{[CD]}{[Far]_{total}} + \left(\phi_{11} + 2\phi_{12} + \frac{\phi_{21}}{2}\right) \quad (20)$$

Entonces, en una hoja de cálculo se pueden dar valores a la [CD] para los parámetros dados de $[Far]_{total}$, las constantes globales de formación, los factores de respuesta y las ecuaciones (5), (6) y (10) a (20). Con ello se pueden obtener curvas de relaciones molares R = f(r_{CD}) o R = g(pCD_{total}) para los sistemas de esta subsección.

En la siguiente sección se presentan algunos ejemplos en los que se aplican las hojas de cálculo construidas con las ecuaciones aquí deducidas.

3. EJEMPLOS DE SISTEMAS EN DONDE SE FORMAN UNO O DOS COMPLEJOS DE INCLUSIÓN, ADEMÁS DEL COMPLEJO FAR(CD)

Los complejos de inclusión que se forman entre la curcumina y las ciclodextrinas han dado lugar a varios trabajos en la literatura científica. Para ejemplificar el caso del modelo desarrollado en la subsección 2.1 de este trabajo se utilizarán los datos de los trabajos reportados en Martínez-Guerra (2021) y Luna-Ortega (2017).

3.1. SISTEMA CURCUMINA/β-CICLODEXTRINA A PH = 3.6 EN SOLUCIÓN ACUOSA

En un estudio espectrofotométrico de soluciones de curcumina no ionizada (H_3Cur) con β-ciclodextrina (βCD), en donde la concentración de curcumina total $[Cur]_{total}$ es igual a 3.25×10^{-5} M y la concentración total de la β-ciclodextrina total varía en el intervalo $0 \leq [\beta CD]_{total} \leq 0.017$ M, se obtuvieron los valores de constantes de equilibrio de formación global y los factores de respuesta de las especies que se muestran en la Tabla 1.

Tabla 1. Parámetros obtenidos por medio de la regresión no lineal de los espectros de absorción de diferentes sistemas de curcumina con β-ciclodextrina a pH = 3.6, utilizando el programa SQUAD (Leggett, 1985; Martínez-Guerra, 2021).

Equilibrio de formación de la especie $H_3Cur(\beta CD)_i$	$\log\beta_{ij}$	Factor de respuesta de la especie $H_3Cur(\beta CD)_i$ $(L\cdot mol^{-1})$*
$H_3Cur \rightleftarrows H_3Cur$	$\log\beta_{10} \equiv 0$	k_{H_3Cur} = 19995
$H_3Cur + \beta CD \rightleftarrows H_3Cur(\beta CD)$	$\log\beta_{11}$ = 4.02	$k_{H_3Cur(\beta CD)}$ = 14983
$H_3Cur + 2\beta CD \rightleftarrows H_3Cur(\beta CD)_2$	$\log\beta_{12}$ = 6.05	$k_{H_3Cur(\beta CD)_2}$ = 36350

* la longitud de onda para esos factores de respuesta es de 416 nm, la longitud de paso óptico es de 1 cm y se considera que la βCD no absorbe luz de esa longitud de onda.

Figura 1. Captura de pantalla que muestra el aspecto de la hoja de cálculo elaborada con las ecuaciones (1) a (9) y los parámetros de la Tabla 1.

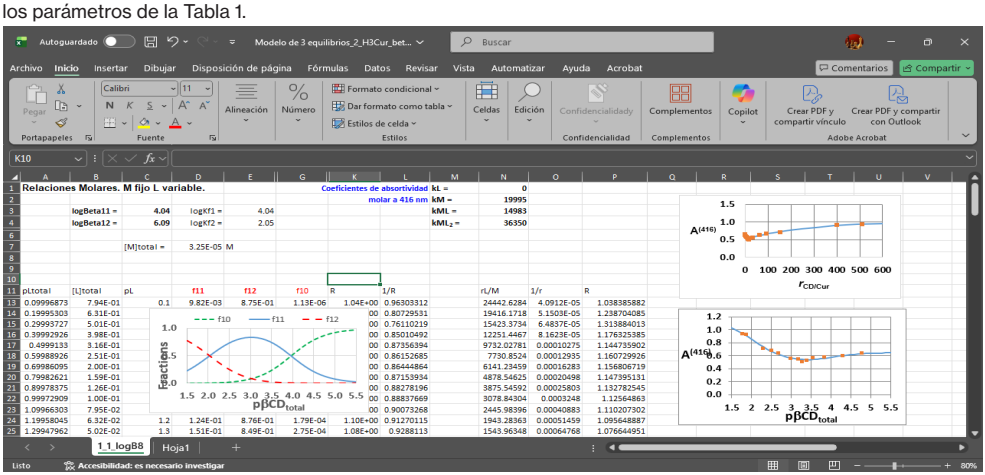

Figura 2. Gráficas obtenidas con el modelo que se muestra en la Tabla 1, construido con la hoja de cálculo que se muestra en la Figura 1, para una [Cur]total = 3.25×10^{-5} M. a) Diagrama de distribución de las especies de curcumina con β-ciclodextrina. b) Curva típica del método de relaciones molares. Los marcadores anaranjados son resultados experimentales. c) Curva de secciones sigmoidales que muestra la presencia de dos complejos de inclusión.

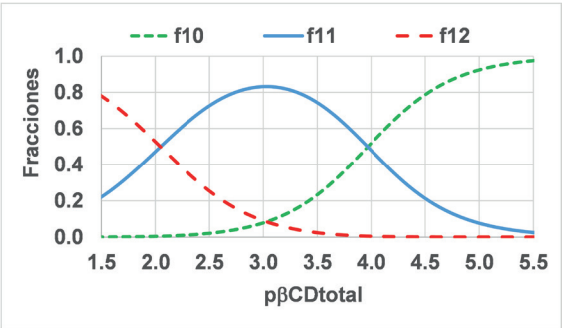

(a)

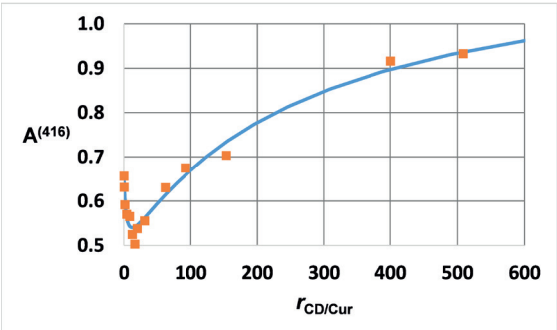

(b)

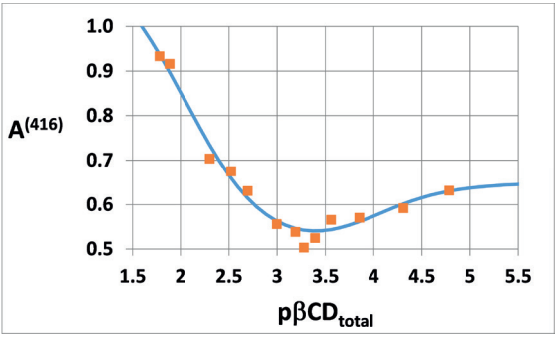

(c)

En la Figura 1 se muestra una imagen de la hoja de cálculo de Excel (Microsoft®), construida con el modelo de la subsección 2.1 para la formación de los complejos de inclusión de estequiometrías $1H_3Cur{:}1\beta CD$ y $1H_3Cur{:}2\beta CD$.

En la Figura 2 se muestran las gráficas más relevantes del método de relaciones molares estudiado en este sistema, para obtener sus constantes de equilibrio.

La Figura 2a muestra que ambos complejos de inclusión son relevantes en el sistema. El anfolito, $H_3Cur(\beta CD)$, predomina en el intervalo de concentraciones totales de β-ciclodextrina que va de 0.0001 M a 0.0100 M., en tanto que el bidonador del sistema, $H_3Cur(\beta CD)_2$, predomina a concentraciones totales de β-ciclodextrina mayores a 0.01 M. Esto muestra la consistencia del modelo.

La Figura 2b es la representación típica de una curva de relaciones molares. Pero, como se observa en la Tabla 1, las tres especies de la curcumina, (el fármaco) contribuyen a la absorbancia del sistema. Las constantes de equilibrio obtenidas muestran que las reacciones no son cuantitativas en las cantidades estequiométricas. De hecho, el mínimo de absorbancia se observa a una relación molar de 16, muy lejos de los valores de 1 ó 2 esperados para reacciones cuantitativas. Sin embargo, el modelo muestra un buen ajuste, representado por la línea continua.

La curva que se muestra en la Figura 2c, inspirada por las curvas que se utilizan en la química ácido-base de Brønsted para determinar constantes de equilibrio (Rodríguez-Barrientos, 2009), permiten ver secciones sigmoidales, relacionadas con la formación de complejos de inclusión en el sistema. En este caso particular se ven dos secciones, cuya parte media está cerca de $p\beta CD_{total} \approx 4$ y $p\beta CD_{total} \approx 2$, que se encuentran cerca de los valores de los logaritmos de las constantes de formación sucesiva, en concordancia con la Tabla 1 (porque en este caso $p\beta CD_{total} \approx p\beta CD$, por la baja concentración de la curcumina en el sistema).

3.2. SISTEMA CURCUMINA/2-HIDROXIPROPIL-β-CICLODEXTRINA A PH = 12.0 EN SOLUCIÓN ACUOSA

En otro estudio espectrofotométrico de soluciones de curcumina totalmente desprotonada (Cur^{3-}) con 2-hidroxipropil-β-ciclodextrina (HPBCD), en donde la concentración de curcumina total $[Cur]_{total}$ es igual a 3.02×10^{-5} M y la concentración total de la β-ciclodextrina total varía en el intervalo $0.00063\ M \leq [HPBCD]_{total} \leq 0.10000\ M$, se obtuvieron los valores de constantes de equilibrio de formación global y los factores de respuesta de las especies que se muestran en la Tabla 2.

Tabla 2. Parámetros obtenidos por medio de la regresión no lineal de los espectros de absorción de diferentes sistemas de curcumina con 2-hidroxipropil-β-ciclodextrina a pH = 12.0, utilizando el programa SQUAD (Leggett, 1985; Luna-Ortega, 2017).

Equilibrio de formación de la especie $(Cur^{3-})(HPBCD)_i$	$\log\beta_i$	Factor de respuesta de la especie $(Cur^{3-})(HPBCD)_i$ $(L{\cdot}mol^{-1}{\cdot}cm^{-1})$*
$Cur^{3-} \rightleftarrows Cur^{3-}$	$\log\beta_{10} \equiv 0$	$k_{Cur^{3-}} = 70000$
$Cur^{3-} + HPBCD \rightleftarrows (Cur^{3-})(HPBCD)$	$\log\beta_{11} = 1.10$	$K_{(Cur^{3-})(HPBCD)} = 49000$
$Cur^{3-} + 2HPBCD \rightleftarrows (Cur^{3-})(HPBCD)_2$	$\log\beta_{12} = 2.20$	$k_{(Cur^{3-})(HPBCD)_2} = 28000$

* la longitud de onda para esos factores de respuesta es de 471 nm, la longitud de paso óptico es de 1 cm y se considera que la HPBCD no absorbe luz de esa longitud de onda.

Figura 3. Gráficas obtenidas con el modelo que se muestra en la Tabla 2, construido con la hoja de cálculo que se muestra en la Figura 1, para una $[Cur]_{total} = 3.02\times10^{-5}$ M. a) Diagrama de distribución de las especies de curcumina con 2-hidroxipropil-β-ciclodextrina. b) Curva típica del método de relaciones molares. Los marcadores anaranjados son resultados experimentales. c) Curva de secciones sigmoidales que haría pensar en la formación de un complejo de inclusión.

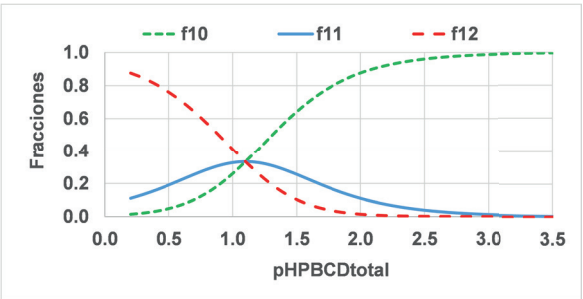

(a)

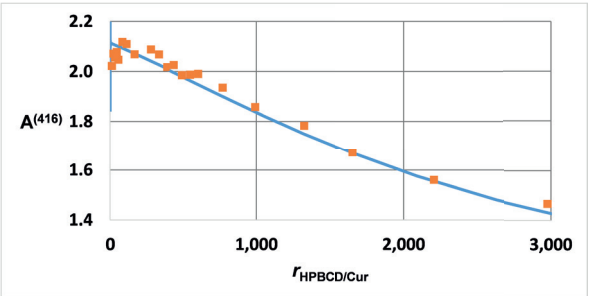

(b)

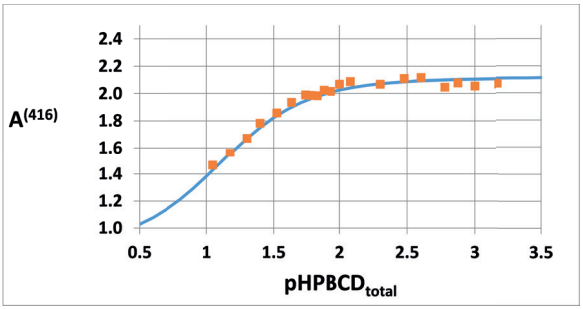

(c)

Con la hoja de cálculo que se muestra en la Figura 1 se obtuvo el modelo para ajustar las curvas experimentales, que se muestran en la Figura 3.

La Figura 3a muestra que, en este caso, el anfolito $(Cur^{3-})(HPBCD)$ no predomina en el sistema, en el intervalo de concentraciones totales de 2-hidroxipropil-β-ciclodextrina (que va de 0.00063 M a 0.10000 M), aunque tampoco se puede decir que no existe. El bidonador del sistema, $(Cur^{3-})(HPBCD)_2$ predomina a concentraciones totales de 2-hidroxipropil-β-ciclodextrina mayores a 0.063 M.

La Figura 3b es la representación típica de una curva de relaciones molares. Pero, como se observa en la Tabla 2, las tres especies de la curcumina, (el fármaco) contribuyen a la absorbancia del sistema. Las constantes de equilibrio obtenidas muestran que las reacciones no son cuantitativas en las cantidades estequiométricas. Sin embargo, el modelo muestra un buen ajuste, representado por la línea continua.

La curva que se muestra en la Figura 3c, permite ver sólo una sección sigmoidal, relacionada con la formación de complejos de inclusión en el sistema. En este caso particular su parte media está cerca de $pHPBCD_{total} \approx 1.5$, que se encuentra cerca del promedio de los valores de los logaritmos de las constantes de formación sucesivas que se deducen de la Tabla 2 (por la baja concentración de la curcumina en el sistema).

Si se comparan los resultados mostrados en las Tablas 1 y 2 y en las Figuras 2 y 3, se puede ver que el pH y la naturaleza de la ciclodextrina afecta a la estabilidad de los complejos de inclusión.

En la Figura 4a se muestra una representación esquemática de una posible estructura para el complejo $1H_3Cur : 1\beta CD$, que parece mucho más estable que el complejo $1Cur^{3-} : 1HPBCD$ (que no puede predominar); en tanto que en la Figura 4b se muestra una representación esquemática de una posible estructura del complejo $1Cur^{3-}: 2HPBCD$, cuya estabilidad parece indicar que el complejo de estequiometría $1Cur^{3-}:1HPBCD$ dismuta mucho (de manera que no pueda predominar), posiblemente para estabilizar la estructura por las cargas eléctricas negativas de los fenóxidos.

Figura 4. Esquemas de las posibles estructuras de complejos de inclusión que se forman entre la curcumina y algunas ciclodextrinas. a) Complejo $1H_3Cur$:1βCD que se forma a pH = 3.6 en solución acuosa. b) Complejo $1Cur^{3-}$:2HPBCD que se forma a pH = 12.0 en solución acuosa. c) Representación esquemática genérica de la estructura de las ciclodextrinas.

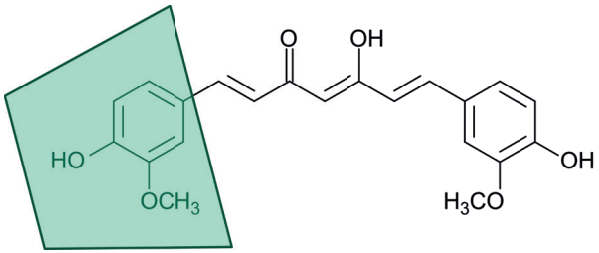

(a)

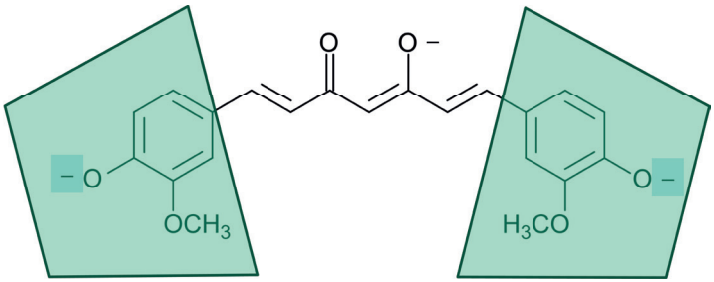

(b)

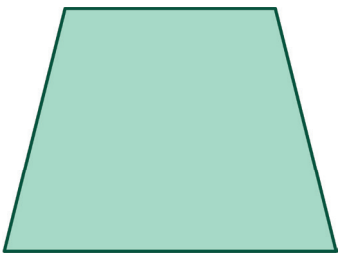

(c)

3.3. SISTEMA DICLOFENACO SÓDICO/2-HIDROXIPROPIL-β-CICLODEXTRINA EN SOLUCIÓN ACUOSA (MUCCI, 1999)

En la Figura 5 se muestra una captura de pantalla con la hoja de cálculo que se construyó con las ecuaciones (4), (5) y (10) a (20), que toma en cuenta la formación de las tres especies: Far(CD), $Far(CD)_2$ y $Far_2(CD)$, en un sistema. Las constantes de equilibrio introducidas en la hoja de cálculo, que se observan en la Figura 5, son las constantes globales ($\log\beta_{ij}$) que se muestran en la Tabla 3, para el sistema de diclofenaco sódico (NaDfc) con 2-hidroxipropil-β-ciclodextrina.

Figura 5. Captura de pantalla que muestra el aspecto de la hoja de cálculo con las ecuaciones (4), (5) y (10) a (20) y los parámetros de la Tabla 3.

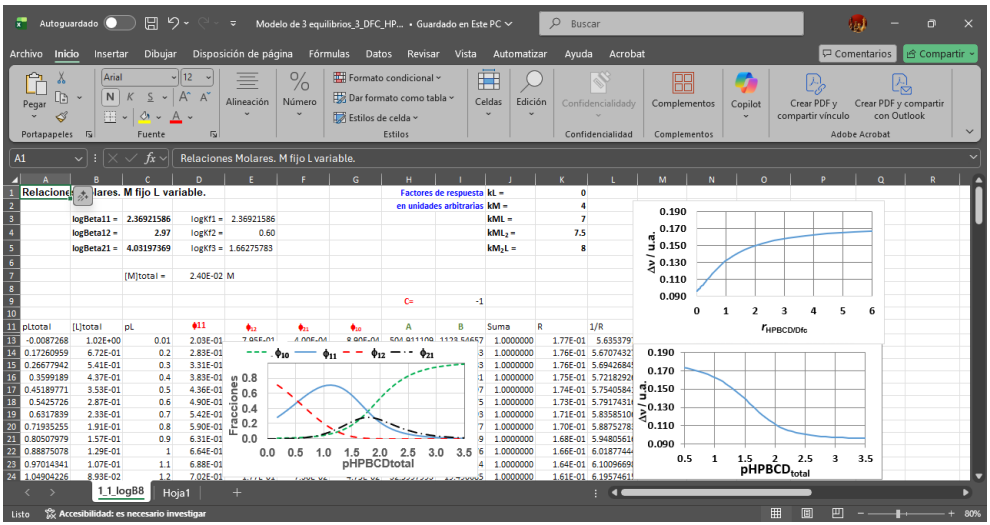

Un cuidadoso y extenso estudio de resonancia magnética nuclear de ^{1}H y ^{13}C, por diferentes métodos, fue publicado en 1999 por Mucci y sus colaboradores. En ese trabajo los autores dan evidencia de la formación de un complejo de estequiometría $Far_2(CD)$, haciendo el ajuste de los desplazamientos químicos de algunas de las señales de diclofenaco y 2-hidroxipropil-β-ciclodextrina. Las constantes que se utilizan en ese trabajo son constantes de formación sucesivas, que se dan por etapas, como se muestra en las ecuaciones (21) a (23).

$$Far + CD \rightleftarrows Far(CD) \quad con \quad K_{11} = \beta_{11} = \frac{[Far(CD)]}{[Far][CD]} \tag{21}$$

$$Far(CD) + CD \rightleftarrows Far(CD)_2 \quad con \quad K_{12} = \frac{\beta_{12}}{K_{11}} = \frac{[Far(CD)_2]}{[Far(CD)]\{CD\}} \tag{22}$$

$$Far(CD) + Far \rightleftarrows Far_2(CD) \quad con \quad K_{21} = \frac{\beta_{21}}{K_{11}} = \frac{[Far(CD)_2]}{[Far(CD)]\{CD\}} \tag{23}$$

Tabla 3. Parámetros tomados del estudio de resonancia magnética nuclear de Mucci (1999) para el sistema de diclofenaco sódico (NaDfc) con 2-hidroxipropil-β-ciclodextrina (HPBCD) en agua deuterada. Las constantes de formación globales fueron calculadas a partir de las ecuaciones (21) a (23).

Equilibrio de formación de la especie $(Dcf^-)_i(HPBCD)_j$	$\log K_{ij}$	$\log\beta_{ij}$
$Dfc^- \rightleftarrows Dfc^-$	$\log K_{10} \equiv 0$	$\log\beta_{10} \equiv 0$
$Dfc^- + HPBCD \rightleftarrows (Dfc^-)(HPBCD)$	$\log K_{11} = 2.37$	$\log\beta_{11} = 2.37$
$(Dfc^-)(HPBCD) + HPBCD \rightleftarrows (Dfc^-)(HPBCD)_2$	$\log K_{12} = 0.60$	–––
$(Dfc^-)(HPBCD) + Dfc^- \rightleftarrows (Dfc^-)_2(HPBCD)$	$\log K_{21} = 1.66$	–––
$Dfc^- + 2HPBCD \rightleftarrows (Dfc^-)(HPBCD)_2$	–––	$\log\beta_{12} = 2.97$
$2Dfc^- + HPBCD \rightleftarrows (Dfc^-)_2(HPBCD)$	–––	$\log\beta_{21} = 4.03$

Haciendo uso de las constantes globales de la Tabla 3, se obtienen las representaciones gráficas de la Figura 6.

En la Figura 6a se muestra el diagrama de distribución de las especies de diclofenaco aniónico (Dfc^-) con 2-hidroxipropil-β-ciclodextrina. Se observa que la especie $(Dfc^-)_2(HPBCD)$ no predomina, pero hay suficiente cantidad de ella para contribuir significativamente a los desplazamientos químicos de algunos átomos de hidrógeno y carbono en las moléculas.

Figura 6. Gráficas obtenidas con el modelo que se muestra en la Tabla 3, con la hoja de cálculo que se muestra en la Figura 5, para una concentración de diclofenaco total igual a 0.024 M. a) Diagrama de distribución de las especies de diclofenaco con 2-hidroxipropil-β-ciclodextrina. b) Curva típica del método de relaciones molares. Los marcadores anaranjados son resultados experimentales. c) Curva de secciones sigmoidales que haría pensar en la formación de un complejo de inclusión.

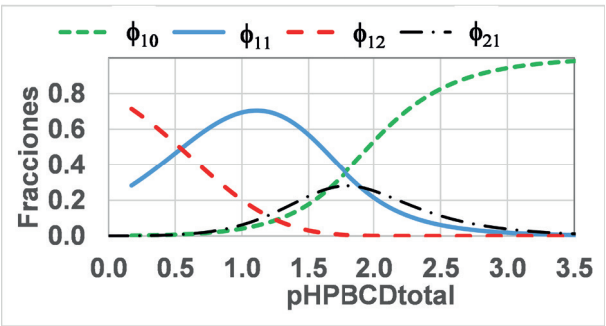

(a)

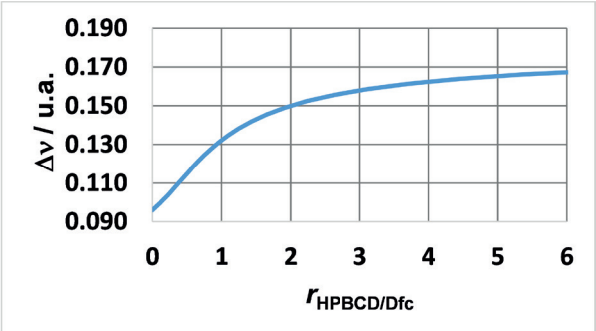

(b)

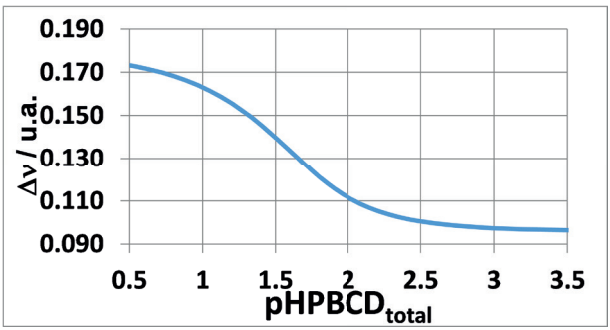

(c)

En la Figura 6b, la representación típica del método de relaciones molares hace pensar que es posible la formación de especies con las estequiometrías: $1Dfc^-$: 1HPBCD, $2Dfc^-$: 1HPBCD y $1Dfc^-$: 2HPBCD. Sin embargo, como las reacciones no son muy cuantitativas la función no está formada por líneas rectas.

Aunque no se han ajustado valores experimentales en el presente trabajo, la tendencia observada (en unidades arbitrarias) es la misma que se observa experimentalmente para algunos desplazamientos químicos de ^1H y ^{13}C (Mucci, 1999).

La representación gráfica en la Figura 6c no está dada ni discutida en el trabajo de Mucci (1999). Esta gráfica podría llevar a pensar en la formación de un solo complejo de inclusión de estequiometría 1:1, pero su punto de inflexión no está tan cerca del valor de $\log\beta_{11}$, por lo que debe haber más especies, aunque no lleguen a predominar en el sistema en estudio.

En la Figura 7 se muestra una representación gráfica que da una idea de una posible estructura del complejo $(Dfc^-)_2$(HPBCD), interpretando la discusión de Mucci y colaboradores en su trabajo de 1999.

4. CONCLUSIONES

En este trabajo se han presentado las ecuaciones de modelos matemáticos para poder ajustar curvas de relaciones molares de sistemas en donde se forman hasta tres complejos de inclusión, del tipo: Far(CD), $Far(CD)_2$ y $Far_2(CD)$.

Figura 7. Esquema de la posible estructura del complejo de inclusión que se forma entre el diclofenaco y la 2-hidroxipropil-β-ciclodextrina: $(Dfc^-)_2$(HPBCD).

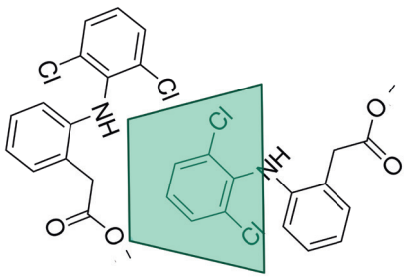

A diferencia de otros trabajos, la construcción de los diagramas de distribución de las especies permite hacer una interpretación de los resultados experimentales con mayor claridad.

Los ajustes que se pueden hacer, a partir de resultados experimentales, permiten determinar las constantes de equilibrio de formación global de las diferentes especies, así como proponer algunas estructuras posibles de las mismas.

REFERENCIAS BIBLIOGRÁFICAS

Escandar. G. M. Analyst. 124, 587-591 (1999).

Luna-Ortega, L. A., Rojas-Hernández, A., Ramírez-Silva, M. T., Álvarez-Romero, G. A., Palomar-Pardavé, M. E. Teoría y Aplicaciones de la Química Analítica en México. Memorias del XXX Congreso Nacional de Química Analítica. AMQA. León. 2017. pp. 490-495.

Legget, D. J., Computational Methods for the Determination of Formation Constants. Capítulo 6. Plenum Press. Nueva York, 1985. pp. 159-220.

Martínez-Guerra, J., Palomar-Pardavé, M. E., Romero-Romo, M., Corona-Avendaño, S., Guzmán-Hernández, D. S., Rojas-Hernández, A., Ramírez-Silva, M. T. ChemElectroChem, 202101534, 1-11 (2021).

Mucci, A.; Schenetti, L.; Vandelli, M. A.; Ruozib, B.; Fornib, F. J. Research Chem. (M). 1999, 1761-1795 (1999).

Rodríguez-Barrientos, D., Rojas-Hernández, A., Gutiérrez, A., Moya-Hernández, R., Gómez-Balderas, R., Ramírez-Silva, M. T. Talanta, 80, 754-762 (2009).

Rojas-Hernández, A., Ramírez, M. T., González, I., Ibanez, J. G. Journal of Chemical Education, 72, 1099-1105 (1995).

Rojas-Hernández, A.; Rodríguez-Laguna, N.; Ramírez-Silva, M. T.; Moya-Hernández, R. Distribution Diagrams and Graphical Methods to Determine or to Use the Stoichiometric Coefficients of Acid-Base and Complexation Reactions. En Innocenti, A. Ed. Stoichiometry in Research: The Importance of Quantity in Biomedicine. In Tech. Cap. 13. 287-310. (2013). ISBN 978-953-51-0198-7. DOI: 10.5772/1875.

CAPÍTULO 3

MODELAGEM MATEMÁTICA E SIMULAÇÃO APLICADAS À DINÂMICA DE FILAS EM SERVIÇOS

Data de submissão: 24/11/2025
Data de aceite: 06/12/2025

Alireza Mohebi Ashtiani
Universidade Tecnológica Federal do Paraná - UTFPR
Londrina - PR
http://lattes.cnpq.br/5025709771742662

Tatielen Demarchi
Universidade Tecnológica Federal do Paraná - UTFPR
Cornélio Procópio - PR
http://lattes.cnpq.br/6161889316551237

Pedro Henrique Rodrigues Petrelli
Universidade Tecnológica Federal do Paraná - UTFPR
Londrina - PR
http://lattes.cnpq.br/7015038369020637

Rebeca Mitiko Ito Faria
Universidade Tecnológica Federal do Paraná - UTFPR
Londrina - PR
http://lattes.cnpq.br/4389932788998212

RESUMO: Atualmente, em diferentes setores e sistemas contemporâneos, a busca por maior eficiência e produtividade tornou-se não apenas relevante, mas indispensável. Entre as diversas metodologias disponíveis, a modelagem e a simulação surgem como ferramentas fundamentais, capazes de oferecer uma análise mais profunda e precisa desses sistemas. Nos setores de serviço, a formação de filas é muitas vezes inevitável, e a busca por qualidade e eficiência pode envolver desde o treinamento adequado das equipes até a adoção de práticas de manutenção preventiva e a reorganização de processos internos. Nesse cenário, o presente estudo tem como objetivo analisar com maior clareza sistemas que envolvem filas, de modo a ampliar a compreensão e a gestão desse tipo de dinâmica operacional.
PALAVRAS-CHAVE: sistemas; modelagem; simulação; filas.

MATHEMATICAL MODELING AND SIMULATION APPLIED TO THE DYNAMICS OF QUEUES IN SERVICE SYSTEMS

ABSTRACT: Currently, across a wide range of contemporary sectors and systems, the pursuit of greater efficiency and productivity has become not only relevant but essential. Among the various methodologies available, modeling and simulation emerge as fundamental tools that provide deeper and more accurate analyses of such systems. In service-oriented environments, the formation of queues is often unavoidable, and efforts to enhance quality and efficiency may involve actions ranging from proper staff training to the adoption of

preventive maintenance practices and the reorganization of internal processes. In this context, the present study aims to provide a more detailed analysis of systems involving queues, thereby contributing to a broader understanding and more effective management of this type of operational dynamic.
KEYWORDS: systems; modeling; simulation; queues.

1. INTRODUÇÃO

Atualmente, em diferentes setores econômicos, como o industrial, o de serviços, o financeiro, o logístico e o portuário, a busca por eficiência e produtividade tornou-se ainda mais urgente. Esse crescimento depende de fatores internos e externos específicos de cada setor, sendo que alguns processos são naturalmente mais complexos que outros. Um exemplo é o setor logístico, frequentemente visto como mais desafiador do que o de serviços ou o financeiro.

No setor de serviços, muitas vezes, ações simples, como o treinamento adequado dos funcionários ou uma reorganização interna dos fluxos de trabalho, já são capazes de elevar a qualidade do atendimento. Ainda assim, em praticamente todos os setores, a permanência em filas é quase inevitável, podendo gerar insatisfação, desgastes e impactos diretos na produtividade.

Pesquisas como as da Mintel (2015) ajudam a ilustrar esse cenário. Segundo os dados apresentados, 33% dos brasileiros evitam locais onde geralmente há filas, 22% procuram serviços que economizem tempo e cerca de 31% afirmam desejar mais tempo com a família, percentual que sobe para 47% entre jovens de 25 a 34 anos. Além disso, 17% utilizam aplicativos para acompanhar tempos de espera e outros 35% demonstram interesse em fazê-lo. Esses números deixam claro que o problema vai muito além da conveniência: o tempo de espera tem uma relação direta com a qualidade de vida, bem-estar e organização da rotina.

Diante desse contexto, empresas de diversos segmentos têm buscado soluções para reduzir a insatisfação causada por longos tempos de espera. Filas excessivas podem fazer clientes desistirem do atendimento, o que significa perda de receita e, muitas vezes, desgaste da imagem da empresa. No setor industrial, atrasos na produção não apenas prejudicam o desempenho, mas podem ocasionar custos elevados e comprometer prazos. Por outro lado, sistemas com ociosidade constante também representam desperdício de recursos. Assim, entender o funcionamento das filas e suas causas é fundamental para encontrar o equilíbrio entre demanda e capacidade de atendimento.

A Teoria das Filas, baseada em conceitos de matemática e estatística, surge justamente para apoiar esse tipo de análise (GROSS & HARRIS, 1985). Em grande parte

dos sistemas, o processo de chegada costuma seguir uma distribuição de Poisson, enquanto o tempo de atendimento tende a se ajustar à distribuição exponencial. Esses modelos permitem prever o comportamento das filas, estimar tempos médios de espera e identificar pontos de melhoria, como ajustes na velocidade de atendimento, reorganização de processos e até melhorias nas condições de trabalho das equipes.

A simulação, quando integrada à Teoria das Filas, amplia ainda mais as possibilidades de análise. Em Ribeiro et al. (2017), por exemplo, os autores demonstram como o uso dessa abordagem contribuiu para reduzir o tempo de espera no setor de embalagem de uma fábrica de móveis em Passos/MG. Já Faria et al. (2024) mostram que combinar simulação com Teoria das Filas pode ser muito eficaz para compreender o comportamento das filas em um restaurante universitário, permitindo propor soluções alinhadas com os dados reais.

Neste trabalho, examinamos dois cenários distintos: (i) o comportamento das filas nos caixas rápidos de um hipermercado, utilizando o modelo M/M/c para investigar a distribuição do atendimento entre quatro servidores; e (ii) os impactos do crescimento da frota de veículos na mobilidade urbana de Londrina, com foco especial em um cruzamento semaforizado de alto fluxo. Em ambos os casos, aplicamos a Teoria das Filas e ferramentas de simulação para entender melhor como os sistemas se comportam, identificar gargalos e refletir sobre ajustes possíveis, seja no ambiente de atendimento ao consumidor, seja na dinâmica do trânsito urbano.

2. TEORIA DAS FILAS: DEFINIÇÕES E ELEMENTOS BÁSICOS

Segundo PRADO (2004), a Teoria das Filas é utilizada para a modelagem de sistemas e constitui um método analítico que aborda o problema por meio de fórmulas matemáticas. Na prática, a Teoria das Filas, quando combinada à Teoria da Simulação, transforma-se em uma ferramenta poderosa, capaz de representar, com fidelidade, um sistema real caracterizado pela presença de filas. Essa abordagem torna possível simular o funcionamento do sistema e, a partir disso, determinar a quantidade ideal de atendentes ou operários em cada setor.

Em muitas situações reais, parte da população solicita determinados serviços, formando filas compostas por aqueles que aguardam atendimento até que este seja realizado. Em essência, filas surgem sempre que a demanda supera a capacidade de atendimento do sistema, ou seja, quando a taxa de chegada é maior que a taxa de atendimento disponível. O termo *cliente* não se restringe a pessoas: pode se referir também a peças em linhas de produção, navios aguardando atracação em portos ou até documentos que circulam em setores administrativos.

O atendimento em sistemas que envolvem filas pode ocorrer por meio de um ou mais canais. As filas mais simples apresentam uma única fila atendida por um único canal; já as mais complexas podem envolver várias filas distribuídas entre múltiplos atendentes. A maioria dos sistemas do cotidiano, incluindo o analisado neste estudo, opera com uma única fila que alimenta diferentes canais de atendimento. Na Figura 1, observamos os elementos básicos de um sistema desse tipo. Nota-se também que parte dos clientes pode abandonar a fila devido à lentidão do atendimento ou à ocorrência de gargalos no sistema.

Figura 1: Elementos básicos de um sistema de fila.

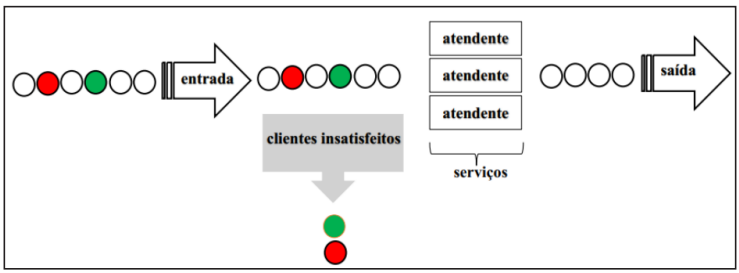

Fonte: Autoria própria.

Com clientes cada vez mais exigentes e com menos tempo disponível, filas longas e demoradas podem levar à desistência e à busca por outros estabelecimentos. No setor industrial, o congestionamento em etapas da produção pode atrasar a entrega do produto final, gerar prejuízos e comprometer a satisfação dos clientes.

As filas apresentam características específicas que permitem sua análise sistemática, conforme descrito por PRADO (2004) e ANDRADE (2009). Entre essas características, destacam-se:

- **Processo de chegada**: definido pela taxa média de chegada, que corresponde à razão entre a quantidade de clientes que chegam em determinado período e o intervalo médio entre chegadas;
- **Processo de atendimento**: relacionado ao ritmo médio e à duração média do serviço;
- **Número de servidores**: sistemas simples possuem um único servidor, mas, à medida que a taxa de chegada aumenta, o número de atendentes pode ser ampliado;
- **Disciplina da fila**: refere-se à ordem de atendimento, podendo ser FIFO (first in, first out – o primeiro que chega é o primeiro a ser atendido) ou LIFO (last in, first out – o último a chegar é o primeiro a ser atendido);

- **Tamanho da fila**: o número de clientes é considerado suficientemente grande para que a população seja tratada como infinita.
- **Tempo médio de espera na fila**: o tempo médio que um cliente permanece no sistema até ser atendido.

De acordo com PRADO (2004), algumas variáveis-chave permitem caracterizar e analisar uma fila. Entre elas, destacam-se: o ritmo médio de chegada (λ) e o ritmo médio de atendimento (μ); a capacidade de atendimento, representada pelo número de atendentes (C); o intervalo entre chegadas, calculado como IC = 1/λ; e o tempo de atendimento ou serviço, definido como TA = 1/μ. A intensidade de tráfego do sistema é dada por I = |λ/μ| = |TA/IC|. Além disso, é possível determinar o número médio de clientes na fila (NF = $\lambda^2/[\mu^*(\lambda-\mu)]$), o tempo médio de espera na fila (TF = $\lambda/[\mu^*(\lambda - \mu)]$), o número médio de clientes sendo atendidos (NA = λ/μ), o tempo médio de atendimento (TA = 1/μ), o tempo médio de permanência na fila (TF = NF/λ) e o número médio de clientes no sistema (NS = NF + NA). Estas variáveis permitem uma análise detalhada do desempenho das filas e auxiliam na tomada de decisões sobre dimensionamento de atendimento e melhoria do serviço.

Estas variáveis referem-se ao sistema como um todo, ao processo de chegada, à fila e ao processo de atendimento. Por exemplo, as variáveis TF e NS estão relacionadas ao sistema, enquanto TA, C e μ correspondem ao processo de atendimento de um determinado sistema.

Quando o sistema possui apenas uma única fila e um único atendente, a taxa de utilização do atendente (número médio de clientes sendo atendidos) é dada por ρ = λ/μ. Para um sistema com uma única fila, mas vários canais de atendimento, a taxa de utilização dos atendentes é calculada como ρ = λ / (cμ), onde C representa o número de atendentes. Essa variável é considerada como o **grau de congestionamento** ou **taxa de intensidade de tráfego do sistema**.

Um sistema é estável quando não há formação contínua de filas, ou seja, quando os atendentes conseguem atender à demanda. Isso ocorre apenas quando o ritmo médio de chegada é menor que o ritmo médio de atendimento, isto é, λ < μ, pois neste caso ρ < 1. Nos sistemas estáveis, o fluxo que entra é sempre igual ao fluxo que sai do sistema. Quando ρ = 1, ocorre que λ = μ, significando que os atendentes estão ocupados 100% do tempo atendendo os clientes. A situação mais crítica ocorre quando ρ > 1, ou seja, quando o ritmo médio de chegada supera o ritmo médio de atendimento. Nessa condição, a fila tende a crescer indefinidamente, caracterizando um sistema **supersaturado**, no qual os atendentes não têm tempo de descanso.

Quanto ao processo de chegada, na maioria dos sistemas sua distribuição ajusta-se bem ao modelo de Poisson. Quando isso ocorre, os intervalos entre chegadas seguem a distribuição exponencial negativa (PRADO, 2004).

3. METODOLOGIA

A metodologia adotada neste estudo foi estruturada em duas etapas complementares, cada uma relacionada a um dos sistemas de filas investigados: (i) o sistema de atendimento em caixas-rápidos de um hipermercado localizado na região central de Londrina (PR) e (ii) o sistema de tráfego urbano em um cruzamento crítico da cidade paranaense, composto por uma interseção semaforizada. Embora tratem de contextos distintos, ambos os estudos compartilham a mesma lógica metodológica, baseada na coleta de dados reais, na modelagem matemática fundamentada na Teoria das Filas e na aplicação de ferramentas computacionais para análise e simulação dos comportamentos observados , buscando sempre aproximar o modelo teórico da realidade prática.

3.1. ESTUDO 1: FILAS EM CAIXAS-RÁPIDOS DE UM HIPERMERCADO

O primeiro estudo tem como objetivo avaliar o comportamento das filas nos caixas rápidos de um grande hipermercado situado no centro de Londrina (PR). Devido à localização estratégica, o estabelecimento apresenta um fluxo especialmente elevado nos horários de pico, principalmente entre 19h00min e 20h30min, quando muitos trabalhadores retornam para casa e aproveitam para realizar pequenas compras. Por esse motivo, as coletas foram realizadas no mês de novembro de 2024, em dias distintos e sempre dentro desse intervalo de maior movimento, a fim de capturar com precisão a dinâmica real do sistema.

Para mensurar os tempos relacionados às etapas do processo – entrada na fila, início do atendimento e término do atendimento – foram utilizados cronômetros digitais acionados por meio de um aplicativo capaz de registrar múltiplos marcadores simultaneamente. Em cada versão de coleta, três tempos foram registrados: (a) o momento em que o cliente entra na fila, (b) o instante em que deixa a fila e inicia o atendimento e (c) o momento em que conclui o atendimento e deixa o caixa. Esses registros permitiram calcular o tempo de espera, o tempo de serviço e o intervalo entre chegadas, fornecendo estimativas empíricas das taxas λ (chegadas) e μ (atendimento).

Como o sistema operava com uma única fila direcionada a quatro atendentes, sua modelagem matemática-estocástica foi conduzida sob o arcabouço do modelo **M/M/c**,

adequado para representar sistemas com múltiplos servidores e chegadas aleatórias. Esse modelo permite avaliar a distribuição do atendimento entre os servidores, a taxa de utilização de cada caixa, o tempo médio de espera e o número médio de clientes no sistema. Os dados coletados constituíram a base para validar empiricamente as hipóteses da Teoria das Filas e, além disso, subsidiar simulações posteriores para verificar o impacto de diferentes configurações de atendimento — como a variação do número de atendentes, ajustes na velocidade média de atendimento ou reorganização operacional.

3.2. ESTUDO 2: FILAS VEICULARES EM UM CRUZAMENTO URBANO SEMAFORIZADO

O rápido crescimento da frota de veículos nas cidades brasileiras tem tornado o trânsito cada vez mais lento e desgastante. Nesse contexto, a cidade de Londrina, localizada na região norte do Paraná, apresenta um cenário típico de grande centro urbano, com alta circulação de veículos e intensa dinâmica de serviços. Fundada em 10 de dezembro de 1934, é atualmente a segunda maior cidade do estado e a quarta maior do Sul do Brasil, contando com aproximadamente 600 mil habitantes e mais de 400 mil veículos.

Segundo dados recentes da Prefeitura de Londrina (2024), o município possui mais de 50 mil estabelecimentos distribuídos entre comércio, prestação de serviços, instituições financeiras e uma ampla rede de saúde — incluindo hospitais e dezenas de Unidades Básicas de Saúde (UBS). Essa diversidade de atividades reforça a complexidade dos fluxos de deslocamento, tornando ainda mais relevante a análise de sistemas de filas em ambientes como o transporte urbano.

Um dos pontos mais críticos da cidade, analisado neste estudo, é o cruzamento entre a Avenida Juscelino Kubitschek (JK) e a Rua Pernambuco, uma interseção muito utilizada pela população e controlada por **dois semáforos sincronizados**. O objetivo deste estudo é, por meio da Teoria das Filas, avaliar o comportamento do cruzamento como um sistema de fila, verificar se está corretamente dimensionado e propor melhorias com base em evidências empíricas.

Como o fluxo varia conforme o período do dia, as coletas foram realizadas no mês de **julho de 2024,** contemplando períodos matutino, vespertino e noturno, garantindo assim uma visão mais completa do comportamento viário. Nesses levantamentos, foram registrados o tempo dos ciclos semafóricos, o tamanho das filas formadas e o tipo de veículos que compunham o fluxo. Esses dados possibilitaram construir um modelo fiel ao que realmente ocorre no cruzamento.

A coleta exigiu um procedimento diferenciado: para identificar quantos veículos atravessavam os semáforos tanto da Av. JK, quanto da Rua Pernambuco, em um intervalo

de 10 minutos, optou-se por realizar uma gravação completa no horário de pico (por volta das 18h00). Posteriormente, os vídeos foram analisados para contabilizar com precisão a quantidade de veículos que passaram por cada via. A partir dessas observações, foram calculadas médias de veículos por minuto e por hora, necessárias para alimentar os modelos matemáticos e computacionais.

A literatura indica que ajustes inteligentes nos ciclos semafóricos, aliados ao uso de ferramentas de simulação, podem melhorar significativamente a fluidez do tráfego (MUNIZ et al., 2019). Por isso, este estudo adotou o software **PTV Vissim** como ferramenta central para modelar e testar diferentes alternativas para o cruzamento. A modelagem considerou dados reais coletados em campo, incluindo tempos de verde, amarelo e vermelho dos semáforos; a quantidade de veículos parados em cada fechamento; e a composição do fluxo por tipo de veículo.

Com o modelo finalizado, indicadores como **Delay** (atraso adicional médio por veículo) e **Number of Stops** (quantidade de paradas ao longo do trajeto) foram avaliados para identificar gargalos e propor melhorias. Além dos benefícios técnicos, o estudo traz impactos sociais diretos, contribuindo para deslocamentos mais rápidos, menos estressantes e mais seguros, especialmente para estudantes e trabalhadores que utilizam essa via diariamente.

4. RESULTADOS E ANÁLISE

Nesta seção, apresentamos e discutimos os resultados obtidos nos dois estudos realizados. Apesar de lidarem com cenários muito distintos, um dentro de um hipermercado movimentado e outro em um cruzamento urbano semaforizado, ambos compartilham uma questão central: a necessidade de compreender como as filas se formam, por que se tornam mais longas em determinados momentos e quais estratégias podem tornar esses sistemas mais eficientes. Para manter a análise mais clara e organizada, esta seção foi dividida em duas partes.

4.1. FILAS EM CAIXAS-RÁPIDOS DE UM HIPERMERCADO

Com o uso do aplicativo *Multi Timer Cronômetro*, que permite acionar vários cronômetros simultaneamente, foi possível registrar com precisão dois momentos essenciais: o instante em que cada pessoa entrava na fila e o momento em que concluía o atendimento e deixava o caixa. Esses registros permitiram compreender, com clareza, tanto o tempo de espera quanto a duração efetiva do atendimento.

Durante o período de coleta, os caixas rápidos operavam com quatro atendentes. A análise dos registros revelou que 165 clientes entraram na fila. Desses, 8 desistiram, alguns por demora, outros por saírem da fila para buscar mais produtos. Assim, 157 clientes foram efetivamente atendidos, como apresentado na Tabela 1.

Tabela 1 – Dados para os cálculo das variáveis do hipermercado.

Clientes que entram na fila	Clientes que saem do caixa	Tempo	Atendentes
165	8	90 min	4

Fonte: Autoria própria.

A partir da Tabela 1, obtém-se $\lambda = 1{,}83$ clientes por minuto. Isso significa que, em média, mais de um cliente entra na fila por minuto, revelando um fluxo constante e intenso. Como discutido anteriormente, a taxa de chegada pode ser modelada por uma distribuição de Poisson, o que possibilitou gerar um gráfico dessa distribuição e compará-la aos dados coletados. Essa simulação foi realizada com o software estatístico **RStudio**. Com base nos registros, as demais variáveis aleatórias foram estimadas como IC = 32,72 e $\mu = 1{,}74$.

Assim, $\rho = 1{,}05$, indicando que o sistema opera acima de sua capacidade. Nesse cenário, o hipermercado sempre apresentará filas e os atendentes não terão intervalos para descanso. Segundo Prado (2004), quando $\rho > 1$, "estranhos fatos ocorrerão", o que reforça o desequilíbrio do sistema.

A partir desses dados, observou-se que o tempo médio de permanência dos clientes na fila (TF) é de aproximadamente 11 minutos e 53 segundos, calculado pela Lei de Little. Esses valores deixam evidente que o tempo de espera e o tamanho da fila ultrapassam a capacidade de atendimento do sistema. Em outras palavras, o fluxo de chegada é maior que o ritmo de atendimento, fazendo com que a fila cresça continuamente e os atendentes permaneçam em estado de sobrecarga.

4.2. RESULTADOS DO ESTUDO 2: CRUZAMENTO SEMAFÓRICO

Com o objetivo de reunir as informações necessárias para avaliar como mudanças nos tempos dos semáforos poderiam otimizar o fluxo de veículos no cruzamento, tanto pela Teoria das Filas quanto por meio da simulação no software, foi realizada uma coleta de dados no cruzamento entre a Av. JK e Rua Pernambuco. Essa etapa consistiu em gravar o fluxo de veículos que atravessava o semáforo da Av. JK em direção à Av. Santos Dumont e, ao mesmo tempo, o movimento no semáforo da Rua Pernambuco no sentido Zerão.

Figura 2 – Cruzamento entre a Av. JK e Rua Pernambuco.

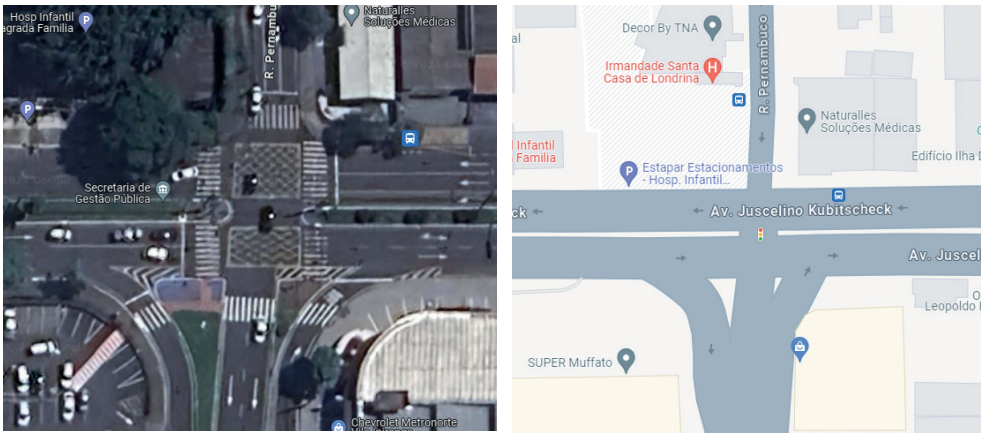

Fonte: Autoria própria.

Após a gravação, o vídeo foi analisado em intervalos de cinco minutos, permitindo calcular o número médio de veículos por minuto e por hora em cada via. Os resultados estão apresentados na Tabela 2.

Tabela 2 – Informações obtidas através da coleta de dados.

Intervalo (minutos)	Rua/Avenida	Veículos	Veículos /min	Veículos /hora
0- 5	Pernambuco	54	10,8	648
5-10	Pernambuco	60	12	720
0-5	JK	86	17,2	1032
5-10	JK	114	22,8	1368

Fonte: Autoria própria.

Esses números mostram uma clara diferença de demanda entre as vias: a Av. JK apresenta fluxo médio de cerca de 1200 veículos por hora, enquanto a Rua Pernambuco registra cerca de 684 veículos por hora. Além disso, registrou-se quantos veículos conseguiam atravessar os semáforos durante o período de abertura (verde). A Tabela 3 apresenta esses dados.

Tabela 3 – Número de veículos que conseguiram ser atendidos.

Atendimento (semáfro verde)	Veículos que foram atendidos na JK	Veículos que foram atendidos na Pernambuco
1	43	20
2	37	17
3	42	25
4	38	28
MÉDIA	40,0	22,5

Fonte: Autoria própria.

A análise do vídeo também permitiu registrar, com precisão, o tempo de duração de cada cor do semáforo nos dois pontos observados, fornecendo assim as informações necessárias sobre os períodos de verde, amarelo e vermelho para cada via.

Tabela 4 – Duração de cada cor nos semáforos da Av. JK e da Rua Pernambuco.

	Duração do semáforo JK (segundos)	**Duração dosemáforo Pernambuco (segundos)**
Verde	45	24
Amarelo	3	3
Vermelho	57	78

Fonte: Autoria própria.

Com todos esses dados em mãos, foi possível alimentar o software PTV Vissim e construir uma simulação fiel ao comportamento real do cruzamento. As mesmas informações também foram aplicadas à Teoria das Filas, permitindo analisar o sistema tanto do ponto de vista matemático quanto por meio da simulação computacional.

Figura 3 – Programação dos semáforos da Rua Pernambuco e da Av. JK.

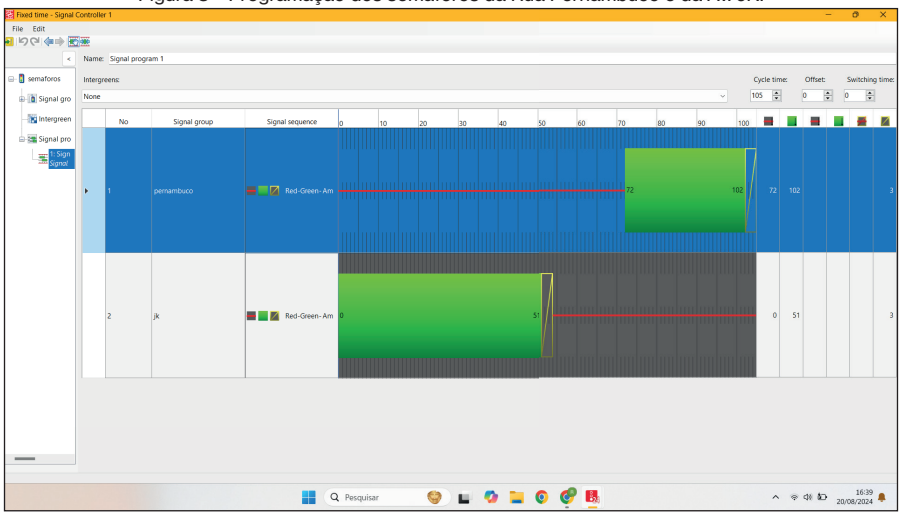

Fonte: autoria própria.

Após a coleta dos dados, iniciou-se a construção do cruzamento estudado no software PTV Vissim. Isto foi feito com base no desenho inicial que o programa fornece da área de estudo e foram acrescentadas ainda as informações obtidas através do vídeo contidas nas tabelas anteriormente apresentadas, como, por exemplo, a programação dos semáforos e a quantidade de veículos que passavam por hora. Na Figura 3, pode ser vista a ferramenta que permite personalizar os tempos de duração de cada cor do semáforo.

Figura 4 – Ferramenta para definir o volume de carros em cada via.

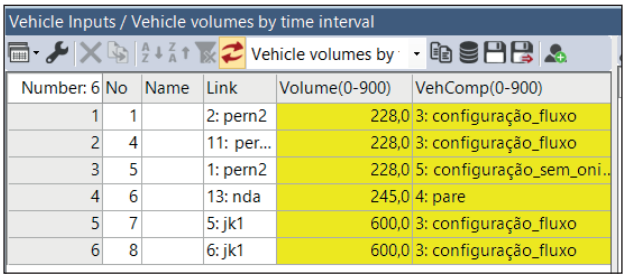

Number: 6	No	Name	Link	Volume(0-900)	VehComp(0-900)
1	1		2: pern2	228,0	3: configuração_fluxo
2	4		11: per...	228,0	3: configuração_fluxo
3	5		1: pern2	228,0	5: configuração_sem_oni...
4	6		13: nda	245,0	4: pare
5	7		5: jk1	600,0	3: configuração_fluxo
6	8		6: jk1	600,0	3: configuração_fluxo

Fonte: autoria própria.

Depois de finalizar a construção do cruzamento com base no cenário real, iniciou-se a etapa de ajustes na programação dos semáforos da Av. JK e da Rua Pernambuco, com o objetivo de identificar configurações que pudessem melhorar o fluxo de veículos. As alterações foram feitas de forma gradual: o tempo de verde e de vermelho foi modificado em incrementos de dois segundos, tanto individualmente, em cada semáforo separadamente, quanto simultaneamente nos dois sentidos.

A cada ajuste realizado, a simulação era executada novamente, permitindo observar com precisão como aquela mudança impactava a formação de filas e o comportamento geral do tráfego. Ao final desse processo, verificou-se que aumentar o tempo de verde em quatro segundos ou mais em ambos os semáforos reduziu significativamente o acúmulo de veículos na Av. JK. No entanto, é importante destacar que nenhuma das alterações testadas trouxe melhorias perceptíveis para o fluxo da Rua Pernambuco, que permaneceu praticamente inalterado mesmo com diferentes combinações de tempos semafóricos.

Posteriormente, foi realizada a análise baseada na Teoria das Filas. A partir dos dados obtidos na gravação, calcularam-se as variáveis necessárias para descrever o comportamento da fila de veículos no cruzamento. No caso específico de uma fila controlada por semáforo, o ritmo médio de atendimento depende diretamente das características do ciclo do sinal. Assim, utilizou-se

$$\mu = [(g - t)/c] \cdot m$$

que considera o tempo total do ciclo (c), o tempo em que o sinal permanece aberto (g) e o tempo médio de atraso na liberação do fluxo (t), isto é, o intervalo entre o instante em que o semáforo fica verde e o momento em que os veículos realmente começam a avançar.

Com todas essas variáveis definidas a partir das observações do vídeo, foi possível calcular o ritmo médio de chegada dos veículos, o ritmo médio de atendimento e, consequentemente, a taxa de utilização do sistema. Esses resultados estão

organizados na Tabela 5 e permitem compreender com mais precisão se o cruzamento opera dentro da sua capacidade ou se há tendência de formação de filas persistentes ao longo do tempo.

Tabela 4 – Valores das principais variáveis para avaliação do cruzamento.

	Ritmo de Chegada (veículo por segundo)	Ritmo de atendimento (veículo por segundo)	Taxa de utilização (ρ)
Av. JK	0,33	0,31	1,06
Pernambuco	0,19	0,15	1,26

Fonte: Autoria própria.

Por fim, após as manipulações matemáticas necessárias, foi possível determinar os tempos ideais de abertura do sinal verde para cada via. O resultado indica que o tempo adequado de verde seria de 46,37 segundos na Av. JK e 28,45 segundos na Rua Pernambuco. Isso significa que, em relação aos tempos originalmente observados, seria necessário um aumento de aproximadamente 1,37 segundos na Av. JK e 4,45 segundos na Rua Pernambuco para que o fluxo de veículos operasse de forma mais eficiente.

5. CONCLUSÕES

Os dois estudos apresentados, o dos caixas-rápidos do hipermercado e o do cruzamento semaforizado, mostram como a Teoria das Filas e a Simulação podem se transformar em ferramentas essenciais para compreender problemas reais do dia a dia e propor soluções simples, eficazes e fundamentadas em dados.

No caso do hipermercado, os resultados deixaram evidente que o sistema opera constantemente acima de sua capacidade. A taxa de utilização dos atendentes é maior que 1, e o tempo médio de espera ultrapassa 11 minutos, caracterizando um sistema supersaturado, em que a fila tende a crescer continuamente. Esse cenário reforça a necessidade de intervenções operacionais, sendo a medida mais eficaz o aumento do número de atendentes nos horários de pico. Tal ajuste reduziria a sobrecarga, evitaria desistências e proporcionaria um atendimento mais fluido e satisfatório aos clientes.

Já no estudo envolvendo o cruzamento entre a Av. JK e a Rua Pernambuco, a combinação entre Teoria das Filas e Simulação computacional também se mostrou extremamente valiosa. As análises indicaram que ampliar o tempo de verde em aproximadamente quatro a seis segundos melhora de forma significativa o fluxo de veículos na Av. JK, resultado consistente entre o modelo matemático e as simulações realizadas no PTV Vissim. Embora a Rua Pernambuco não apresente ganhos expressivos mesmo após os ajustes, a convergência entre as abordagens confirma que a Teoria

das Filas oferece um diagnóstico confiável, sobretudo quando ainda não há acesso a softwares especializados.

A simulação, por sua vez, amplia as possibilidades de análise, permitindo avaliar cenários mais complexos e prever o impacto de mudanças no sistema, especialmente quando se deseja estudar áreas maiores ou múltiplos cruzamentos.

Em conjunto, os dois estudos reforçam a relevância da modelagem matemática e da simulação como ferramentas capazes de diagnosticar problemas, orientar decisões e apoiar intervenções práticas que fazem diferença direta na experiência dos usuários. Os resultados mostram que ajustes relativamente pequenos, seja aumentando o número de atendentes, seja reorganizando o tempo semafórico, podem gerar melhorias substanciais na qualidade do serviço, na fluidez dos processos e no bem-estar das pessoas que dependem desses sistemas.

REFERÊNCIAS

ANDRADE, E. L. Problemas de congestionamento das filas. In: ANDRADE, E. L. **Introdução à Pesquisa Operacional: métodos e modelos para análise de decisões**. 4. ed. Rio de Janeiro: LTC, 2009. cap. 6, p. 104-120.

FARIA, R. M. I.; ASHTIANI, A. M.; PETRELLI, P. H. R. O estudo do tempo de espera de um restaurante universitário através da Teoria das Filas e da Simulação. In: ENCONTRO DE ENGENHARIA DE PRODUÇÃO DA UTFPR – ENENPRO, 2024, Londrina. Anais [...]. Londrina: UTFPR, 2024.

GROSS, D.; HARRIS, C. M. **Fundamentals of Queueing Theory**. 2. ed. New York: John Wiley & Sons, 1985.

MINTEL. Um terço dos brasileiros evita ir a lugares com fila. 2015. Disponível em: https://brasil.mintel.com/imprensa/estilos-de-vida/um-terco-dos-brasileiros-evita-ir-a-lugares-com-filas-revela-mintel. Acesso em: 02 dez. 2025.

MUNIZ, A. B.; CARVALHO, A. C.; SOARES, V. T. Simulação do tráfego urbano e avaliação de cenários de sinalização semafórica. **Revista Brasileira de Engenharia de Tráfego**, v. 10, n. 2, p. 45-58, 2019.

PRADO, D. S. **Teoria das filas e da simulação**. Série Pesquisa Operacional – v. 2. Nova Lima, MG: INDG Tecnologia e Serviços LTDA, 2004.

RIBEIRO, G. H. S.; PEREIRA, R. S.; SANTOS FILHO, V. H.; HOLETZ, M. G.; PONTAROLO, M. L. Aplicação da teoria das filas para redução do tempo de espera no setor de embalagem de uma fábrica de móveis no município de Passos/MG. In: CONGRESSO BRASILEIRO DE ENGENHARIA DE PRODUÇÃO, 2., 2017. Anais [...]. 2017.

CAPÍTULO 4

MATHEMATICAL METHODS IN POPULATION DYNAMICS

Data de submissão: 03/11/2025
Data de aceite: 20/11/2025

Alberto Gutiérrez Borda
Faculty of Sciences, National University of San Luis Gonzaga – Ica, Perú
https://orcid.org/0000-0001-6260-2419

ABSTRACT: Without a doubt, the study in mathematical modeling is current, it is of vital importance in ecological studies, naturally some arise in population dynamics, highlighting the role of mathematical analysis that allows optimizing decision making in a certain behavior. The main objective is the study of the logistic model, to give way to the classic model of the Lotka -Volterra type without diffusion. At the end, an analysis of the model case with diffusion is made, and much attention is paid to linear and nonlinear models. Algorithmic results make sense to explain natural phenomena, growth that can be: a cell, an organ, a human being, a plant or a population, better if it is a fundamental problem of biology.
KEYWORDS: population dynamics; model without dissemination; diffusion model.

1. INTRODUCTION

Mathematics is useful in the study of certain phenomena that exhibit important characteristics. Linear and nonlinear models exist, and their study is currently relevant in the scientific community. To describe nonlinear models, one must understand how linear models operate and function; since they are not exact, approximations are made for the most part. In general, for unpredictable results, theories are not definitive, which allows for the refinement of theories and sustained work on the experimental aspect. The fact is that nonlinear models explain a greater number of phenomena.

A concern about the subject is evident in the work of the Belgian demographer Verhulst (1845), using data on the North American population from 1870 to 1840 to predict its population up to the year 1930; his hypothesis was that it would continue to satisfy the logistic equation.

Another important theoretical reference is found in the study by marine

biologist Umberto D'Ancona, (Israel, et al., 2002; Margalef, 1998), in relation to the variations of fish populations, their growth was associated with competition for food.

A fundamental problem in biology is growth: cell, organ, plant, human, population. For this essential case, we have the differential equation.

$$\frac{dx(t)}{dt} = kx(t) \tag{1}$$

the general solution of (1) is

$$P(t) = ce^{kt} \tag{2}$$

where it behaves as a positive constant (Malthus, 1998). It can be deduced that growth occurs if $k > 0$, while decay occurs for $k > 0$. A flaw observed in equation (1) and the associated solution (2) is that when $k > 0$, then it turns out that $x \to \infty$ when $t \to \infty$, as time passes, growth is unlimited, which is in conflict with reality, especially if we consider that after a certain time a cell stops growing, just like a human being, having reached a maximum size.

The function $P(t)$ follows an unbounded exponential growth pattern. In most cases, this differential equation provides an unrealistic model of population growth, thus generating controversy between what is predicted and what is observed.

To make changes, one can cite the Belgian mathematician and biologist P.F. Verhulst, who around 1840 was interested in mathematical formulations to predict the populations of several countries; this equation is

$$\frac{dP(t)}{dt} = P(t)(k - bP(t)) \tag{3}$$

where the initial condition is $P(0) = P_0$, that is, an initial population P_0 at an initial time $t=0$, and where k and are b positive constants. Later, equation (3) became known as the *logistic equation*, whose solution is called *the logistic function*, and therefore its graph is also a *logistic curve*. It turns out that when the population is very large, equation (3) does not provide a very accurate result regarding population growth.

An exhaustive analysis of this equation, for $k > 0$, where k represents a constant average birth rate, when the average death rate is assumed, at any given instant, to be proportional to the population $P(t)$, then, if $\frac{1}{P(t)} \cdot \frac{dP(t)}{dt}$ is the growth rate per individual in a population (Boyce and DiPrima, 2005), we have

$$\frac{1}{P(t)}\cdot\frac{dP(t)}{dt} = (tasa\ media\ de\ natalidad) - (tasa\ media\ de\ mortalidad)$$

$$\frac{1}{P(t)}\cdot\frac{dP(t)}{dt} = k - bP(t) \tag{4}$$

In this case b, a positive constant of proportionality is considered, where multiplying (4) by $P(t)$ yields equation (3), (Gutiérrez, 2019). On the other hand, if equation (4) is written as $\frac{dP(t)}{dt} = kP(t) - bP^2(t)$, the term $-bP^2\,(t)$ with $b > 0$ is interpreted as an inhibition or competition term. How is it k with respect to b? The question remains open.

2. ESTIMATION EQUATION

First, we want to show that the solution of (4) is bounded when $t\to\infty$. The equation is nonlinear, but separable $\frac{dP}{kP - bP^2} = dt$, $P(0) = P_0$, it is solvable see (Gutiérrez, 2019; Scudo, 1971)

$$P(t) = \frac{kP_0}{bP_0 + (k - bP_0)e^{-kt}} \tag{5}$$

in equation (5), given that time can elapse without limit, when $t\to\infty$, being $k > 0$, we obtain $P_{máx} = \lim_{t\to\infty} P(t) = \lim_{t\to\infty}\left[\frac{kP_0}{bP_0 + (k - bP_0)e^{-kt}}\right]$, from which

$$P_{máx} = \frac{k}{b} \tag{6}$$

Result (6) confirms that a growth limit occurs $P(t)$, as biological facts dictate, and further underscores the validity of this mathematical model. To analyze result (5), it would be useful to assign two times to $P(t)$, let these times be $t = 1$ and $t = 2$, with some unit of time, resulting in the populations P_1 and P_2 respectively. Using equation, we obtain, for $t = 1$

$$P_1 = \frac{\frac{k}{b}}{1 + \left(\frac{\frac{k}{b}}{P_0} - 1\right)e^{-k}} \tag{a}$$

of (a)

$$\frac{k}{b}\left(1 - e^{-k}\right) = \frac{1}{P_1} - \frac{e^{-k}}{P_0} \tag{b}$$

Similarly, when $t = 2$, one has

$$P_2 = \frac{\frac{k}{b}}{1 + \left(\frac{\frac{k}{b}}{P_0} - 1\right)e^{-2k}} \tag{c}$$

of (c),

$$\frac{k}{b}\left(1-e^{-2k}\right)=\frac{1}{P_2}-\frac{e^{-2k}}{P_0} \tag{d}$$

Clearly the idea is to obtain $\frac{k}{b}$ and that depend on P_0, P_2 and P_2, we proceed from (b) and (c) to divide each member respectively. $1+e^{-k}=\frac{P_1\left(P_0-P_2e^{-2k}\right)}{P_2(P_0-P_1e^{-k})}$ Thus, it turns out

$$e^{-k}=\frac{P_0(P_2-P_1)}{P_2(P_1-P_0)} \tag{7}$$

Substituting equation (7) into result (b), we get

$$\frac{k}{b}=\frac{P_1^2-P_0P_2}{P_1(P_0P_1-2P_0P_2+P_1P_2)} \tag{8}$$

Thus, the maximum population is a limit value of $P(t)$, and depends on P_0, P_1 and P_2, that is $P(t)_{máx}=\lim_{t\to\infty}P(t)=\frac{k}{b}=\frac{P_1^2-P_0P_2}{P_1(P_0P_1-2P_0P_2+P_1P_2)}$.

3. MODEL WITHOUT DISSEMINATION

A model is established that is based on the following assumptions:

(a) A fish population is divided into two mutually exclusive classes: on one side, the *predators* (selachians) and on the other, the *prey*, with $u(t)$ y being $v(t)$ the number of fish of each class at time t.

(b) During the growth of each of the classes, only the number of their respective individuals and the number of contacts per unit of time between the two species are involved.

The objective is to determine the growth of predators, which is affected proportionally and negatively by their number (due to food scarcity) and proportionally and positively by the number of prey. Conversely, prey growth is affected proportionally and positively by their number (reproductive effect) and proportionally and negatively by the number of contacts. Considering the absence of fishing intensity and based on the interpretation of the derivative (Edwards and Penney, 2009), Vito Volterra proposed the model

$$\begin{aligned}\frac{du(t)}{dt}&=u(t)(m-nv(t))\\ \frac{dv(t)}{dt}&=v(t)(-p+qu(t))\end{aligned} \tag{9}$$

In equation (9), indicates time, while m, n, p and are positive constants that explain the indicated proportionalities; that is, these constants affect the growth of the species positively or negatively. It turns out that this same model was proposed by Lotka for some problems involving concentrations and chemical reactions (Lotka, 1925). Therefore, system (9) is also called the *Lotka -Volterra model*.

3.1. MODEL ANALYSIS

Equation (19) is a system of first-order ordinary differential equations. According to the provided data, it presents different types of solutions where the initial condition is fundamental. $(u(0),v(0))=(u_0,v_0)$ A biological interpretation of this system is facilitated, with primary interest being the solutions that $u(t), v(t)$ are both positive, regardless of the initial condition $t \geq 0$. With these limitations, the following solutions are distinguished:

(i) Equilibrium solutions. Those that change over time. We have when $u_0=0, v_0=0$, then $u(t)=0, v(t)=0$, that is, is the zero solution. For the case where $u_0 = \frac{p}{q}$, $v_0 = \frac{m}{n}$, the solution is also constant.

(ii) Semi-trivial solutions. This is when the species has no individuals. In this case, one could have,
Yes $u_0=u_0$, $v_0=0$ with $u_0 > 0$ this system it turns out $\frac{du(t)}{dt} = mu(t)$ (s)
$\frac{dv(t)}{dt} = 0$

In this case (s) is a separable equation whose solution is written as $u(t)=ce^{mt}$, if $u_0=u_0$, then $c=u_0$, therefore $u(t)=u_0 e^{mt}$. For $v(t)=c_1$ with $v_0=0$ results $c_1=0$, therefore $v(t)=0$. Therefore, the only solution is $(u(t),v(t))=(u_0 e^{mt},0)$. If $(u_0,v_0)=(0,v_0)$ with $v_0=0$, produces the system $\frac{du}{dt} = 0, \frac{dv(t)}{dt} = -pv(t)$. Therefore, the solution is $(u(t),v(t))=(0,v_0 e^{-pt})$.

(iii) State of non-trivial coexistence. This occurs when both components are non-trivial and positive. In this case, in system (12), if the initial condition satisfies $u_0 > 0, v_0 > 0$, then the unique resulting solution $(u(t),v(t))$ satisfies $u(t) > 0, v(t)>0, \forall\ t>0$, and the set of points of the form $\{(u(t),v(t))/t \geq 0\}$
It is a closed curve in $\mathbb{R}^2$, this implies that the solution is periodic.

Specifically, if $(u(t),v(t))$ it is a coexistence state for (9), then by applying the inverse function theorem, it follows $\frac{dv}{du} = \frac{v(-p+qu)}{u(m-nv)}$ that, being an equation of separable variables, the solution is given by by $\ln(|v|^m |u|^n)=nv+qu+c$, which exponentiating and making it $c_1=e^c$ results,

$$v^m u^p = c_1 e^{nv} e^{qu} \quad (10)$$

for some constant c_1. It is shown that the curve of equation (13) is closed at $\mathbb{R}^2$ (Lee, 1967).

Lemma 1. For $u > 0, v > 0$ the equation given in (13) describes a closed curve.

Proof . Given $u > 0, v > 0$, let us consider the functions $f(u) = \frac{u^p}{e^{qu}}, g(v) = \frac{v^m}{e^{nv}}$,

The behavior of these functions is determined. It is observed that $g(0)=0, g(\infty)=0$ since it is positive, it is $v > 0$ observed that the function has a critical point and reaches a maximum value at. $g(v)$ Differentiating the function $g, \frac{dg(v)}{dv} = \frac{v^{m-1}(m-nv)}{e^{nv}}$ by doing $\frac{dg(v)}{dv} = 0, e^{nv} > 0$ we obtain that $v = \frac{m}{n}$, so $g(v)$ it has a critical point and reaches a maximum value at $g\left(\frac{m}{n}\right) = \frac{\left(\frac{m}{n}\right)^m}{e^m} = M_v$.

It can be seen that the graph is a curve with an extreme maximum and asymptotic to the X-axis, as shown in Figure 1.

Figure 1. Graph of $g(v)=v^n e^{-nv}$.

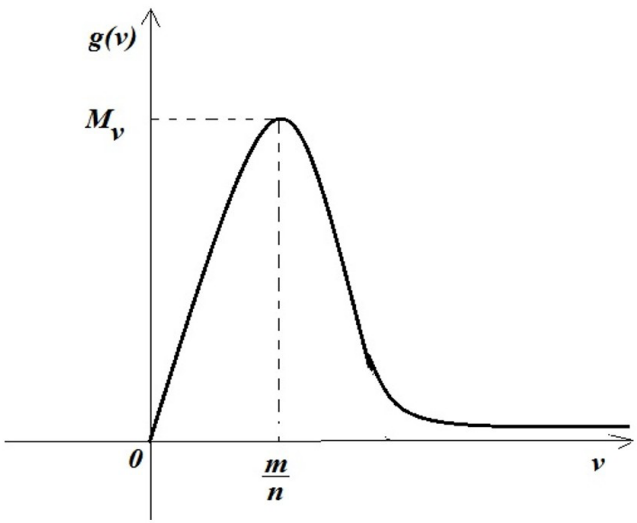

For the function $f(u)$, we proceed similarly. We observe that $f(0)=0, f(\infty)=0$, since it is $u > 0$ and $e^{qu} > 0$ we have that it $f(u)$ is positive. Differentiating the function f, $\frac{df(u)}{du} = \frac{u^{q-1}(p-qu)}{e^{qu}}$, by doing $\frac{df(u)}{du} = 0$, we obtain that $u = \frac{p}{q}$, so $f(u)$ it has a critical point and reaches a maximum value at $f\left(\frac{p}{q}\right) = \frac{\left(\frac{p}{q}\right)^p}{e^p} = M_u$, the graph is a curve with an extremum a maximum and asymptotic with the horizontal axis, as shown in figure 2.

Figure 2. Graph of $f(u)=u^p e^{qu}$.

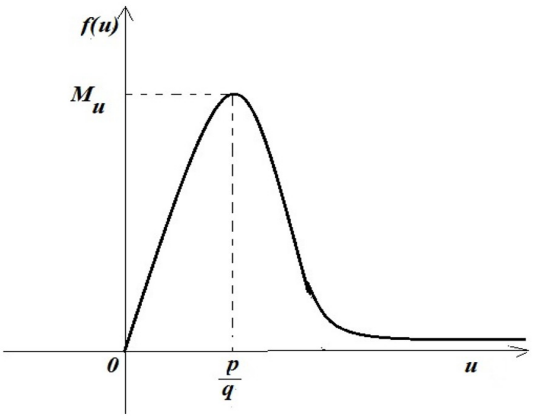

Therefore, according to the previous analysis, it is concluded that equation (9) does not admit solutions $u > 0, v > 0$ for some constant $c_1 > M_u M_v$, and for $c_1 = M_u M_v$ has the solution $u = \frac{p}{q}. v = \frac{m}{n}$. Then, it would only be necessary to consider the case when $c_1 = \delta M_v$, where δ is a positive number and $\delta < M_u$. It can be observed that the equation $\delta = \frac{u^p}{e^{pu}}$ admits one solution $u = u_r < \frac{p}{q}$ and another solution $u = u_R > \frac{p}{q}$. Therefore, the equation $g(v) = \frac{v^m}{e^{-nv}} = \left(\frac{\delta}{u^p e^{-qu}}\right) M_v$, has no solution and if u is less than u_r, or greater than u_R. If $u = u_r$ or $u = u_R$ results only in the solution $v = \frac{m}{n}$, while for each u between u_r and u_R has two solutions $v_1(u)$ and $v_2(u)$. In this case, the lesser solution $v_1(u)$ is always less than $\frac{m}{n}$ and the greater solution $v_2(u)$ is always greater than $\frac{m}{n}$. When tends to u_r o a u_R, then both $v_1(u)$ tend $v_2(u)$ to $\frac{m}{n}$, (Blat, 1984; Logan, 1987).

Therefore, the curves defined by (10) are closed for u and v positive, and take the form as shown in Figure 3.

Figure 3. Orbit of (12) for u, v positives.

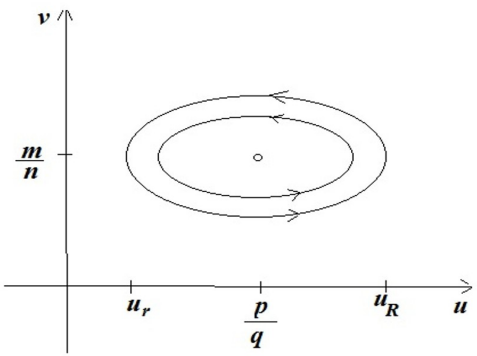

Lemma 2. Let be $(u(t), v(t))$ any coexistence state of (9), with period $T > 0$, then its average values are $\bar{u} = \frac{1}{T}\int_0^T u(t)dt$, $\bar{v} = \frac{1}{T}\int_0^T v(t)dt$, that is $\bar{u} = \frac{p}{q}$, $\bar{v} = \frac{m}{n}$.

Proof. This lemma specifies that the average values of $u(t)$ y $v(t)$ are the equilibrium values. From equation (12), we have

$$\frac{du(t)}{dt} = mu(t) - nu(t)v(t) \text{ and } \frac{1}{u}\frac{du(t)}{dt} = m - nv(t) \quad \text{(d)}$$

so that, in (d) integrating both sides $\frac{1}{T}\int_0^T \frac{u'(t)}{u(t)}dt = \frac{1}{T}\int_0^T (m - nv(t))dt$, We have $\frac{1}{T}(Lnu(T) - Lnu(0)) = \frac{1}{T}\int_0^T mdt - \frac{n}{T}\int_0^T v(t)\,dt$, but since $u(T)=u(0)$, it turns out $0 = m - \frac{n}{T}\int_0^T v(t)dt$, that is, $\frac{1}{T}\int_0^T v(t)dt = \frac{m}{n}$. Therefore, $\bar{v} = \frac{m}{n}$. Similarly, from equation (9), we have $\frac{dv(t)}{dt} = -pv(t) + qu(t)v(t)$ and $\frac{1}{v}\frac{du(t)}{dt} = -p + qu(t)$ (m) so that in (m) integrating into both sides $\frac{1}{T}\int_0^T \frac{v'(t)}{v(t)}dt = \frac{1}{T}\int_0^T (-p + qu(t))dt$

We have $\frac{1}{T}(Lnv(T) - Lnv(0)) = \frac{1}{T}\int_0^T pdt - \frac{q}{T}\int_0^T u(t)\,dt$, but since $v(T)=v(0)$, it turns out $0 = -p - \frac{q}{T}\int_0^T u(t)dt$, that is, $\frac{1}{T}\int_0^T u(t)dt = \frac{p}{q}$. Therefore, $\bar{u} = \frac{p}{q}$.

The analysis shows that even when it is not possible to obtain it $(u(t),v(t))$ explicitly, it is possible to calculate it $(\bar{u}, \bar{v})$, resulting in the fact that, regardless of the chosen coexistence state, it is always the case $(\bar{u}, \bar{v}) = \left(\frac{p}{q}, \frac{m}{n}\right)$.

4. CONCLUSIONS

We can observe that model (9) does not account for how fishing intensity might affect the growth of a species. To address this, the following hypothesis is proposed: "the fishing intensity of a species u is directly proportional to the total population over time t and negatively impacts its growth." This occurs similarly for the species v. Therefore, the new, corrected model is written

$$\begin{aligned} \frac{du}{dt} &= u(t)(m - nv(t)) - \varepsilon u(t) \\ \frac{dv}{dt} &= v(t)(-p + qu(t)) - \varepsilon v(t) \end{aligned} \quad (11)$$

where $\varepsilon > 0$ indicates the fishing intensity. The system given in (11) is the same as system (9), provided that m< ε, that is, $\frac{du}{dt} = u(t)(m - \varepsilon - nv(t))$ and $\frac{dv}{dt} = v(t)(-p - \varepsilon + qu(t))$; however, it must be specified that fishing reduces the population of edible fish at a rate $\varepsilon u(t)$, in the

same way as the sharks, at a rate $\varepsilon v(t)$. It can be deduced that the constant ε indicates the fishing intensity. Therefore, the average values of the corresponding solutions are $\bar{u} = \frac{p+\varepsilon}{q}$, $\bar{v} = \frac{m-\varepsilon}{n}$.

Finally, the decrease in the intensity of fishing; that is, decreasing it ε, causes a decrease in prey u and an increase in predators v; this result corresponds to the Volterra principle (Volterra, 1931).

REFERENCES

Boyce W. and DiPrima R. (2005), *Elementary Differential Equations and Boundary Value Problems*. Edit. Wiley.

Blat, J. and Brown, K. J. (1984). *Bifurcation of steady-state solutions in predator prey and competition systems*. Proceedings of the Royal Society of Edinburgh.

Gutierrez B., Alberto. (2019). *Ecuaciones diferenciales ordinarias I*. Ica: Editorial Gráfica Señor de Luren.

Edwards, C. Henry y Penney, David E. (2009), *Ecuaciones diferenciales y problemas con valores en la frontera*, México: Pearson Education.

Israel, G. and Gasca, A. M. (2002). *Letters between Umberto D'Ancona and Vito Volterra*. In the Numbers (pp. 130-200). Birkhauser Basel.

Lee, E. B. and Markus, L. (1967). *Foundations of optimal control theory*. New York, Wiley-Interscience.

Logan, J. D. (1987). *Applied Mathematics, a Contemporary Approach*. New York, Wiley-Interscience.

Lotka, A. J. (1925). *Elements of Physical Biology*. USA, Williams and Wilkins.

Malthus, T. R. (1998). *Ensayo sobre el principio de la población*, México, FCE.

Margalef, R. (1998), *Ecología*, Madrid, Ediciones Omega.

Scudo, F. M. (1971). *Vito Volterra and theorical ecology*. Theoretical Population Biology, 2(1), 1-23.

Volterra, V. (1931). *Lecons sur la Thériee Mathematique de la luthe pour la vie*. USA, Editorial Gauthier-Villars.

CAPÍTULO 5

REMOCIÓN DE CROMO (VI) EN SOLUCIÓN ACUOSA POR LA BIOMASA DE LA CASCARA DE SEMILLA DE GIRASOL (*Helianthus annuus*)

Data de submissão: 10/11/2025
Data de aceite: 28/11/2025

Pedro Pablo Zapata Hernández
Laboratorio de Micología Experimental
Facultad de Ciencias Químicas
Universidad Autónoma de
San Luis Potosí, S.L.P.
San Luis Potosí, S.L.P., México

Claudia M. Martínez Rodríguez
Laboratorio de Micología Experimental
Facultad de Ciencias Químicas
Universidad Autónoma de
San Luis Potosí, S.L.P.
San Luis Potosí, S.L.P., México
https://orcid.org/0000-0002-5335-6137

Adriana Rodríguez Pérez
Universidad Autónoma de
San Luis Potosí
Centro de Investigación y Extensión
de la Zona Media. El Balandran
Calle Escontría No. 230
Barrio 3, C.P. 79660
Cd. Fernández, San Luis Potosí
https://orcid.org/0000-0002-6570-6579

Juan Fernando Cárdenas González
Universidad Autónoma de
San Luis Potosí
Centro de Investigación y Extensión
de la Zona Media. El Balandran
Calle Escontría No. 230
Barrio 3, C.P. 79660
Cd. Fernández, San Luis Potosí
https://orcid.org/0000-0002-3502-5959

Víctor Manuel Martínez Juárez
Área Académica de Medicina
Veterinaria y Zootecnia
Instituto de Ciencias Agropecuarias
Universidad Autónoma del
Estado de Hidalgo
Avenida Universidad Km. 1 s/n
Exhacienda Aquetzalpa, 43600
Tulancingo de Bravo, Hidalgo, México
https://orcid.org/0000-0002-7426-6835

Ismael Acosta Rodríguez
Laboratorio de Micología Experimental
Facultad de Ciencias Químicas
Universidad Autónoma de
San Luis Potosí, S.L.P.
San Luis Potosí, S.L.P., México
https://orcid.org/0000-0001-8620-2727

RESUMEN: El objetivo de este trabajo fue analizar la capacidad de remoción de Cromo (VI) por la biomasa de la cáscara de semilla de girasol (*Helianthus annuus*), encontrando que 10 g de la biomasa analizada eliminan el 100% del metal a las 4 horas de incubación a pH de 1.0, 28°C, 100 mg/L de Cromo (VI), mientras que a mayores valores de pH, la remoción es menor. Además, a mayor temperatura de incubación, la remoción es más eficiente, pues a 60°C, se remueve el 100% del metal a los 90 minutos, y a diferentes concentraciones de Cromo (VI) analizadas (200-1000 mg/L), se obtuvo una remoción similar (91-96%) a 28°C, mientras que a 60°C la remoción es

total a las 2 horas, con las diferentes concentraciones del metal analizadas. A diferentes concentraciones del bioadsorbente, se observó que con 1 g de biomasa se eliminó un 55.5 % en 8 h, con 5 g de biomasa un 97.3%, en el mismo tiempo de incubación, y con 10 g de biomasa, se eliminó el 100% de cromo (VI) en solución a las 4 h. Cuando se analizó la remoción del metal a partir de tierra y agua contaminadas con Cromo (VI), se eliminó el 100% del metal a los 3 días a partir de tierra contaminada, mientras que a los 4 días se remueve el 73% del metal a partir de agua contaminada.
PALABRAS CLAVE: cromo (VI); biomasa; girasol; biorremediación; aguas residuales.

REMOVAL OF CHROMIUM (VI) FROM CONTAMINATED SOIL AND WATER USING SUNFLOWER SEED HULL BIOMASS

ABSTRACT: The objective of this work was to analyze the Chromium (VI) removal capacity of sunflower seed hull biomass (*Helianthus annuus*). It was found that 10 g of the analyzed biomass removed 100% of the metal after 4 hours of incubation at pH 1.0, 28°C, and 100 mg/L of Chromium (VI). At higher pH values, the removal was lower. Furthermore, at higher incubation temperatures, the removal was more efficient. At 60°C, 100% of the metal was removed after 90 minutes. At different Chromium (VI) concentrations (200-1000 mg/L), similar removal rates (91-96%) were obtained at 28°C, while at 60°C, complete removal was achieved after 2 hours. At different concentrations of the bioadsorbent, it was observed that 1 g of biomass removed 55.5% of the metal in 8 h, 5 g of biomass eliminate 97.3% in the same incubation time, and 10 g of biomass removal 100% of the chromium (VI) in solution after 4 h. When the removal of the metal from soil and water contaminated with chromium (VI) was analyzed, 100% of the metal was removed from contaminated soil after 3 days, while 73% of the metal was removed from water contaminated, after 4 days.
KEYWORDS: chromium (VI); biomass; sunflower; bioremediation; wastewater.

1. INTRODUCCIÓN

Los metales pesados tóxicos son compuestos químicos inorgánicos que afectan al medio ambiente, causando contaminación debido a su no biodegradabilidad, acumulación en la cadena alimentaria y biomagnificación (Xie, 2024). Además, las actividades humanas como el curtido de pieles, la minería y el cromado de metales, así como algunos eventos naturales como incendios forestales y la erosión del suelo provocan la contaminación de cuerpos de agua superficiales y subterráneas con cromo (VI), lo cual puede provocar diversas afectaciones en el cuerpo humano y en la fauna acuática y terrestre, siendo la principal consecuencia la formación de células cancerígenas, debido a su alta solubilidad y permeabilidad en las membranas, lo que permite la formación de estrés oxidativo y la formación de un complejo con el ADN (Shruthi y Hemavathy, 2024), y el cromo (Cr), un metal pesado, se encuentra en los residuos de industrias como la del cuero, la cerámica, el caucho, la impresión y el teñido de textiles, y los componentes metálicos cromados (Ukhurebor, et. al., 2021). Se han

reportado diferentes estados de oxidación del cromo, siendo los más comunes el Cr(0), el Cr(III) o forma trivalente, y el Cr(VI) o forma hexavalente (Pushkar, et. al., 2021), el cual es un contaminante común de los metales pesados, y es un vertido por las industrias, que contamina tanto los suelos agrícolas como los cuerpos de agua, (Ovens, et. al., 2017). El cromo hexavalente existe en diferentes formas según su pH, en un rango de 1 a 6, la especie dominante es el ácido hidrocrómico, $HCrO_4^-$, y cuando el pH es mayor que 7, el cromato, CrO_4^{2-} (Ukhurebor, et. al., 2021). En comparación con el Cr(III), el Cr(VI) es altamente tóxico y móvil en la naturaleza (Jiang, et. al., 2019). Tanto el Cr(III) como el Cr(VI) tienen consecuencias nocivas para los organismos vivos, como alterar la forma celular e interactuar con sustancias químicas, proteínas y ADN a través de los sistemas digestivo, respiratorio y epidérmico, lo que conduce a la destrucción de la expresión génica, respectivamente (Karthik, et. al., 2017). La USEPA (Agencia de Protección Ambiental de los Estados Unidos) recomienda que el agua potable contenga solo 0,05 mg/L de cromo (Pushkar, et. al., 2021). Por lo tanto, la eliminación del cromo junto con un método eficaz y rentable resulta importante. Entre los diferentes métodos existentes para el control de metales pesados se han reportado: precipitación, óxido-reducción, intercambio iónico, filtración, tratamiento electroquímico, tecnologías de membranas y recuperación por evaporación, adsorción y bioadsorción, y algunos metales pesados que se consideran peligrosos son: plomo, cobalto, estaño, hierro, cadmio, mercurio, cromo, vanadio, entre otros (Zaynab et al., 2022).

Por otro lado, la generación de residuos agrícolas es inevitable debido al procesamiento de materias primas para la producción de alimentos. El crecimiento poblacional requiere aumentar la demanda alimenticia para subsistir, lo que provoca un incremento desmedido en la cantidad de residuos agrícolas (Aguirre de los Santo, et. al., 2025). En México, se producen más de 70 Mt de residuos agrícolas, el 79.4 % corresponde a residuos primarios (paja de cereales, residuos del procesamiento de frutas y hortalizas y residuos de cultivos), y el resto corresponde a residuos de cultivos industriales (arroz, café, tabaco y caña de azúcar). (Quintero et al., 2023). Actualmente, estos residuos forman parte del problema ambiental en México y en el mundo, por ello, se han estado buscando propuestas para darles un tratamiento para reducir su efecto en el ambiente, reutilizarlos como materia prima o emplearlos como fuentes de componentes de interés, y en base a eso, se han propuesto materiales obtenidos de los residuos agrícolas como adsorbentes económicos y respetuosos con el medio ambiente (Ince & Kaplan, 2020). Los materiales de origen agrícolas, en particular contienen celulosa han mostrado un alto potencial para la eliminación de los metales tóxico (Ranjan et al., 2009). El proceso de adsorción de metales

tóxicos en solución acuosa por los adsorbentes de bajo coste procedentes de residuos vegetales puede llevarse a cabo con o sin modificaciones químicas, y se ha reportado que los residuos vegetales naturales tienen una mayor capacidad de adsorción que las formas no modificadas (Shruthi and Hemavathy, 2024). Algunos materiales estudiados son: *Mentha piperita* (González Padilla et al., 2024), tabaco (*Nicotiana tabacum*) (Huerta Veláquez et al., 2024), cáscara de sandía (*Citrulus lanatus*) (García Luis, et. al., 2023), cascara de toronja (*Citrus Paradise*) (Rodríguez Pérez et al., 2024), y la semilla de girasol (*H. annuus*), de la cual se ha reportado su utilidad en la remoción de diferentes metales pesados como: la remoción de Arsénico (Flores Herrera, 2016), cadmio (II) (Almouei et. al., 2013), gasolina (Almazan-Casteñada y cols., 2024), la acumulación de plomo, zinc y cadmio por el tallo, y cobre, níquel y manganeso por las raíces de *H. annuus* en residuos mineros (Hernández-Acosta, y cols., 2016), y la recuperación de plomo por girasol y vermicompost (Sarmiento y Febres, 2021|). Por lo anterior, el objetivo de este trabajo fue analizar la remoción de cromo (VI) en solución acuosa por la biomasa de la cáscara de semilla de girasol (*Helianthus annuus*).

2. MATERIAL Y MÉTODOS

2.1. BIOADSORBENTE

Las semillas de girasol (*H. annuus*), se obtuvieron a partir de caña comercial obtenida de una tienda de herbolaria de un mercado popular de la zona centro de la ciudad capital de San Luis Potosí, S.L.P., México, en el mes de julio del 2024. Para la obtención de la biomasa, las semillas se lavaron durante 24 horas con EDTA (10% p/v), el cual sirve como agente quelante, con el fin de eliminar metales contaminantes, después se lavaron con agua tridesionizada por una semana con cambios de agua cada 12 horas. Posteriormente, se calentaron a ebullición por una hora, y después se secaron en una estufa a 80°C por 3 días, se molieron en una licuadora y se guardaron en envases de vidrio ámbar a temperatura ambiente hasta su uso.

2.2. MÉTODOS

2.2.1. Soluciones de Cromo (VI)

Se utilizó una solución de cromo (VI) con una concentración de 100 mg/L, obtenida por dilución de una solución patrón de 1.0 g/L, preparada en agua tridesionizada, a partir de dicromato de potasio De acuerdo con el pH empleado para cada prueba, éste se modificó con soluciónes de NaOH y/o H_2SO_4, antes de adicionarla a la biomasa.

2.2.2. Determinación de remoción de Cromo (VI) en distintas condiciones

De la biomasa a analizar, se pesaron 10 g y se añadieron a matraces Erlenmeyer de 500 mL y posteriormente se mezclaron con 200 mL de una solución del metal [100 mg/L de cromo (VI], se incubaron a una temperatura de 28°C con agitación constante (100 rpm) bajo diferentes condiciones de pH (1.0, 2.0, 3.0 y 4.0), temperatura (28°C, 40°C, 50°C y 60°C), concentración de cromo (VI) (200 mg/L, 400 mg/L, 600 mg/L, 800 mg/L y 1000 mg/L) y diferentes concentraciones de biomasa (1 g, 5 g y 10 g), y de la misma manera se determinó la remoción del metal a partir de agua y tierra contaminadas.

Posteriormente, a diferentes tiempos de incubación, se tomaron alícuotas de 5 mL, removiendo la biomasa por centrifugación a 3 000 rpm (10 min) y al sobrenadante se le determinó la concentración de cromo (VI) en solución, utilizando el método colorimétrico de la Difenilcarbazida, determinando la cantidad del metal presente en solución por medio de la producción de una coloración rosa violeta, las muestras se leyeron por duplicado en un espectrofotómetro a una longitud de onda de 540 nm (Greenberg et al., 1992). Todos los experimentos se realizaron mínimo 2 veces y por duplicado.

3. RESULTADOS Y DISCUSIÓN

3.1. EFECTO DEL TIEMPO DE INCUBACIÓN Y PH

La capacidad de remoción de la cascara de semilla de girasol fue la siguiente: Se obtuvo una remoción del 100% a las 4 horas a pH de 1.0, mientras que se obtuvo una remoción de 58.2%, 29.4% y 38% a pH 2.0, 3.0 y 4.0 respectivamente, estos últimos a las 5 horas (Figura 1).

Figura. 1. Efecto del tiempo de incubación y pH sobre la remoción de cromo (VI) en solución.100 mg/L Cr (VI), 100 rpm, 28°C, 10 g biomasa.

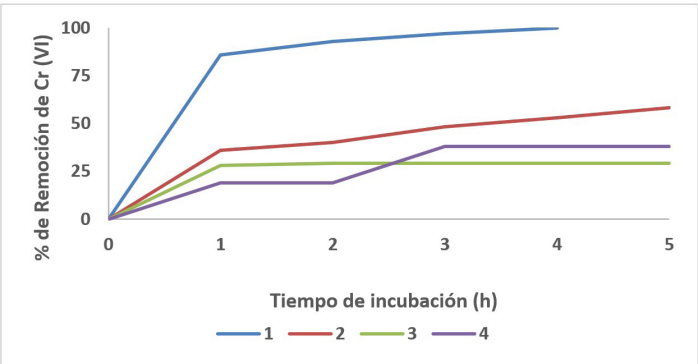

3.2. EFECTO DE LA TEMPERATURA DE INCUBACIÓN

En relación con la temperatura, se obtuvo una remoción del 100% en las diferentes temperaturas, a 28°C, la remoción fue total a las 4 horas, a 40°C a las 3 horas, a 50°C a las 2.5 horas y a 60°C se completó a 1.5 horas, confirmando que a mayor temperatura es más rápida la remoción del cromo (VI) (Figura 2).

Figura 2. Efecto de la temperatura de incubación sobre la remoción de cromo (VI). 100 mg/L Cr (VI). pH 1.0. 100 rpm. 10 g de biomasa. 5 h.

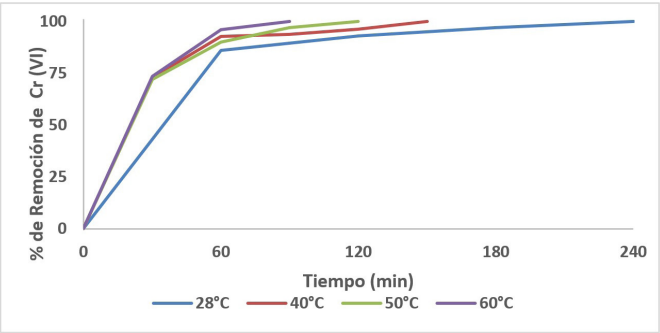

3.3. EFECTO DE LA CONCENTRACIÓN INICIAL DEL METAL SOBRE LA ADSORCIÓN DEL MISMO

Por otro lado, a las diferentes concentraciones de cromo (VI) en solución analizadas, a las 5 h se obtuvieron remociones de 96.6%, 95.15%, 93.4%, 92.2% y 91.6% a concentraciones de 200, 400, 600, 800 y 1000 mg/L respectivamente, con una temperatura de 28°C, a las 6 horas de incubación (Figura 3), mientras que a 60°C, se observó una remoción total del metal analizado a las concentraciones analizadas entre 90 y 120 minutos de incubación (Figura 4).

Figura 3.- Efecto de la concentración de cromo (VI) sobre la remoción del mismo. 10 g de biomasa. 100 rpm, pH 1.0. 28°C.

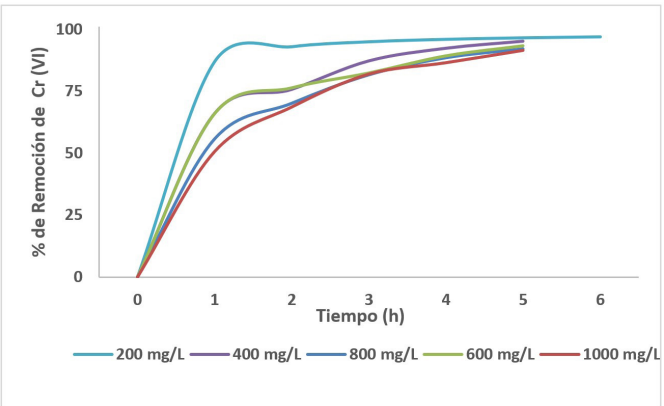

Figura 4.- Efecto de la concentración de cromo (VI) sobre la remoción del mismo. 10 g de biomasa. 100 rpm, pH 1.0. 60°C.

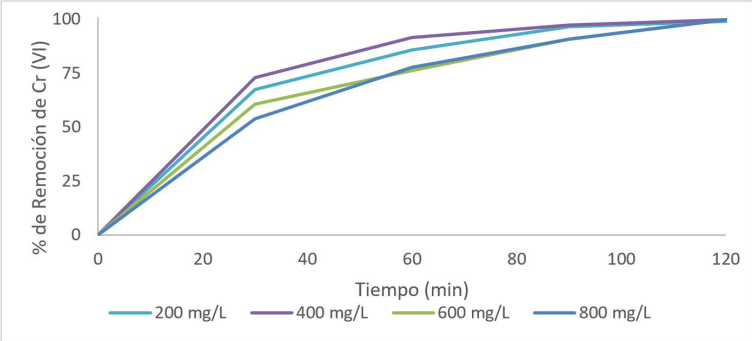

3.4. EFECTO DE LA CONCENTRACIÓN DEL BIOADSORBENTE

En la figura 5, se muestra el efecto de la concentración inicial de la biomasa sobre la remoción del metal, encontrando que con 1 g de biomasa se eliminó un 55.5 % en 8 h, con 5 g de biomasa un 97.3%, en el mismo tiempo de incubación, y con 10 g de biomasa se eliminó el 100% del cromo (VI) en solución a las 4 h (Figura 5).

Figura 5.- Efecto de la concentración del bioadorbente sobre la remoción de cromo (VI). 100 rpm, pH 1.0. 28°C. — 1 g, — 5 g, — 10 g.

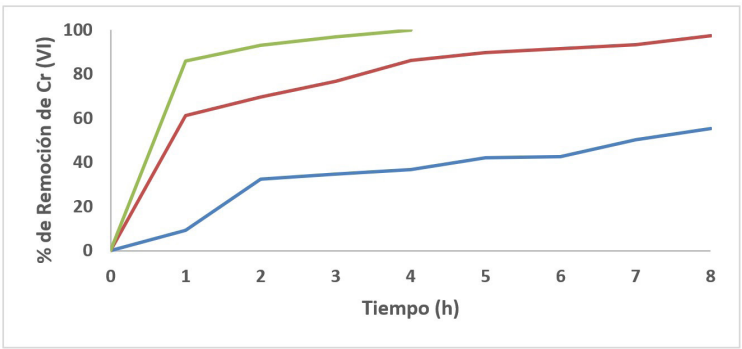

3.5. REMOCIÓN DE CROMO (VI) A PARTIR DE RESIDUOS INDUSTRIALES CONTAMINADOS

Se realizó un ensayo de biorremediación de cromo (VI), a partir de agua y suelo contaminados con 200 mg/g de tierra y 200 mg/L de agua contaminada (ambos ajustados), a partir de muestras obtenidas de una tenería de Celaya, Gto, México, utilizando 10 g de la biomasa a analizar, observando que la biomasa elimina el 100% de cromo (VI) presente en tierra a los 3 días de incubación (Figura 6), mientras se eliminó el 73% del metal a los 4 días de incubación en agua contaminada, a 28°C y 100 rpm (Figura 7).

Figure 6. Remoción de cromo (VI) a partir de residuos industriales. 10 g de biomasa. 28°C, 100 rpm, 10 g de tierra contaminada, 180 mL de agua tridesionizada estéril (200 mg Cr (VI)/L, ajustado, pH 6.8.

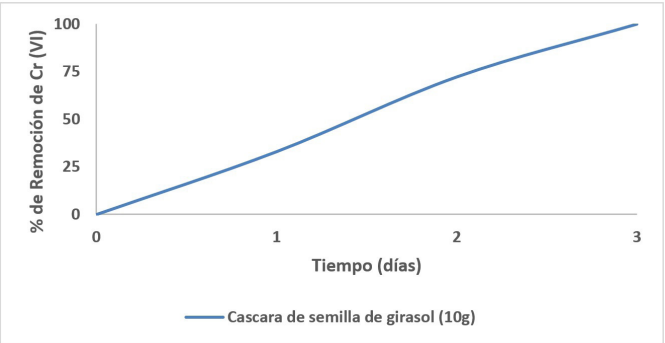

Figure 7.- Remoción de cromo (VI) a partir de aguas residuales industriales. 10 g de biomasa. 28°C, 100 rpm, 190 mL de agua contaminada, (200 mg Cr (VI)/L de agua, ajustado, pH 7.2).

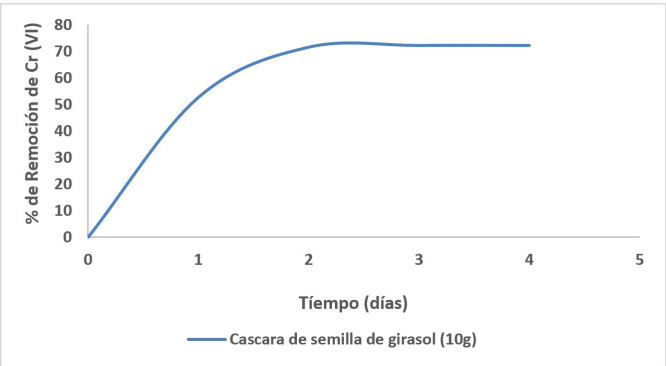

Finalmente, en la tabla 1, se muestran los porcentajes de adsoción de Cromo (VI) utilizando diferentes bioadsorbentes.

Tabla 1. Comparación de los porcentajes de remoción de Cromo (VI) con otros bioadsorbentes.

Adsorbente	**pH**	**Capacidad de adsorción (mg/L)**	**Referencia**
Avena sativa	1.0	100	Pacheco *et al*., 2017
Dioscorea rotundata	2.0	325.88	Villabona *et al*., 2022
Emblica Officinalis	2.0-3.0	416	Kushwah & Chakra-Borty, 2021
Oriza sativa L.	1.0	50	Rodríguez-Pérez *et al.* 2022
Heinsia crinita	2.0	49.45	Dawodu *et al*., 2020
Pisum sativum	2.0	5	Kebede et al., 2022
Eichhornia crasipes	1.5	2.5	Ardila-Arias *et al*., 2022
Nicotiana tabacum	2.0	72	Huerta Velázquez et al., 2024
Helianthus annus	1.0	100	Este trabajo

4. DISCUSIÓN

Los resultados obtenidos en este trabajo, sugieren la potencial aplicabilidad de la biomasa de la cáscara de semilla de girasol (*H. annus)* para la remoción de cromo (VI), y otros metales pesados de aguas residuales. Sin embargo, la capacidad de remoción puede verse afectada por altas concentraciones de los mismos contaminantes, o la presencia de otros metales pesados, disminuyendo la capacidad de remoción de las biomasas estudiadas, aunque, actualmente, el uso de biomasas de desecho, es una gran alternativa para tratar de eliminar los metales pesados de los diferentes sitios contaminados. Actualmente, el uso de biomasas naturales vivas y/o muertas, es una gran alternativa para tratar de eliminar éstos y otros contaminantes de sitios contaminados, debido a su bajo costo, gran capacidad de adsorción, fácil accesibilidad, su producción en grandes cantidades y la facilidad de obtención, pues la mayoría se estos productos se desecha y no se utiliza para el beneficio de la humanidad.

También, se ha reportado, que la biomasa de la semilla de *H. annus* puede acumular eficientemente diferentes metales pesados (Flores Herrera, 2016; Almouei et. al., 2013; Almazan-Casteñada y cols., 2024), pero, hay pocos reportes relacionados con la remoción de cromo (VI por esta biomasa, por lo cual este trabajo es relevante para estudios posteriores para eliminar y mejorar la capacidad de remoción de esta biomasa natural.

5. CONCLUSIONES

Con la biomasa de la cáscara de semilla de girasol (*H. annus),* se obtuvo una buena capacidad de remoción del metal analizado en las condiciones descritas, lo cual sugiere su potencial aplicación para la biorremediación de sitios contaminados con este metal.

REFERENCES

Aguirre de los Santo, Y.L., Vázquez-Sánchez, A.Y., Abatal, M., Quiroz-Rodriguez, A. 2025. Potencial de Residuos Agrícolas Mexicanos para la Remoción de Metales Pesados desde Soluciones Acuosas, p. 251-268. En: J.G. Cerón Bretón, R. M. Cerón Bretón y M. López Cisneros (ed.). Tópicos Selectos de Contaminación Ambiental. Universidad Autónoma de Campeche. 366 p. ISBN 978-607-8907-33-5. doi 10.26359/EPOMEX01202512.

Almazán-Casteñada, P.J., Alarcón, A., García-Barradas, O., Mendarte-Alquisira, C. y Ferrera-Cerrato, R. 2024. Fitotoxicidad y fitorremediación de un suelo contaminado con fasolina utilizando plantas de girasol asistidas por bacterias rizosférixcas nativas. Revista Internacional de Contaminación Ambiental. 40, 351-362. https://doi.org/10.20937/RICA.55039

Amouei, A.I., Amooey, A.A., Asgharzadeh, F. 2023. A study of cadmium removal from aqueous solutions by sunflower powders and its modeling using artificial neural network. Iranian journal of health sciences. 1:3 28-34. http://jhs.mazums.ac.ir

Ardila-Arias A.N., Arriola-Villaseñor E., Álvarez-González W., Hernández-Maldonado J.A. & Barrera-Zapata R. 2022. Aprovechamiento de residuos de *Eichhornia crasipes* para la remoción de Cr (VI) en Aguas simuladas. Revista Politécnica.18(35): 71-83. DOI: https://doi.org/10.33571/rpolitec.v18n35a5

Dawodu F.A., Akpan B.M. & Akpomie K.G. 2020. Sequestered capture and desorption of hexavalent chromium from solution and textile wastewater onto low cost *Heinsia crinita* seed coat biomass. Applied Water Science. 10(1):1-15. https://doi.org/10.1007/ s13201-019-1114-6

Flores Herrera, M.B. 2016. Remoción de arsénico con cáscara de Semilla de Girasol mediante el proceso de adsorción en aguas del manantial Puncomachay, Jauja 2016. Tesis Profesional para obtener el Título Profesional de Ingeniero Ambiental. Escuela Profesional de Ingeniería Ambiental. Facultad de Ingeniería. Universidad Cesar Vallejo. Lima, Perú.

García Luis, M.F., Ramos Arteaga, A., Sánchez Lucio, L.S., Rodríguez Pérez, A., Cárdenas González, J.F. & Acosta Rodríguez, I. 2023. Remoción de cromo (VI) en solución acuosa por la biomasa de la cáscara de sandía (*Citrulus lanatus*). Sociedad Química de México. 255-259. ISSN: 2448-914X. Versión digital. www.sqm.org.mx.

González Padilla, M.J., Martínez Rodríguez, C.M., Contreras Briones, D., Navarro Castillo, J.F. & Acosta Rodríguez, I. 2024. Removal of chromium (VI) in solution by the *Mentha piperita* biomass. Journal of Multidisciplinary and Environmental Science and Technology. (JMEST). Vol. 11, No. 11. pp. 16522-16527. January 31. ISSN: 2458-9403. JMESTN42354307. www.jmest.org

Greenberg A.E., Clesceri L.S. & Eaton A.D. 1992. Standard Methods for the Examination of Water and Wastewater. American Public Health Association, American Water Works Association, Water Environment Federation, Washington, DC, USA, 18th edition. 3.58-3.60.

Hernández-Acosta, E., Juárez-Santos, Y., Robledo-Santoyo, E., Díaz-Vargas, P. y Cristobal-Acevedo, D. 2016. Acumulación de metales pesados en Helianthus annuus desarrollado en residuos de mina. Revista Iberoamericana de Ciencias. 3:6. 27-36. www.reibci.org

Huerta-Velázquez, C.C., Cruz-García, K.B. & Acosta-Rodríguez, I. 2024. Usefulness of the Biomass of Tobacco (*Nicotiana tabacum*) for The Elimination of Chromium (VI) from Polluted Waters. Universal Journal of Green Chemistry. Vol. 2, No. 1. pp. 1-10. 21/02/2024. DOI: https://doi.org/10.37256/ujgc.2120242220. https://ojs.wiserpub.com/index.php/UJGC/

Ince, M., & Kaplan Ince, O. 2020. Heavy Metal Removal Techniques Using Response Surface Methodology: Water/Wastewater Treatment. Biochemical Toxicology-Heavy Metals and Nanomaterials, 1–19. DOI: 10.5772/intechopen.88915

Jiang, B., Gong, Y., Gao, J., Sun, T., Liu, Y., Oturan, N., Oturan, M.A. 2019. The reduction of Cr(VI) to Cr(III) mediated by environmentally relevant carboxylic acids: state-of- the-art and perspectives, Journal of Hazardous Materials. 365, 205–226, https://doi.org/10.1016/j.jhazmat.2018.10.070

Karthik, C., Barathi, S., Pugazhendhi, A., Ramkumar, V.S., Thi, N., Arulselvi, P.I. 2017. Characterization of multifarious plant growth promoting traits of rhizobacterial strain AR6 under Chromium(VI) stress, Microbiological Research. 204, 65–71, https://doi.org/10.1016/j.micres.2017.07.008

Kebede A., Kedir K., Melak F. & Girma-Asere T. 2022. Removal of Cr(VI) from Aqueous Solutions Using Biowastes: Tella Residue and Pea (*Pisum sativum*) Seed Shell. Hindawi Scientific World Journal. Vol. 2022, Article ID 7554133, 12 pages https://doi.org/10.1155/2022/7554133

Kushwaha P. & Chakraborty, S. 2021. Removal of Cr(VI) from Synthetic Wastewater by Low Cost Adsorbent Developed from Amla Wood Sawdust (*Emblica officinalis*). International Journal of Engineering Research & Technology (IJERT). 10(02): 246-248. http://www.ijert.org

Ovens, M., Khan, M.S., H.A. Qari, H.A. 2017. Ensifer adhaerens for heavy metal bioaccumulation, biosorption, and phosphate solubilization under metal stress condition, Journal of Taiwan Institute Chemical Engineering. 80, 540–552, https://doi.org/10.1016/j.jtice.2017.08.026

Pacheco-Castillo N.C., Cárdenas-González J.F., Moctezuma-Zárate M.G., Martínez-Juárez V.M., Rodríguez-Pérez A. & Acosta Rodríguez I. 2017. Removal of chromium (VI) in aqueous solution by oat biomass (*Avena sativa*). Mexican Journal of Biotechnology. 2(2): 196-205. https://doi.org/10.29267/mxjb.2017.2.2.196

Pushkar, B., Sevak, P., Parab, S., Nilkanth, N. 2021. Chromium pollutiom and its bioremediation mechanisms in bacteria: a review, Journal of Environmental Management. 287, 112279. https://doi.org/10.1016/j.jenvman.2021.112279

Quintero, S., Zwolinski P., Evrard D., Cano, J. & Rivas, P. (2023). Turning food loss and waste into animal feed: A Mexican spatial inventory of potential generation of agro-industrial wastes for livestock feed. Sustainable Production and Consumption. 41, 36-48.

Rodríguez-Pérez A., Pacheco-Castillo N., Tovar-Oviedo J., Martínez-Juárez V.M., Acosta-Rodríguez I., Muñoz-Morales A. & Cárdenas-González J.F. 2022. Remoción de Cromo (VI) en solución acuosa por la biomasa modificada de la cáscara de arroz (*Oriza sativa* L.). Tecnología y Ciencias del Agua. Instituto Mexicano de Tecnología del Agua. 13(3): 478-502. DOI: 10.24850/j-tyca-2022-03-10.

Shijie, Xie. 2024. Water contamination due to hexavalent chromium and its health impacts: exploring green technology for Cr (VI) remediation, Green Chemistry Letters and Reviews. 17:1, 2356614, DOI: 10.1080/17518253.2024.2356614

Shruthi, S. Hemavathy, R.V. 2024. Myco-remediation of chromium heavy metal from industrial wastewater: A review. Toxicology Reports. 13, 101740. 1-8. doi.org/10.1016/j.toxrep.2024.101740.

Ukhurebor, K., Aigbe, U.O., Onyancha, R.B., Nwankwo, W., Osibote, O.A., Paumo, H.K., Ama, O.M., Adetunji, C.O., Siloko, I.U. 2021. Effect of hexavalent chromium on the environment and removal techniques:a review. Journal of Environmental Management. 280, 111809. 1–25, https://doi.org/10.1016/j.jenvman.2020.111809.

Villabona-Ortíz A., González-Delgado Á. & Tejada-Tovar C. 2022. Equilibrium, Kinetics and Thermodynamics of Chromium (VI) Adsorption on Inert Biomasses of *Dioscorea rotundata* and *Elaeis guineensis*. Water. 14(844): 1-15. https://doi.org/10.3390/w14060844

Zaynab M., Al-Yahyai R., Ameen A., Sharif Y., Ali L., Fatima M., Ali-Khan K. & Li S. 2022. Health and environmental effects of heavy metals. Journal of King Saud University–Science. 34(101653): 1-8. https://doi.org/10.1016/j.jksus.2021.101653

Villabona-Ortíz A., González-Delgado Á. & Tejada-Tovar C. 2022. Equilibrium, Kinetics and Thermodynamics of Chromium (VI) Adsorption on Inert Biomasses of *Dioscorea rotundata* and *Elaeis guineensis*. Water. 14(844): 1-15. https://doi.org/10.3390/w14060844

Zaynab M., Al-Yahyai R., Ameen A., Sharif Y., Ali L., Fatima M., Ali-Khan K. & Li S. 2022. Health and environmental effects of heavy metals. Journal of King Saud University–Science. 34(101653): 1-8. https://doi.org/10.1016/j.jksus.2021.101653

CAPÍTULO 6

DE RESIDUO AGROINDUSTRIAL A SOLUCIÓN AMBIENTAL: DISEÑO DE ADSORBENTES CATIÓNICOS SUSTENTABLES A PARTIR DE SUBPRODUCTOS DE LA SOJA

Data de submissão: 15/11/2025
Data de aceite: 02/12/2025

Enrique David Victor Giordano[1]
CONICET-IPROBYQ
Instituto de Procesos
Biotecnológicos y Químicos
Univesidad Nacional de
Rosario (UNR), Argentina
https://orcid.org/0000-0002-1117-7149

Malena Castagnino Schirmer
CONICET-IPROBYQ
Instituto de Procesos
Biotecnológicos y Químicos
Universidad Nacional de
Rosario (UNR), Argentina

Nerina Meglio
Instituto de Procesos
Biotecnológicos y Químicos
Universidad Nacional de
Rosario (UNR), Argentina

Gonzalo Benedetti
CONICET-IPROBYQ
Instituto de Procesos
Biotecnológicos y Químicos
Universidad Nacional de
Rosario (UNR), Argentina

Fernando Ariel Bertoni
Instituto de Procesos
Biotecnológicos y Químicos
Universidad Nacional de
Rosario (UNR), Argentina
https://orcid.org/0000-0002-0141-1253

RESUMEN: Este trabajo presenta el diseño y caracterización de un adsorbente catiónico sustentable obtenido a partir de la cascarilla de soja mediante una ruta de síntesis “one-pot”, que integra en un solo paso la extracción de celulosa y su modificación química. El material resultante, una celulosa microcristalina cuaternizada (CS-Cat), fue analizado mediante FTIR, XRD, SEM y estudios termoanalíticos, confirmando su funcionalización, mayor cristalinidad y cambios morfológicos significativos. La CS-Cat exhibió alta afinidad por colorantes aniónicos, con capacidades de adsorción excepcionales (509–596 mg/g) y cinética ultrarrápida, ajustándose al modelo de Langmuir y a una cinética de pseudo-primer orden. Su comportamiento termodinámico indica un proceso espontáneo y exotérmico, manteniendo eficiencia incluso en medios salinos. Estos resultados posicionan a la CS-Cat como un material avanzado, sostenible y competitivo para el tratamiento de efluentes textiles.

[1] Corresponding author.

PALABRAS CLAVE: adsorción; celulosa microcristalina; síntesis one-pot; cascarilla de soja; colorantes textiles; biorremediación química.

FROM AGROINDUSTRIAL WASTE TO ENVIRONMENTAL SOLUTION: DESIGN OF SUSTAINABLE CATIONIC ADSORBENTS FROM SOYBEAN BY-PRODUCTS

ABSTRACT: This work presents the design and characterization of a sustainable cationic adsorbent obtained from soybean husk through a one-pot synthesis route that combines cellulose extraction and chemical modification in a single step. The resulting material, a quaternized microcrystalline cellulose (CS-Cat), was analyzed using FTIR, XRD, SEM, and thermal methods, confirming successful functionalization, increased crystallinity, and significant morphological changes. CS-Cat exhibited high affinity for anionic dyes, achieving exceptional adsorption capacities (509–596 mg/g) with extremely fast kinetics, fitting the Langmuir isotherm and a pseudo-first-order kinetic model. Thermodynamic analysis revealed a spontaneous and exothermic process, with the material maintaining efficiency even in saline environments. These results position CS-Cat as an advanced, sustainable, and competitive material for tertiary treatment of textile wastewater.
KEYWORDS: adsorption; microcrystalline cellulose; one-pot synthesis; soybean husk; textile dyes; chemical remediation.

1. INTRODUCCIÓN

La industria textil enfrenta el desafío crítico de gestionar efluentes cargados con colorantes sintéticos, los cuales son recalcitrantes y visibles incluso a bajas concentraciones (10-50 mg/L). Asimismo, la problemática ambiental contemporánea exige la búsqueda de estrategias de Economía Circular que permitan transformar residuos en recursos de alto valor añadido. En este contexto, la cascarilla de soja (CS) emerge como un subproducto agroindustrial de interés estratégico. Dada la magnitud de la producción global de granos de soja (superando las 420 millones de toneladas en las campañas recientes), y considerando que la cascarilla representa aproximadamente entre el 5% y el 8% del peso del grano, se estima la generación anual de entre 21 y 33 millones de toneladas de este residuo a nivel mundial.

Ante este desafío de gestión, se propone una solución innovadora: la valorización de la CS mediante una ruta de síntesis química 'one-pot' (en un solo paso) para obtener un adsorbente funcionalizado: la Celulosa Microcristalina Cuaternizada (CS-Cat). Este enfoque metodológico integra eficientemente la extracción de la celulosa (deslignificación y eliminación de hemicelulosa) y su modificación química, lo que permite reducir drásticamente el consumo de agua, tiempo de reacción y uso de reactivos en comparación con los procesos de aislamiento y funcionalización tradicionales.

2. METODOLOGÍA DE SÍNTESIS “ONE-POT”

La innovación central radica en evitar la purificación previa de la celulosa. La síntesis se basa en una reacción de eterificación directa sobre la matriz de biomasa cruda.

- **Protocolo de Síntesis:** Se parte de cascarilla de soja molida (tamiz 60 mesh). La reacción ocurre en medio alcalino a temperaturas entre 70°C y 80°C durante un periodo de 14 a 16 horas bajo agitación constante. El agente cationizante utilizado es el cloruro de N-(3-cloro-2-hidroxipropil) trimetilamonio (CHPTAC).

3. CARACTERIZACIÓN FISICOQUÍMICA

La transformación de la biomasa cruda (CS) al material funcionalizado (CS-Cat) se valida mediante cambios drásticos en sus propiedades estructurales y superficiales.

3.1. ESPECTROSCOPÍA INFRARROJA (FTIR)

El análisis espectral confirma dos fenómenos simultáneos:

- **Funcionalización:** Aparición de un nuevo pico a 1478 cm^{-1}, atribuido a la vibración de flexión de los grupos metilo del amonio cuaternario -$N(CH_3)_3^+$, ausente en la biomasa original.
- **Purificación:** Desaparición completa del pico a 1743 cm^{-1} (estiramiento C=O de grupos acetatos/urónicos en hemicelulosa y ésteres en lignina), confirmando la eliminación efectiva de componentes no celulósicos durante la síntesis.

3.2. DIFRACCIÓN DE RAYOS X (XRD) Y CRISTALINIDAD

Los difractogramas revelan una transición polimórfica y un aumento en el ordenamiento estructural:

- **Transición de Fase:** La estructura cristalina cambia de Celulosa I (nativa) a **Celulosa II** (mercerizada), evidenciada por el desplazamiento de los picos de difracción característicos.
- **Índice de Cristalinidad (CrI):** Se observa un incremento notable del 58.1% en la cascarilla original al 76.4% en la CS-Cat. Esto indica que la eliminación de la matriz amorfa (lignina/hemicelulosa) deja expuestos los dominios cristalinos de la celulosa.

- **Tamaño del Cristal:** Se reduce a 2.72 nm en CS-Cat (comparado con 5.07 nm de una celulosa estándar), sugerente de un reordenamiento estructural intra-fibrilar.

3.3. MORFOLOGÍA (SEM)

Las micrografías electrónicas muestran un cambio textural radical:

- **Biomasa Nativa (CS):** Fibras largas (80-110 µm) y superficie rugosa cubierta de impurezas (ceras, lignina).
- **CS-Cat:** Fibras cortas en forma de varilla (*rod-shaped*) con longitud promedio de 30.93 µm y diámetro de 8.33 µm. La superficie es lisa y limpia, típica de la celulosa microcristalina, confirmando la hidrólisis de las regiones amorfas.

3.4. PROPIEDADES TÉRMICAS Y SUPERFICIALES

- **Análisis Térmico (TGA/DSC):** CS-Cat muestra una menor estabilidad térmica inicial (pico de degradación máx. a ~266°C vs ~336°C de la CS), debido al efecto catalítico de los grupos amonio cuaternario que aceleran la degradación de la celulosa. Sin embargo, no deja residuo carbonoso (char), a diferencia de la CS (3.3%).
- **Carga Superficial (punto de carga cero, pH_{PZC}):** A diferencia de la biomasa nativa (pH_{PZC}= 5.27), CS-Cat no presenta punto de carga cero en el rango de pH 2-12. Mantiene una carga positiva neta constante ($\Delta pH > 0$), lo que la hace un adsorbente aniónico ideal independiente del pH del medio.
- **Hinchamiento (Swelling):** La capacidad de retención de agua se duplica respecto a la materia prima, favoreciendo la difusión de contaminantes acuosos hacia los sitios activos.

4. PROCESO DE ADSORCIÓN (SISTEMA BATCH)

El material se evaluó frente a colorantes aniónicos de gran relevancia industrial: Azul Reactivo 21 (AR-21) y Negro Directo 22 (ND-22).

4.1. ISOTERMAS DE ADSORCIÓN Y CAPACIDAD MÁXIMA

Las isotermas relacionan la cantidad de colorante adsorbido en el equilibrio (Q_e) con la concentración en solución (C_e).

- **Modelo de Ajuste:** Los datos experimentales se ajustan preferentemente al modelo de Langmuir ($R^2 > 0.99$), lo que indica una adsorción en monocapa sobre sitios energéticamente homogéneos (los grupos amonio).
- **Valores de Q_{max}:**
    - Para **AR-21**: Se alcanzan capacidades excepcionales de ~596 mg/g a 25°C.
    - Para **ND-22**: La capacidad máxima es de ~509 mg/g.
    - *Comparativa*: Estos valores son muy superiores a los de otros adsorbentes biológicos citados en la literatura (ej. cáscara de nuez ~131 mg/g, residuos de hongos ~15 mg/g).

4.2. CINÉTICA DE ADSORCIÓN

La velocidad de captura es extremadamente rápida, un factor crítico para aplicaciones industriales.

- **Rapidez:** Se logra eliminar >90% del colorante en el primer minuto de contacto para concentraciones altas (1200 ppm).
- **Modelado:** La cinética sigue un modelo de *pseudo*-primer Orden (PPO**)**, lo que demuestra una interacción electrostática fuerte entre el grupo $-N(CH_3)_3^+$ del adsorbente y los grupos SO_3^- del colorante.

4.3. TERMODINÁMICA Y EFECTO DE VARIABLES

- **Efecto de la Temperatura:** Se observó que el proceso es exotérmico, implicando que la adsorción es más eficiente a temperaturas moderadas, aunque mantiene un alto rendimiento a 60°C. La energía libre de Gibbs es negativa y aumenta con la temperatura, indicando espontaneidad.
- **Efecto de la Fuerza Iónica (Sales):** Contrario a lo que ocurre con muchos adsorbentes, la presencia de sales (5% y 7.5 % de NaCl) no modificó de manera significante a la capacidad de adsorción.

5. CONCLUSIÓN

La celulosa microcristalina cuaternizada (CS-Cat) obtenida mediante la ruta “one-pot” representa un material avanzado que combina la sustentabilidad de la química verde con un rendimiento técnico superior. Su capacidad de carga positiva permanente, alta cristalinidad y cinética rápida la posicionan como una alternativa competitiva al carbón activado para el tratamiento terciario de efluentes textiles, especialmente aquellos con alta salinidad.

CAPÍTULO 7

ENFRIAMIENTO DE PANEL FOTOVOLTAICO PARA AUMENTAR SU DESEMPEÑO ELÉCTRICO

Data de submissão: 09/11/2025
Data de aceite: 02/12/2025

Vicente Flores Lara
Doctor en Ingeniería
Instituto Tecnológico de Apizaco
Departamento de Metal Mecánica
Apizaco, Tlaxcala, México
https://orcid.org/0000-0001-5029-9707

Jorge Bedolla Hernández
Doctor en Ciencias de Ingeniería Mecánica
Instituto Tecnológico de Apizaco
Departamento de Metal Mecánica
Apizaco, Tlaxcala, México
https://orcid.org/0000-0003-3856-6061

Carlos Alberto Mora Santos
Doctor en Ciencias de Ingeniería Mecánica
Instituto Tecnológico de Apizaco
Departamento de Metal Mecánica
Apizaco, Tlaxcala, México
https://orcid.org/0000-0002-6050-6578

RESUMEN: La temperatura de diseño de la tecnología fotovoltaica es de 298 K para lograr su máximo desempeño eléctrico, sin embargo, durante su operación se alcanza temperaturas superficiales, de hasta 365 K, reduciendo significativamente su potencia y eficiencia eléctrica, así como, su nivel de vida útil. En el presente, se estudia técnicas de enfriamiento pasivas aplicadas a 2 paneles fotovoltaicos de diferente capacidad, 110 W y 150 W de potencia nominal respectivamente y 15% de eficiencia eléctrica en ambos. En la parte posterior del panel se hace el acoplamiento del sistema de enfriamiento, a continuación, se hace fluir aire o agua a temperatura ambiente provocando la remoción de calor al panel. Lo anterior genera el enfriamiento con lo que se aumenta su potencia y eficiencia eléctrica, al mismo tiempo que se dispone de energía térmica a través del calentamiento del fluido. Se aumentó su potencia 9 W y la eficiencia eléctrica 5% para el panel de 150 W enfriado con aire, en el caso del panel de 110W enfriado con agua se aumentó la potencia 8 W y la eficiencia eléctrica 2.3%.

PALABRAS CLAVE: enfriamiento; panel; fotovoltaico; desempeño; eléctrico.

COOLING PHOTOVOLTAIC PANELS TO INCREASE THEIR ELECTRICAL PERFORMANCE

ABSTRACT: The design temperature of photovoltaic technology is 298 K to achieve its maximum electrical performance; however, during operation, surface temperatures of up to 365K are reached, significantly reducing its power and electrical efficiency, as well as its lifespan. This study investigates passive cooling techniques applied to two photovoltaic

panels of different capacities, 110 W and 150 W nominal power respectively, both with 15% electrical efficiency. The cooling system is mounted on the back of the panel, and ambient air or water is then circulated through it, removing heat from the panel. This process generates cooling, thereby increasing its power and electrical efficiency, while simultaneously providing thermal energy through fluid heating. The power output increased by 9 W and the electrical efficiency by 5% for the 150 W air-cooled panel; for the 110 W water-cooled panel, the power output increased by 8 W and the electrical efficiency by 2.3%.
KEYWORDS: cooling; panel; photovoltaic; performance; electric.

1. INTRODUCCIÓN

Una de las fuentes de energía sostenible con mayor aprovechamiento, es la solar, considerada como la energía no convencional más utilizada en todo el mundo. La radiación solar es la fuente de todos los tipos de energía renovable. Puede convertirse directa o indirectamente en energía eléctrica mediante sistemas fotovoltaicos (P·V) con eficiencia que oscila entre el 10% y el 20%, o sistemas térmicos, con eficiencia entre 40 % y el 60 % (Ali Maka et al, 2022). Cuando la radiación solar incide sobre las celdas fotovoltaicas, los fotones son absorbidos por los materiales semiconductores de las celdas y aquellos con energía superior a la banda prohibida de dichos materiales constituyen el flujo de corriente eléctrica desde la celda fotovoltaica hacia la carga externa (Aghaei et al, 2022).

Existen diversos parámetros ambientales que afectan al panel solar. Entre ellos, la radiación solar, la temperatura ambiente, la temperatura de la superficie del módulo, la velocidad del viento, la humedad, el sombreado, el polvo, la altura de instalación sobre el nivel del mar. De acuerdo con diversas investigaciones, la irradiancia solar y la temperatura son factores clave en el desempeño eléctrico del panel solar (Aghaei et, al 2022; Espinosa et al, 2023; Pushpendu et al, 2020).

Figura 1. Efecto en la potencia por el aumento de temperatura del panel (Espinosa et al, 2023).

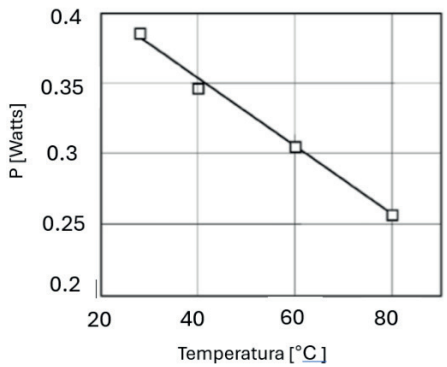

La temperatura de los módulos fotovoltaicos se incrementa por la radiación solar absorbida que no se convierte en electricidad, ocasionando una disminución de su potencia y eficiencia eléctrica y, en consecuencia, su tiempo de vida útil, (Sargunanathan et al, 2016).

Figura 2. Efecto de la temperatura del panel en el desempeño eléctrico (Espinosa et al, 2023).

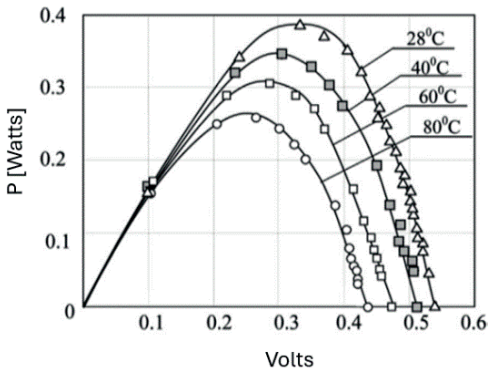

La temperatura de la celda posee un efecto importante en la potencia eléctrica a través de la tensión en circuito abierto y se observa en la curva I-V, figura 2. Así, al aumentar la temperatura, la tensión de circuito abierto disminuye del orden de unos pocos milivoltios por cada grado Celsius de aumento de la temperatura, 2.3 mV/°C para el silicio y entre 2 mV/°C y 2.2 mV/°C en el caso de arseniuro de galio. En el caso de la eficiencia eléctrica, se reduce en alrededor de un 0.45% por cada grado Celsius de aumento de temperatura. Para las celdas de silicio amorfo (a-Si), el impacto es menor, con una disminución de alrededor de un 0,25% por cada grado Celsius de incremento de temperatura, dependiendo del diseño del módulo. Este impacto indeseable puede evitarse parcialmente por medio de remoción de calor idónea con una circulación de algún fluido. Es por ello por lo que se han realizado estudios que han demostrado que al enfriar el panel fotovoltaico aumenta su eficiencia eléctrica considerablemente en celdas solares de silicio monocristalino (c-Si) y policristalino (pc-Si) (Baloch Ahmer et al, 201; Kaiser et al, 2014).

2. MATERIALES Y METODOS

Se emplearon dos paneles fotovoltaicos para evaluar su desempeño eléctrico con diferente capacidad como se indica en las tablas 1 y tabla 2, que incluyen sus datos técnicos, así también, se emplearon dos técnicas de enfriamiento, la primera empleando insertos cónicos adheridos en la superficie posterior del panel fotovoltaico y un canal

rectangular para hacer fluir aire a temperatura ambiente, como fluido de transferencia de calor y provocar el enfriamiento del panel, figura 1. En la segunda técnica figura 2, se empleó una placa de policarbonato alveolar, adherida en la parte posterior del panel, a través de los alveolos se hace transferir agua a temperatura ambiente, la placa alveolar y el flujo de agua hacen la función de intercambiador de calor, retirando calor al panel y enfriándolo.

Tabla 1. Datos técnicos de los paneles fotovoltaicos experimentales 110 W y 150 W respectivamente, para una irradiancia de 1000 W/m² y temperatura ambiente de 25°C [Datos del fabricante].

Ficha técnica del panel solar 110 W				**Ficha técnica del panel solar 150 W**		
Descripción	**Símbolo**	**Valor**	**Unidad**	**Símbolo**	**Valor**	**Unidad**
Potencia nominal	P.max.	110	W	P. max	150	W
Tensión en máxima potencia	V.Mmp	18.1	V	V.Mmp	18	V
Corriente en máxima potencia	I. Mpp	6.12	A	I. Mpp	8.34	A
Tensión de circuito abierto	V.	22.9	V	V.	22.1	V
Corriente de corto circuito	Isc	6.43	A	Isc	9.05	A
Tolerancia de potencia nominal	Pmax	+0-3	W	Pmax	+0-3	W

Figura 3. Obstrucciones en la superficie posterior del panel.

La figura 4, muestra el proceso de enfriamiento del panel. Colocadas las aletas en la superficie posterior del panel, que al mismo tiempo funcionan como obstrucciones al flujo, se hace fluir aire a temperatura ambiente mediante un ventilador axial, el aire se conduce a través de un canal para guiar el fluido hacia las aletas y provocar el enfriamiento.

Figura 4. Esquema del proceso de enfriamiento del panel.

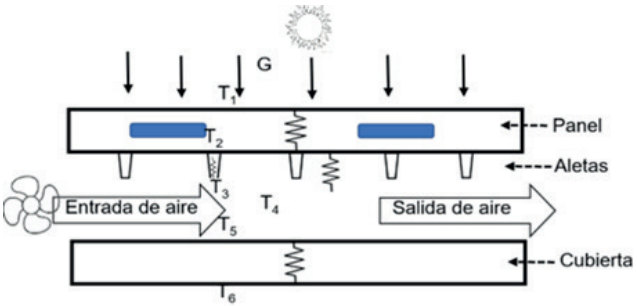

3. RESULTADOS Y ANALISIS

Se monitoreo la temperatura de la superficie del panel solar para diferentes niveles de irradiancia solar, la figura 5 muestra un caso típico, donde los niveles de irradiancia promedio registrados son de 960 W/m². Las temperaturas del panel se registraron en 15 puntos y graficados, se observa que en horarios cercanos al medio día, la temperatura supera los 60°C. La influenciada por la velocidad del viento y la temperatura ambiente provocan fluctuaciones de la temperatura, sin embargo, para el desempeño eléctrico del panel los valores son significativos de tal forma que provocan en la reducción de su capacidad eléctrica.

Figura 5. Temperatura de operación del panel con velocidad de viento de 1.3 m/s y temperatura ambiente de 26°C.

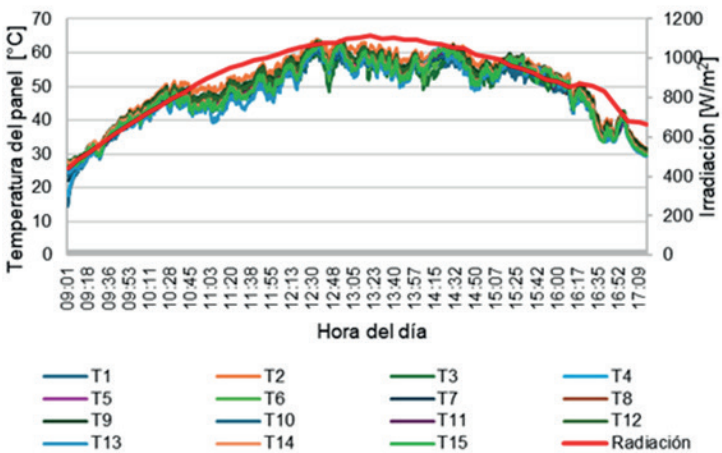

El objetivo del enfriamiento es hacer que los parámetros eléctricos del panel mejoren. Un caso se muestra en la figura 6 empleando un panel con capacidad nominal de 150W, el efecto que tiene disminuir la temperatura del panel en su eficiencia eléctrica, la temperatura disminuye 23°C y su eficiencia aumenta 2%. Para lograr el enfriamiento

se empleó flujo de aire forzado con valor de 0.0469 kg/s. Para comparar los resultados de enfriar el panel con respecto a cuándo no se enfría, la figura 7 muestra a través de la potencia y la eficiencia, el efecto que tiene el enfriamiento, para ello se trabajó con flujo másico de 0.034 kg/s., la mejora en la potencia es 6W mayor con enfriamiento que sin él, en la eficiencia eléctrica es mayor en 1.3% con enfriamiento. Entre la figura 6 y la figura 7, puede notarse la influencia que tiene el valor del flujo másico, con el aumento del flujo se genera mayor enfriamiento y crece la eficiencia.

Figura 6. Aumento de la eficiencia eléctrica por el enfriamiento con aire 0.0469 kg/s, 150W.

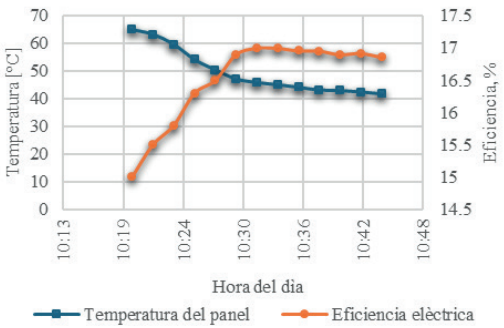

Figura 7. Desempeño eléctrico del panel 150W, con y sin enfriamiento con aire, 0.034 kg/s.

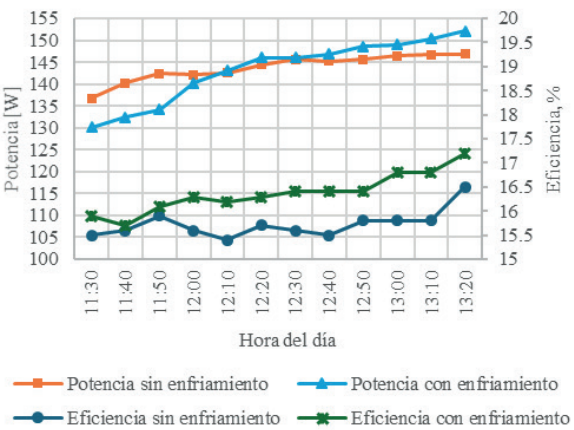

Un tercer caso se muestra en la figura 8, en el que se aumenta el flujo másico hasta 0.08 kg/s, con ello se logra que la potencia aumente 9W y la eficiencia 5% respectivamente, con respecto cuando no se tiene enfriamiento.

Figura 8. Desempeño eléctrico del panel con y sin enfriamiento 150W.

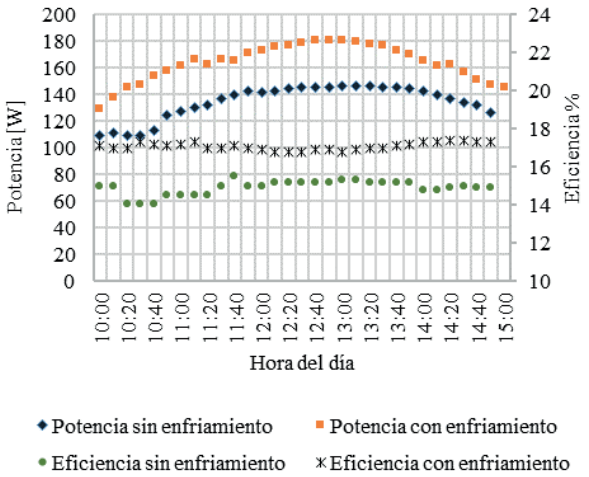

Los siguientes resultados corresponden al enfriamiento del panel de 110W y eficiencia 15%, se emplea la placa de policarbonato y se hace fluir agua a través de los alveolos, el agua a temperatura ambiente (22ºC), irradiancia solar promedio de 820 W/m2, con flujo de 0.076 kg/s. En la figura 9, se muestra que a temperatura del panel de 60°C la eficiencia se reduce a 13.3% y esta va aumentando conforma la temperatura del panel se reduce. En la figura 10, el agua de enfriamiento fue de 23.5°C, e irradiancia solar de 900 W/m² y el mismo flujo 0.076 kg/s. El aumento de la irradiancia y de la temperatura de enfriamiento con respecto al primer caso, provocaron menor enfriamiento del panel con un gradiente de 21.5°C y 28.1°C para el primer caso. De la misma forma con la eficiencia, en el segundo caso se aumentó 2% y para el primero 2.3% respectivamente. En la figura 10, también se muestra el aumento de la potencia con respecto a la disminución de la temperatura.

Figura 9. Eficiencia eléctrica del panel 110 W con enfriamiento a base de agua.

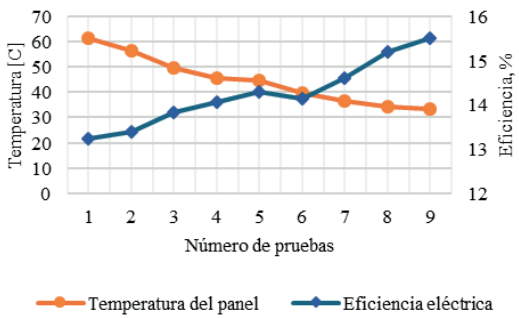

Figura 10. Desempeño eléctrico del panel fotovoltaico 110W enfriamiento con agua.

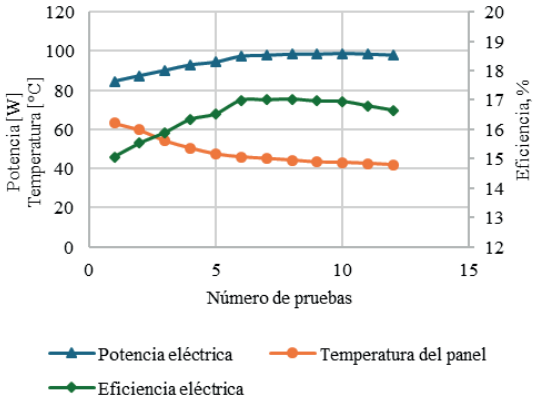

4. CONCLUSIONES

Se estudiaron dos técnicas de enfriamiento de paneles fotovoltaicos para analizar el efecto en el desempeño eléctrico, a través de la potencia y la eficiencia eléctrica respectivamente. Una técnica correspondió al enfriamiento de un panel de 150W usando elementos obstructores de flujo adheridos al panel, así como, un canal rectangular por el cual se hizo fluir el aire con dos valores de flujo másico, para este caso se observa que, a mayor flujo, mejor enfriamiento y así el desempeño eléctrico, que en el mejor de los casos se aumentó la potencia 9W y la eficiencia 5% con flujo másico de 0.08 kg/s. La segunda técnica correspondió al uso de una placa de policarbonato alveolar adherida al panel haciéndose fluir agua a través de los alveolos, el mejor caso es el que se presenta, con un valor de flujo de agua de 0.076 kg/s elevando la potencia 8W y la eficiencia 2.3%. Con base en las propiedades termofísicas de los fluidos principalmente el calor especifico, siendo 4 veces mayor en el agua que en el aire, en el caso del aire se provocó un gradiente de 23.2ºC mientras que con el agua de 28ºC a pesar de que el contacto entre el agua y el panel no es directo como entre el aire y el panel. Finalmente, se probó en este trabajo que es posible aumentar el desempeño del panel fotovoltaico mediante técnicas de enfriamiento, atención especial requiere el conocer el valor del flujo másico que mejoré el enfriamiento, ya que al incrementarse se logra mayor enfriamiento, pero se requiere más energía para mover el flujo, por lo que podría resultar contraproducente. La razón por la cual se busca el enfriamiento de paneles fotovoltaicos es para operarlos donde sus parámetros eléctricos alcanzan valores cercanos a los de diseño, otra razón es que a través del enfriamiento con un fluido puede disponerse de energía eléctrica y energía calorífica de forma simultánea, esta última para procesos térmicos, como es el caso de

calefacción, tratamiento de alimentos para su conservación mediante la deshidratación o la disposición de agua caliente.

REFERENCIAS

Ali Maka O.M., and Jamal Alabid M. Solar energy technology and its roles in sustainable development. Clean Energy, (2022), 6, 476–483.

Aghaei M., Fairbrother A., Gok A., Ahmad S., Kazim S., Lobato K., Reinders A., Schmitz J., Theelen M., Yilmaz P., Kettl J. Review of degradation and failure phenomena in photovoltaic modules. Renewable and Sustainable Energy Reviews 159 (2022) 112160.

Espinosa-Ramírez B., Garrido-Hernández A., García-Domínguez G., Vargas-Leóna J. E., Castillo-Minjarez M. Efecto de la temperatura en la eficiencia de paneles fotovoltaicos. Publicación Semestral Pädi Vol. 11, No. Especial 5(2023) 184-190. https://doi.org/10.29057/icbi.v11iEspecial5.11841

Pushpendu D., Sudhakar K., Archana S., Kirpichnikova I. Advanced cooling techniques of P.V. modules: A state of art. Case Studies in Thermal Engineering 21 (2020) 100674.

Sargunanathan S., Elango A., Tharves Mohideen S. Performance enhancement of solar photovoltaic cells using effective cooling methods: A review, Renewable and Sustainable Energy Reviews, 64 (2016) 382–393.

Baloch Ahmer A.B., Bahaidarah Haitham M.S., Palanichamy G., Al-Sulaiman Fahad A. Experimental and numerical performance analysis of a converging channel heat exchanger for PV cooling, Energy Conversion and Management 103 (2015) 14–27.

Kaiser A.S., Zamora B., Mazón R., García J.R., Vera F. Experimental study of cooling BIPV modules by forced convection in the air channel, Applied Energy 135 (2014) 88–97.

CAPÍTULO 8

ECODESIGN: SHAPING A SUSTAINABLE FUTURE WITH PLASTIC PRODUCTS

Data de submissão: 11/11/2025
Data de aceite: 02/12/2025

Ana Barroso
PIEP - Pólo de Inovação em Engenharia de Polímeros
Guimarães, Portugal
https://orcid.org/0009-0009-4572-0478

André Gomes
PIEP - Pólo de Inovação em Engenharia de Polímeros
Guimarães, Portugal
https://orcid.org/0009-0007-3345-0226

Bruno Sousa
PIEP - Pólo de Inovação em Engenharia de Polímeros
Guimarães, Portugal
https://orcid.org/0000-0003-0388-8087

Ângelo Marques
PIEP - Pólo de Inovação em Engenharia de Polímeros
Guimarães, Portugal
https://orcid.org/0009-0008-8667-8731

Rui Oliveira
PIEP - Pólo de Inovação em Engenharia de Polímeros
Guimarães, Portugal
https://orcid.org/0000-0001-5480-5056

Filipa Carneiro
PIEP - Pólo de Inovação em Engenharia de Polímeros
Guimarães, Portugal
https://orcid.org/0000-0002-4439-4166

ABSTRACT: In a context where plastic is often negatively perceived for its environmental impact, there's a noticeable trend towards replacing it with alternatives like paper or composites. However, these transitions often occur without thorough assessment, potentially leading to the development of new products that may not be environmentally beneficial. Ecodesign emerges as a key solution for sustainability. This research highlights innovations and best practices for designers working on plastic-centric projects. It explores how ecodesign utilizes technological advances to reduce the environmental impact of plastic products. Emphasizing early-stage research and planning, the research advocates principles like life cycle assessment, biomimicry, and circular economy, demonstrating their integration for projects with environmental, social, and economic responsibility. To demonstrate the practical application of this approach, the PRR "NIRVANA" project will serve as a reference and result to analyse the development of sustainable modular systems for more sustainable hydroponics.

KEYWORDS: ecodesign; plastic; sustainability; education; biomimicry.

[1] Uma versão anterior deste trabalho foi publicada em DESIGN COMMIT – 1st International Conference on Design and Industry, 2024.

1. INTRODUCTION

During the 18th and the 19th century, the world underwent significant industrial evolution. New technologies were developed, mass production increased significantly, and urban spaces expanded as well. This evolution, despite being of great importance for technological and economic progress for humanity, also posed a significant environmental threat (Allen, 2017). It wasn´t long until industrial growth started to affect the environment with severe problems. The entire bionetwork and natural system components like water, air, soil and bio-diversity started to face relentless consequences. Realizing the seriousness of the problem, the impacts needed to be analysed and there was a demand for conscious environmental response or solution (Patnaik, 2018). Ecodesign has emerged as a proposed solution to these current problems. It seeks to combat the adversities resulting from industry and excessive consumption by developing alternatives or improving existing products with a smarter and more environmentally responsible approach (Dewberry, 1996). Sustainable design, or ecodesign, is based on fundamental rules that assist in making informed decisions regarding the product under development. These 'rules' must be based on facts, and therefore, extensive preliminary research is necessary to ensure that the product will truly be more sustainable than its competitor (DeArmitt, 2020).

It could be argued that industrial design is one of the most harmful professions towards the planet, however industrial designers can be the problem as well as the solution (Papanek, 2005). With this said, designers have a huge opportunity to propose solutions that could mitigate the global ecological crisis and improve the quality of life for the future. This should be the design challenge of this generation (Ramirez, 2007).

This research will explore this theme focused on a specific type of material: polymers, delving into their various applications, environmental impact, public perception, and, most importantly, how they can be utilized as a more sustainable alternative.

2. ECODESIGN

In the search for a solution to the ascending environmental threats, the United Nations held the Conference on the Human Environment in Stockholm in 1972. This event allowed for the worldwide recognition of the importance of protecting the environment, changing habits and approaches with this goal in mind, and adopting more environmentally responsible measures. It was during this conference that sustainable development was brought up for the first time (Handl, 2012). Later it was described in this manner:

> "Sustainable development is development that meets the needs of the present without compromising the ability of future generations to meet their own needs" (*UN World Commission on Environment and Development, Ed., Report of the World Commission on Environment and Development*, 1987)

In the subsequent years, efforts were made to thoroughly understand the problem and explore ways to address it. It was concluded that some of the main issues included the indiscriminate extraction of limited natural resources, excessive production, dangerous emissions, improper waste disposal, and the widespread use of toxic chemicals (Patnaik, 2018). In response to this adversity, the concept of ecodesign emerged. It seeks to combine the principles of industrial design with environmental ideologies by developing products that take into account their entire life cycle, materials, waste, applications, and production from an early stage. This type of design is considered an integral part of global efforts to combat climate change and preserve the environment. Furthermore, it is increasingly recognized by businesses and governments as a sound investment, as it also meets the demands of environmentally conscious consumers. Ecodesign is a concept that integrates multifaceted aspects of design and environmental considerations and the objective is to create sustainable solutions that satisfy human needs and desires Its main goal is to develop products that contribute to sustainability by reducing its environmental impact throughout the life cycle, along with requirements such as functionality, quality, safety, cost, ease of production, ergonomics and aesthetics (Karlsson & Luttropp, 2006).

2.1. ECODESIGN TOOLS

When discussing ecodesign it's essential to highlight the importance of the research phase, since it plays a pivotal role in the design process by providing a foundation for informed decision-making. With this in mind, a series of processes were developed to serve as ecodesign tools. These tools must be integrated into the product development process as early as possible to avoid possible errors in a more advanced phase of the development, implying larger costs and risks (Camocho, 2022).

> "Rational planning constitutes an essential tool for reconciling any conflict between the needs of development and the need to protect and improve the environment." – (*Report of the United Nations Conference on the Human Environment, Stockholm, 5-16 June 1972*, 1972)

In addition to guidelines, which will also be presented, there are two very useful tools for this purpose.

2.1.1. Life cycle assessment (LCA)

Life-cycle assessment (LCA) is a process created to evaluate the effects that a product has on the environment over the entire period of its life thereby increasing resource-use efficiency and decreasing liabilities. It can be used to study the environmental impact of either a product or the function the product is designed to perform. It attempts to measure the total environmental effects of a product "from cradle to grave" (Duda & Shaw, 1997). It is used to analyse and quantify environmental impacts in various categories, such as natural resource consumption, greenhouse gas emissions, air and water pollution, among others. This analysis has a major importance for the development of products since it provides lots of information to the developers about the impact of the product in each stage of its life cycle. The general categories of environmental impacts in need of consideration are human health, use of resources and ecological consequences. This knowledge is vital to understand what needs to be improved and to compare the impact of different materials, manufacturing processes allowing the designer to make more conscious choices when developing a product (Klöpffer & Grahl, 2014).

The life cycle of a product can be based on a linear economy or in a circular economy. In a linear product life cycle, the product is designed in a way that it is produced, distributed and discarded as waste after it is used or after it stops serving its purpose. This type of economy is known as a non-sustainable one because it shortens the product life cycle, it generates more waste and it causes pollution and resource depletion (Nasir et al., 2017).

Nowadays, when developing eco-friendly products, the goal is to bet in a circular economy. This model pretends to minimize waste and environmental impact by aiming to keep products and materials in use for as long as possible. It promotes a "cradle to cradle" approach implying that, at the end of a life cycle, the product doesn't need to turn into full waste, and instead it can be repurposed (Mestre & Cooper, 2017)

After understanding what is a product life cycle, it's possible to comprehend how a LCA (Life Cycle Assessment) is made. In a simplified manner, when making a LCA it's necessary to collect data on everything involved (energy, materials, waste ...) at every stage of the cycle, study this information and analyse the impact on the environment (emissions, resource use...), understanding what the results mean and in which stages the product is more impactful, etc (Duda & Shaw, 1997). After having a well-done LCA it's possible to improve the product in a much more informed and intelligent manner. Understanding what stages are the most impactful in a product life cycle can result in upgrades adjusted to that data.

2.2. BIOMIMICRY

Biomimicry can be defined as a branch of science that emulates nature in the search for optimized solutions to a variety of problems. It is often considered a tool or approach within the field of ecodesign and its underlying concept is that designers and engineers pay attention to the details and designs of natural systems, using them as a source of inspiration for effective, sustainable and renewable solutions to problems that compete with environmental sustainability. (Kennedy et al., 2015).

A good example of biomimicry being used for ecodesign is the design process in the development of the "Shinkansen" the Japanese Bullet Train inspired by the kingfisher. The kingfisher is a bird that is able to cut through the air and dive into the water to catch prey without causing any splashes. Many tests were conducted and the conclusion was that aquatic kingfishers had improved drag reduction properties in their beak structures and thus were more suited for diving in comparison to their terrestrial relatives. Using biomimicry principles, the front part of the train was redesigned to resemble the shape of the kingfisher's beak. This adaptation massively decreased the drag, improving the speed and fuel economy (Sreeramagiri, 2021).

Fig. 1. Japan's Shinkansen Bullet Train and a kingfisher - Biomimicry example.

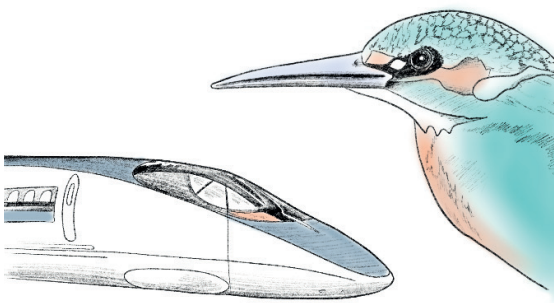

2.3. ECODESIGN GUIDELINES

Nowadays where environmental sustainability is paramount, the concept of Ecodesign has emerged as a powerful tool for fostering innovation and reducing the environmental impact of products. In an effort of developing a simple tool in ecodesign education, the checklist and guidelines approach started to be used for a quick evaluation of the product's environmental profile. The purpose of these guidelines is to present to designers intelligent questions and suggestions for the design team to consider to solve

problems. Many checklists and guidelines were formulated, however the Ten Golden Rules, proposed by Luttropp and Lagerstedt (2006), represent the most significant example of this typology of design recommendations (Rossi et al., 2016). By adhering to these principles, we can not only mitigate the environmental footprint of our creations but also align our efforts with the global imperative for a more sustainable future.

2.3.1. "Ten Golden Rules" by (Luttropp & Lagerstedt, 2006)

1 - Do not use toxic substances and utilize closed loops for necessary but toxic ones.

When developing a product, it's important to plan it with its potential environmental risks in mind so that they can be eliminated or minimized. Many times products end up in the municipal household waste. The consequence is that valuable materials are not recovered and hazardous substances will be problematic at disposal. An appropriate ecodesign strategy should focus on minimizing the content of materials with a heavy "ecological rucksack" as these are not always recycled, and of hazardous materials which cause additional expenses and efforts in treatment processes. It's possible to reduce of negative environmental impacts through the use of environmentally friendly materials, recycled materials, renewable raw materials so when the use of this kind of materials is possible, it should always be pursued. However, in cases in which this substitution is not possible, it's important to find ways to minimize the use of these materials and ways to reuse them (Schischke et al., 2005).

2 - Minimize energy and resource consumption in the production phase and transport through improved housekeeping.

If it's the manufacture stage that's making the most trouble, the focus should be in studying the possibility of using manufacture procedures that use less resources (energy, water...) or that bet on renewable energy sources, Designing the product so that the material needs to go through less manufacturing processes, can also have a big influence on sustainability of its production. Increasing material efficiency through sorting and recycling of waste is a good way to keep the materials in a circular economy and it could also bring economic benefits to the company. The distribution can also be a problematic stage, ecodesign can be used to soften its impacts by designing the products in a shape that optimizes its organization so that a single truck, for example, can transport more units at a time, or by making the product lighter so that the fuel consumption is lower (Nebe et al., 2018).

3 - Use structural features and high-quality materials to minimize weight in products, if such choices do not interfere with necessary flexibility, impact strength or other functional priorities.

By reducing the required amount of material in a product and its packaging, the start and the end of the life cycle of the product can be greatly improved since it would now be possible to produce more products with the same amount of material. This can be done through design for optimum strength, integration of functions, etc. Nowadays a new design assisting process is in use: Topology optimization is a mathematical method that has been used to reduce material usage of a given structure through optimizing its design considering a given set of loads, boundary conditions or constraints. The technique has been used in the mechanical, civil, and the aerospace industries improving fuel efficiency by reducing the weight of its mechanical parts without compromising the strength (Lee et al., 2023) .

4 - Minimize energy and resource consumption in the usage phase, especially for products with the most significant aspects in the usage phase.

Even though energy is consumed across all of the phases of a product life cycle the level of energy consumed in each phase varies significantly depending on the product. Electrical products are typically great contributors to environmental impact due to the consumption of electricity during the “use stage”. To prevent and reduce ecological consequences of a product when it is being used the design can be really useful. The handling of products can be improved through adaptability, ergonomics, short set-up time, ... Principles of action aiming at waste prevention should be applied so that waste resulting on the use of the product can also be minimized. For example, when developing a coffee maker, the capsules should also be considered and designed in an ecological way since they will produce most of the waste during the product use stage (Seow et al., 2016).

5 - Promote repair and upgrading, especially for system-dependent products. (e.g. cell phones, computers and CD players).

Improved functionality through up-grading, multiple functions, can have positive impacts in the planet. An example of an improvement like this is when a product has more than one functionality, this type of products can substitute many different products possibly reducing the demand for their production. Facilitating reparability and easy-maintenance in eco-design is essential for promoting sustainability. Products that are easy to repair extend their useful life, reduce the need for frequent replacements and minimise environmental impact. By making products easy to maintain, we promote repairability,

extending their useful life and reducing the environmental impact associated with manufacturing and disposal. This approach is in line with a circular economy, encouraging responsible consumption and the conservation of resources. The maintenance of a product can be improved by choosing or developing replaceable components, ensuring maintenance with standard tools, betting on a design for assembly and disassembly, etc (Kishore, 2022).

6 - Promote long life, especially for products with significant environmental aspects outside of the usage phase.

When developing a product, it´s crucial to ensure it has an appropriate life time. A bad design practice regarding this topic is programmed obsolescence which refers to the design and production of goods with the intention of having a limited lifespan, becoming obsolete or non-functional after a certain period. This business strategy aims to create mass consumption harming the environment. A result of shorter lifespan is that more waste is produced which in many circumstances ends up in landfills. From a life cycle thinking perspective, the resource efficiency of such systems is said to be very low (King et al., 2006). With this in mind, it's easy to recognize that the product's lifespan from the outset is an important factor in the sustainability of a product, which should be extended as much as possible (Rivera & Lallmahomed, 2016).

7 - Invest in better materials, surface treatments or structural arrangements to protect products from dirt, corrosion and wear, thereby ensuring reduced maintenance and longer product life.

The selection of the materials for a product can represent a great improvement in the sustainability of a product. When a material is better and able to resist the loads and environment that the product will be exposed to, the product life-cycle can be extended without needing much maintenance or substitution of components (Luttropp & Lagerstedt, 2006).

8 - Prearrange upgrading, repair and recycling through accessibility, labelling, modules, breaking points and manuals.

The upgrading and repairability of a product can and should be facilitated by making the accessibility to components easy, clear labelling for identification and sorting, modular design for disassembly, strategically placed breaking points to aid in disassembly, and comprehensive manuals to guide users through maintenance and repair processes (Luttropp & Lagerstedt, 2006).

9 - Promote upgrading, repair and recycling by using few, simple, recycled, not blended materials and no alloys.

When developing a product, it's advisable to minimize the number of materials used, favouring simple material compositions, giving priority to recycled materials, avoiding blended materials, and refraining from using alloys, which can complicate recycling processes. The use of recyclable materials helps divert waste from landfill, conserves resources and reduces the environmental impact associated with the extraction of raw materials and manufacturing. Recycling plays a crucial role in promoting a circular economy, closing the loop on the use of materials and encouraging a more sustainable approach to resource management. (Pigosso et al., 2010)

10 - Use as few joining elements as possible and use screws, adhesives, welding, snap fits, geometric locking, etc. according to the life cycle scenario.

Facilitating disassembly in design involves making products easy to take apart for maintenance, repair or recycling. This approach enhances sustainability by promoting resource recovery, recycling efficiency and reducing environmental impact. Design for disassembly can be applied by minimizing the use of joining elements, especially the ones that require the use of an extra component or material (Favi et al., 2019).

3. POLYMERS

The German chemist Hermann Staudinger presupposed, in 1920, the existence of lengthy molecules. The idea was that macromolecules could be made by stringing together a chain of many short molecules, causing some skepticism amongst his peers. In 1950 the term "polymer" was internationally adopted as the standard for this type of material (Lintsen et al., 2017). It was discovered a way to produce man-made polymers which are typically addressed as plastics.

> "Polymers can be defined as macromolecules formed by linking together repeating monomer units. This definition may seem a little daunting and confusing to those unfamiliar with this field, but it turns out that polymers are all around us and are present in nature." (DeArmitt, 2020)

This discovery has boosted many technological advances that resulted in a huge improvement in our quality of life since they are very versatile materials. In the field of medicine, plastics played a huge role and contributed to reduce the risk of infection and improved healthcare since it can be found in lots of equipment. Its use revolutionized the food industry, its use in the packaging extended the shelf life of the products and, in consequence, food waste was reduced. The use of plastics in transportation made

vehicles lighter, safer and more efficient. In short, with the appearance of this new material in the industry, it was possible to innovate in product design, architecture and technology since it was now possible to create things that previously would not have been possible or as efficient (DeArmitt, 2020).

3.1. SUSTAINABILITY IN POLYMERS

Since plastics started being used their growth hasn't stopped. Their many properties and applications aligned with the easy and cheap manufacturing are greatly related to this increase. In a time where environmental awareness and sustainability are key topics in society, the public is demanding for environmental change. This well-intentioned goal, when driven by misconceptions and poorly supported info, can inadvertently lead to the opposite effect increased waste, carbon emissions, and pollution. With this in mind the question arises: Are plastics sustainable?

Considering the materials and manufacture involved it's possible to conclude that the main starting material used for plastics is crude oil. The current reliance on crude oil for plastic production is unsustainable, as the rate of consumption far outpaces the natural formation of fossil fuels, however it's also important to keep in mind that only 4% of crude oil is applied in plastics. On top of that, the refining of crude oil releases SO_2 contributing to acidification and the production of plastics as a whole also releases chemicals. On the other hand, there's room for improvement in the manufacturing of plastics. The emissions resulting from plastics manufacturing have been reducing noticeably during the last 20 years. The crude oil can be substituted by other materials like coal, which has much larger reserves, natural gas or, ideally, vegetable raw materials that are biodegradable. Biologically degradable plastics may represent a great approach relating to the disposal and use of limited resources but when they are analysed in LCA they tend to have a negative result caused by the energy expenses associated with agriculture. It's also critical to consider that the use of crude oil to make plastics is preferable than direct burning since it may save energy during the period of use and some energy can be exploited at the end of the life cycle. This small advantage in plastic waste incineration will decrease in importance since nowadays energy is turning renewable making it an extra way to emit CO_2 and other harmful gases (Mulder, 1998).

Regarding the distribution phase of plastic products, these represent great improvement. Their low weight represents a reduction of costs regarding fuel and energy of transportation (Mulder, 1998). Moreover, the significant design flexibility offered by plastic can be harnessed to create products that are easier to arrange, thereby optimizing space and allowing for the transportation of more products in a single shipment.

Single-used products also represent a problem in plastic usage. Although some products need to be single-use (due to hygiene or health reasons for example) there are many products that should be developed to sustain a longer use stage (DeArmitt, 2020). It is estimated that 50% of plastic objects are developed for single-use and just 20% to 25% is intended for long-term use. The best way to combat this problem is to invest in producing products that are able to endure a long time in use. When a good material selection is made it is possible to respond to this requirement successfully since plastics have many qualities that make them durable (Geyer et al., 2017).

According to Industrial Ecology Professor Roland Geyer, despite the potential for recovery, approximately 50% of the plastics produced lack sufficient value to make their recovery economically viable. As a result, only 2% of the plastic waste generated since the 1950s has been recycled, while 6% has been incinerated, and the vast majority (about 92%) has been landfilled or disposed of in the natural environment. (Geyer et al., 2017). According to the book "The Plastics Paradox" by Chris DeArmitt, a leading authority in materials engineering, it doesn't take too much energy to recycle most plastics many times and without a major loss in properties. About 87% of plastics, type one through six, can be recycled. Given this perspective, Chris DeArmitt argues that the United States has the potential to significantly increase its recycling efforts, especially considering that Europe is way ahead in recycling rates. One factor contributing to this gap is the higher cost of recycled plastic, coupled with its less appealing colour options, which presents challenges in marketing and selling of these materials. (DeArmitt, 2020) (Wecker, 2018).

The end of the life cycle of plastic products sparks lots of controversy and contradictory information making it harder for most people to understand what is true or false. When reading an article like "Plastic: Reduce, Recycle, and Environment" it's implied that plastics take roughly 500 to 1000 years to break down into little pieces making them not biodegradable. With this in mind it is also recommended to ban polystyrene shopping bags and the increasing level of plastic manufacturing until the recycling process is greatly improved or another solution comes up (Bano et al., 2020). In contrast Chris DeArmitt states that the claims suggesting that plastics persist for 1000 years are unfounded, that plastics are unstable materials and a regular grocery bag breaks down and disappears in less than a year when left outside (DeArmitt, 2020).

3.2. PUBLIC PERCEPTION

Plastics have been a subject of public scrutiny, often blamed for environmental issues without substantial evidence. One example of poor decision due to lack of proper

research done beforehand is the substitution of plastic bags for paper bags in some supermarket brands. This change is seen as sustainable and a good initiative by the general public since plastics are usually perceived as the worst material for the environment unlike paper. However, upon conducting thorough research on the subject and analysing numerous life cycle assessments (LCAs) of plastic bags produced with various materials, it becomes evident that this decision leans more towards being a marketing strategy rather than an ecological one. (DeArmitt, 2020)

By consulting many LCA it's possible to conclude that both of the materials with the least ecological impact were plastics: the standard polyethylene bag emerged as the most environmentally sustainable option when used singularly but the eco-friendliness of a reusable polypropylene bag surpassed that of its single-use counterpart after several uses. Considering the paper bags that emerged as an alternative, it is confirmed that even when produced from recycled material, these represent a significantly greater environmental impact than plastic since it demands higher energy consumption increasing CO2 emissions, uses more water, and involves a greater quantity of chemicals. Another disadvantage of this alteration in material is that paper bags are more fragile making its reutilization harder than a plastic bag. (Kimmel, Sc.D., 2014; Morris & Seasholes, 2014; O'Farrell, 2009)

> "The study results support the conclusion that any decision to ban traditional polyethylene plastic grocery bags in favour of bags made from alternative materials (compostable plastic or recycled paper) will be counterproductive and result in a significant increase in environmental impacts across a number of categories from global warming effects to the use of precious potable water resources." (Franklin Associates & Council for Solid Waste, 1990)

To consider if a change in a product is for the better or for the worst it's necessary to study a LCA of the current product and a LCA of the product with the change implemented to understand which version is the most sustainable. On top of choosing the right material, it's vital to understand that it is the human behaviour that is primarily responsible for littering and not the material itself. Education and responsibility are considered key to addressing the litter problem. (DeArmitt, 2020)

4. RESULTS "NIRVANA"

To demonstrate the practical application of this approach, the "NIRVANA" project will serve as a reference to analyse the development of modular systems for more sustainable hydroponics.

Currently, in line with the increasing need for higher and more efficient water management, coupled with a growing demand for large quantities of quality agricultural

products, hydroponic farming has been gaining more prominence compared to traditional agriculture. Here, we propose the development of a system using recycled plastic as a base instead of the typical metallic materials used in similar products.

Within the Sustainable Plastics project, under PPS8: NIRVANA, led by the Logoplaste Innovation Lab, as part of the Mobilizing Agendas (PRR) for Sustainable Plastics, several ecodesign principles were implemented in the development of this product. The co-promoters of this project are “J.Prior”, “PIEP” and “Prilux”. A life cycle assessment (LCA) will be conducted to ensure its sustainability. The plastic will be chosen with durability and recyclability in mind, with the aim of achieving 100% recyclability and incorporating recycled materials. The design was optimized for assembly and disassembly, allowing for easy distribution and storage by ensuring that the systems fit together seamlessly. Transitioning from metallic to polymeric materials also aids in distribution. Additionally, these systems facilitate a semi-closed water cycle for hydroponics, prolonging water reuse and reducing waste.

In order to fulfil the objective of having a reduced weight and at the same time improving the structural performance of the system, the methodology of combining engineering with eco-design was applied. This was achieved using structural simulations to analyze the forces applied to the gutter during the hydroponic process in order to understand where it was possible to remove material without compromising the performance.

Fig. 2. Concepts for ribs in the “W” profile.

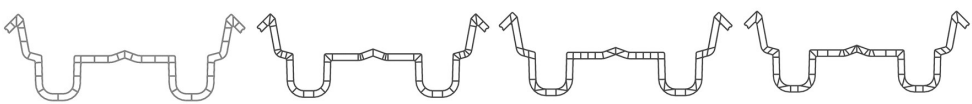

Fig. 3. Structural simulation of selected concept.

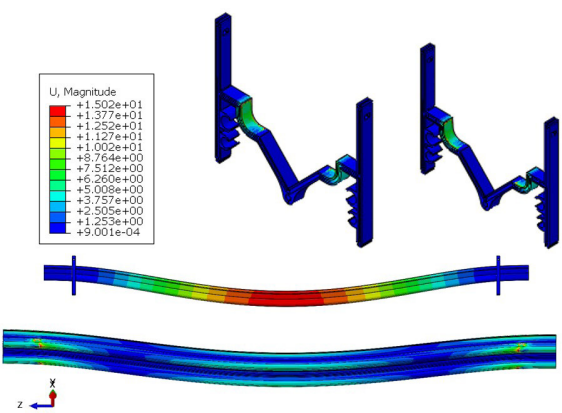

All case studies were subjected to a load equivalent to the weight of the plantings (70kg/3m), and the maximum displacement of each concept was analyzed, searching for the one that would have the lowest maximum displacement. The concept selected was the third one because it had the lowest weight with the best performance ratio. This decision was done having in mind the durability, performance and the material usage. These measures not only seek to optimise the system's efficiency, but are also in line with ecodesign principles, promoting sustainability and efficiency throughout the product's life cycle (Luttropp & Lagerstedt, 2006).

5. DISCUSSION

In light of this, it's accepted that the materials as a whole are not the enemy and they need to be well understood to use them in the most responsible way. Plastics, even though they have an infamous reputation, offer lots of advantages. They have very versatile properties so they can be used to perform the same function as other materials using less quantity, making it lighter and with less residue and they contribute greatly to the sustainability of many products. Overall, this material can enable a modern lifestyle while also protecting the environment as long as it's used in a responsible manner. This can only be done by understanding the impacts and characteristics of the polymer intended to use to make sure it is a good option that will allow the production of a product as functional and ecologic as possible.

Designers bear significant responsibility as they are instrumental in shaping the future products, which should prioritize sustainability. Plastics, in many instances, can offer the most appropriate and environmentally friendly solution. It is up to us to discern these instances and leverage this material to safeguard our environment. For this to happen, it's important that information about material impacts gets clearer and free from misinformation so that everyone can better understand materials and make informed decisions, not only in the development of new products but also in their acquisition. When people lack sufficient knowledge about something, it becomes easier to manipulate their perception of it, and individuals typically gravitate toward things they believe they understand better.

6. RECOMMENDATIONS FOR FUTURE WORK

Concerning the "NIRVANA" project, there are opportunities for enhancement. Improving the stackability of the gutters through minor modifications can ensure seamless fitting during distribution. Additionally, developing the gutter in two separate parts could

facilitate the separation of black and white components for recycling. An intriguing solution to explore could involve developing a bio-based polymer for certain components, utilizing bio-waste generated during cultivation.

Research and innovation should be encouraged to continue to seek and develop materials with better environmental outcomes. These efforts and transitions should be incentivized and embraced by product developers in order to contribute to change.

7. CONCLUSION

Ecodesign has the potential to significantly improve the environmental condition of the world. For it to be effectively implemented, it is important for it to be integrated into the education of designers and consistently encouraged and valued. In the decision-making process of product development, all stages of its lifecycle should be considered. The manufacturing processes, materials, and morphology should be adjusted to ensure the product is as environmentally friendly as possible while remaining economically viable. With these concepts as a foundation, understanding which materials to apply in specific situations is crucial. Often, plastic will be the chosen material, and for it to be applied responsibly, understanding its properties and impacts is essential. When materials are well understood, they can be utilized to maximize their benefits and contribute to a greener future.

This research also explores the intersection between engineering and eco-design, using the project "NIRVANA" project as a practical example to develop modular systems for more sustainable hydroponics. Faced with the growing importance of sustainability in product design, the combination of these disciplines emerges as a multifaceted approach to address both ecological concerns and consumer demands. The paper sets out a new approach that seeks to optimise the structure of the product, reduce its weight, making it more durable and recyclable.

REFERENCES

Allen, R. C. (2017). *The Industrial Revolution: A Very Short Introduction*. Oxford University Press.

Bano, N., Younas, T., Shoaib, F., Rashid, D., & Jaffri, N. (2020). Plastic: Reduce, Recycle, and Environment. Em I. Dincer, C. O. Colpan, & M. A. Ezan (Eds.), *Environmentally-Benign Energy Solutions* (pp. 191–208). Springer International Publishing. https://doi.org/10.1007/978-3-030-20637-6_10

Camocho, D. (2022). *Transition to Circular and Sustainable Economy through Design*. IADE - UE - Faculdade de Design, Tecnologia e Comunicação.

DeArmitt, C. (2020). *The plastics paradox: Facts for a brighter future* (First printing). Phantom Plastics LLC.

Dewberry, E. (1996). *Ecodesign - Present Attitudes and Future Directions: Studies of UK company and design consultancy practice* [Phd, The Open University]. https://oro.open.ac.uk/19845/

Duda, M., & Shaw, J. S. (1997). Life cycle assessment. *Society*, *35*(1), 38–43. https://doi.org/10.1007/s12115-997-1054-x

Favi, C., Marconi, M., Germani, M., & Mandolini, M. (2019). A design for disassembly tool oriented to mechatronic product de-manufacturing and recycling. *Advanced Engineering Informatics*, *39*, 62–79. https://doi.org/10.1016/j.aei.2018.11.008

Franklin Associates, & Council for Solid Waste. (1990). *Resource and environmental profile analysis of polyethylene and unbleached paper grocery sacks: Final report*. Franklin Associates, Ltd. https://nrellibrary.nrel.gov/store/Alma/02LIB050120.pdf

Geyer, R., R. Jambeck, J., & Law, K. L. (2017). *Production, use, and fate of all plastics ever made*. https://doi.org/10.1126/sciadv.1700782

Handl, G. (2012). *DECLARATION OF THE UNITED NATIONS CONFERENCE ON THE HUMAN ENVIRONMENT (STOCKHOLM DECLARATION), 1972 AND THE RIO DECLARATION ON ENVIRONMENT AND DEVELOPMENT, 1992*.

Karlsson, R., & Luttropp, C. (2006). EcoDesign: What's happening? An overview of the subject area of EcoDesign and of the papers in this special issue. *Journal of Cleaner Production*, *14*(15), 1291–1298. https://doi.org/10.1016/j.jclepro.2005.11.010

Kennedy, E., Fecheyr-Lippens, D., Hsiung, B.-K., Niewiarowski, P. H., & Kolodziej, M. (2015). Biomimicry: A Path to Sustainable Innovation. *Design Issues*, *31*(3), 66–73.

Kimmel, Sc.D., R. (2014). Life Cycle Assessment of Grocery Bags in Common Use in the United States. *Environmental Studies*. https://tigerprints.clemson.edu/cudp_environment/6

King, A. M., Burgess, S. C., Ijomah, W., & McMahon, C. A. (2006). Reducing waste: Repair, recondition, remanufacture or recycle? *Sustainable Development*, *14*(4), 257–267. https://doi.org/10.1002/sd.271

Kishore, V. (2022). *Integrating Eco-design Thinking in Redesigning of a Communication Device: Eco-design strategies for sustainable product design and development*. https://urn.kb.se/resolve?urn=urn:nbn:se:lnu:diva-115762

Klöpffer, W., & Grahl, B. (2014). *Life Cycle Assessment (LCA): A Guide to Best Practice*. John Wiley & Sons.

Lee, A. W. L., Chung, S. Y., Low, J. S. C., & Lu, W. F. (2023). Beyond light weighting, adapting topology optimisation to support ecodesign. *Procedia CIRP*, *116*, 366–371. https://doi.org/10.1016/j.procir.2023.02.062

Lintsen, H., Hollestelle, M., & Hölsgens, R. (2017). *How the Netherlands Became a Global Player in Plastics*.

Luttropp, C., & Lagerstedt, J. (2006). EcoDesign and The Ten Golden Rules: Generic advice for merging environmental aspects into product development. *Journal of Cleaner Production*, *14*(15), 1396–1408. https://doi.org/10.1016/j.jclepro.2005.11.022

Mestre, A., & Cooper, T. (2017). Circular Product Design. A Multiple Loops Life Cycle Design Approach for the Circular Economy. *The Design Journal*, *20*(sup1), S1620–S1635. https://doi.org/10.1080/14606925.2017.1352686

Morris, J., & Seasholes, B. (2014, junho 18). *How Green Is that Grocery Bag Ban?* Reason Foundation. https://reason.org/policy-study/how-green-is-that-grocery-bag-ban/

Mulder, K. F. (1998). Sustainable Consumption and Production of Plastics? *Technological Forecasting and Social Change*, *58*(1), 105–124. https://doi.org/10.1016/S0040-1625(97)00129-7

Nasir, M. H. A., Genovese, A., Acquaye, A. A., Koh, S. C. L., & Yamoah, F. (2017). Comparing linear and circular supply chains: A case study from the construction industry. *International Journal of Production Economics*, *183*, 443–457. https://doi.org/10.1016/j.ijpe.2016.06.008

Nebe, K., Ingrassia, D., & Durmaz, A. (2018). *Eco-Design-Sprint for Makers: How to make makers think about the sustainability of their products*. https://doi.org/10.5281/zenodo.1344434

O'Farrell, K. (2009). *Life cycle analysis of plastic bag alternatives (2009)*. https://www.greenindustries.sa.gov.au/resources/life-cycle-analysis-of-plastic-bag-alternatives-2009-

Papanek, V. (2005). *Design for the Real World: Human Ecology and Social Change* (2nd edition). Chicago Review Press.

Patnaik, R. (2018). Impact of Industrialization on Environment and Sustainable Solutions – Reflections from a South Indian Region. *IOP Conference Series: Earth and Environmental Science*, *120*, 012016. https://doi.org/10.1088/1755-1315/120/1/012016

Pigosso, D. C. A., Zanette, E. T., Filho, A. G., Ometto, A. R., & Rozenfeld, H. (2010). Ecodesign methods focused on remanufacturing. *Journal of Cleaner Production*, *18*(1), 21–31. https://doi.org/10.1016/j.jclepro.2009.09.005

Ramirez, M. J. (2007). *Sustainability integration in industrial design education: A worldwide survey*. ConnectED International Conference on Design Education. https://doi.org/10.26190/unsworks/450

Report of the United Nations Conference on the Human Environment, Stockholm, 5-16 June 1972. (1972). UN Conference on the Human Environment (1972: Stockholm). https://digitallibrary.un.org/record/523249

Rivera, J. L., & Lallmahomed, A. (2016). Environmental implications of planned obsolescence and product lifetime: A literature review. *International Journal of Sustainable Engineering*, *9*(2), 119–129. https://doi.org/10.1080/19397038.2015.1099757

Rossi, M., Germani, M., & Zamagni, A. (2016). Review of ecodesign methods and tools. Barriers and strategies for an effective implementation in industrial companies. *Journal of Cleaner Production*, *129*, 361–373. https://doi.org/10.1016/j.jclepro.2016.04.051

Schischke, K., Hagelüken, M., & Steffenhagen, G. (2005). *An Introduction to EcoDesign Strategies – Why, what and how?*

Seow, Y., Goffin, N., Rahimifard, S., & Woolley, E. (2016). A 'Design for Energy Minimization' approach to reduce energy consumption during the manufacturing phase. *Energy*, *109*, 894–905. https://doi.org/10.1016/j.energy.2016.05.099

Sreeramagiri, S. (2021). *Biomimetics: Applications in Structural Design an overview*. https://doi.org/10.15680/IJIRSET.2021.1007055|

UN World Commission on Environment and Development, ed., Report of the World Commission on Environment and Development: Our Common Future. (1987). Environment & Society Portal. https://www.environmentandsociety.org/mml/un-world-commission-environment-and-development-ed-report-world-commission-environment-and

Wecker, K. (2018). *Plastic waste and the recycling myth – DW – 10/12/2018*. Dw.Com. https://www.dw.com/en/plastic-waste-and-the-recycling-myth/a-45746469

CAPÍTULO 9

EL DR. BRACACCINI, SU PASO POR YPF (1932-1955)[1]

Data de submissão: 08/11/2025
Data de aceite: 02/12/2025

Ricardo Juan Calegari
Consultor Independiente
Ciudad del Neuquén
Neuquén-República Argentina
https://orcid.org/0009-0006-1983-3303

RESUMEN: El Dr. Bracaccini se destaca como una figura clave en la Geología Práctica de Argentina, con aportes significativos en la industria del petróleo, la hidrogeología y la geotecnia. Este hijo de inmigrantes italianos comenzó su historia laboral, ingresando a Yacimientos Petrolíferos Fiscales (YPF) a principios de la década de 1930, en calidad de alumno-geólogo. Gracias a su capacidad técnica y de gestión, tras más de veinte años de trabajo, logró acceder a uno de los cargos más relevantes dentro de la empresa. La especialidad del Dr. Bracaccini fue la geología estructural. Esta preferencia se hace evidente desde los temas abordados en su tesis doctoral, experiencia que fue enriqueciendo y profundizando durante toda su carrera profesional. Sus numerosas publicaciones reflejan una gran capacidad de trabajo, la incorporación constante de nuevas ideas para resolver problemas estructurales complejos y el rigor técnico con el que elaboraba sus informes. Por los logros técnicos alcanzados y, especialmente, por su calidad humana, es considerado uno de los geólogos más destacados del siglo XX en Argentina. Su legado permanece vigente a través de su contribución al desarrollo profesional y técnico de la geología en el país.

PALABRAS CLAVE: alumno-geólogo; YPF; geología estructural; legado.

DR. BRACACCINI: HIS YEARS AT YPF (1932–1955)

ABSTRACT: Dr. Bracaccini stands out as a key figure in the field of Applied Geology in Argentina, with significant contributions to the petroleum industry, hydrogeology, and geotechnics. The son of Italian immigrants, he began his professional career at *Yacimientos Petrolíferos Fiscales* (YPF) in the early 1930s as a trainee geologist. Thanks to his technical expertise and managerial skills, after more than twenty years of service he rose to one of the most prominent positions within the company. Dr. Bracaccini's area of specialization was structural geology – a focus that became evident in the subject of his doctoral thesis and one he continued to develop and refine throughout his professional

[1] La versión denominada: El Dr. Bracaccini, de alumno-geólogo a Sub Administrador General de YPF, (1932-1955), fue publicada en las actas del VI Congreso Argentino y I Congreso Latinoamericano de Historia de la Geología, Tucumán, octubre 2023.

career. His numerous publications reflect not only an exceptional work ethic but also a constant incorporation of new ideas to address complex structural problems, along with the technical rigor that characterized all his reports. For his technical achievements and, above all, his human qualities, is regarded as one of the most distinguished geologists of the 20th century in Argentina. His legacy endures through his lasting contribution to the professional and technical development of geology in the country.
KEYWORDS: trainee-geologist; YPF; structural geologist; legacy.

1. INTRODUCCION[2]

A partir de la investigación realizada, se han identificado los principales hitos de la trayectoria profesional del Dr. Bracaccini en la Gerencia de Exploración de Yacimientos Petrolíferos Fiscales (YPF). El autor de este trabajo también se desempeñó en dicha Gerencia durante más de treinta y cinco años (1984–2020), lo que le permitió, aun con décadas de distancia, recorrer muchos de los mismos lugares en los que la empresa desarrolló sus tareas de exploración. Esta coincidencia histórica y geográfica aporta una perspectiva privilegiada para reconstruir su legado profesional.

2. LOS PRIMEROS AÑOS

A partir del entorno familiar se logró reconstruir parcialmente su árbol genealógico, confirmándose que Inocencio Osvaldo Bracaccini nació en la localidad de Bernal, partido de Quilmes (provincia de Buenos Aires), el 7 de julio de 1913. Fue hijo de don Osvaldo, inmigrante italiano originario de la provincia de Ancona, región de Las Marcas, y de doña Cristina Leonardi (Family Search).

El hecho de portar el nombre Inocencio, al igual que su abuelo materno, sugiere que no fue el primogénito, ya que ello contradiría la tradición, muy arraigada entre las familias italianas y españolas, de asignar al primer hijo varón el nombre del abuelo paterno y al segundo, el del abuelo materno (My Heritage). En su vida profesional, firmó habitualmente como Osvaldo Bracaccini, pues no apreciaba el nombre Inocencio (Ramos, V., comunicación personal septiembre 2019). (Fig.1). Tras finalizar la escuela primaria, la familia Bracaccini se radicó en la ciudad de Paraná, provincia de Entre Ríos, donde Osvaldo pasó gran parte de su adolescencia. El contacto cotidiano con las barrancas del río Paraná, pudo haber despertado en él, un temprano interés por las Ciencias de la Tierra.

[2] Toda la información referida a cargos, ascensos y traslados del Dr. Bracaccini, ha sido extraída del L.P n° 378, la cual fue autorizada por el Centro de Gestión Documental del Archivo de RRHH de YPF SA.

Figura 1: Árbol genealógico (parcial) de la Familia Bracaccini-Carena (investigación del autor en Family Search).

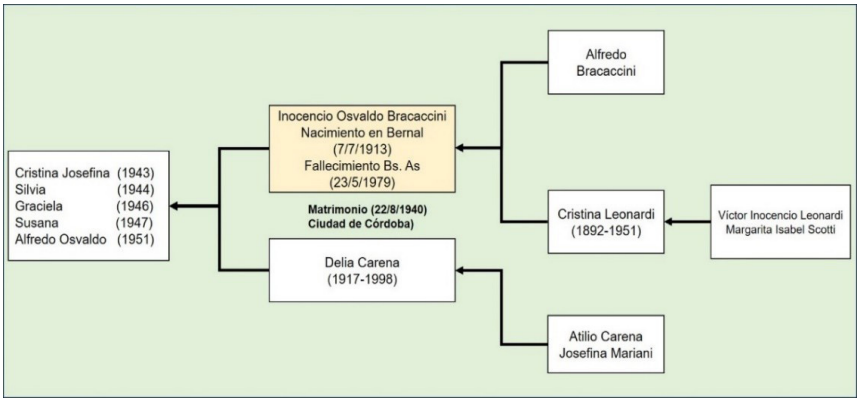

A los 16 años regresó a la ciudad de Buenos Aires, finalizando en el año 1931 sus estudios secundarios en el Colegio Nacional de Quilmes. Al año siguiente se trasladó a la ciudad de Córdoba para iniciar la carrera de Ciencias Naturales en la Universidad Nacional (Ramos, 1979).

3. DECADA DE 1930: FORMACIÓN Y SUS PRIMEROS AÑOS EN YPF

3.1. PROGRAMA DE BECAS Y FORMACIÓN INICIAL (1932–1934)

Por iniciativa del entonces Gerente de Exploración, el Dr. Enrique Fossa Mancini (1928–1939), YPF implementó en 1932 un programa de becas destinado a estudiantes argentinos de geología (Calegari, 2022). Este plan pionero buscaba fortalecer la formación técnica nacional en exploración petrolera. Dentro de ese grupo de becarios se encontraba Inocencio Osvaldo Bracaccini, junto con Freiberg, Dessantis, Catinari, De Ferraris, Daniel, González, Vittori, Leguizamón, Márquez, Echeverría y Bekenstein. Todos ellos fueron asignados a prestar servicios como alumnos-geólogos en la Comisión Geológica Golfo San Jorge, dependiente del Departamento de Geología y Minería.

Hasta enero de 1934, Bracaccini trabajó junto al también becario Altavino Catinari, realizando numerosos relevamientos en la zona de Comodoro Rivadavia. Su desempeño destacado le valió el primer ascenso dentro del programa, en reconocimiento a la calidad técnica de sus observaciones de campo y su compromiso con los objetivos de la empresa.

3.2. TESIS DOCTORAL Y CAPACITACIÓN INTERNACIONAL (1935–1940)

En marzo de 1935, bajo la dirección del Dr. Fossa Mancini, fue enviado junto a Carmelo De Ferraris a realizar un relevamiento geológico-petrolero en la zona de Tres

Cruces, provincia de Jujuy. Ese mismo año se graduó en la especialidad de Mineralogía y Geología, consolidando su formación académica y su experiencia de campo.

A pesar de sus obligaciones laborales, en agosto de 1936 defendió su tesis doctoral, titulada “Observaciones geológicas del Batolito de Achala, en la provincia de Córdoba”. El jurado, integrado por destacados académicos como Guillermo Bodenbender, Miguel Fernández, Juan Olsacher, lo calificó con la máxima nota, destacando la solidez metodológica de su trabajo (Bracaccini, 1936). (Fig. 2)

Tras obtener su título, accedió al cargo de Primer Ayudante Geólogo y fue destinado a la provincia de Mendoza para realizar relevamientos estructurales en las zonas de Huayquerías de San Carlos–Lunlunta Carrizal, en la Cuenca Cuyana. (Fossa Mancini et al., 1938).

Desde estos primeros años en la industria hidrocarburífera demostró una notable capacidad de análisis, proponiendo ideas innovadoras para la resolución de problemas geológico-estructurales.

Figura 2: Fotografía izquierda: tapa legajo personal, Centro: tapa de tesis doctoral, Derecha: noticia de la defensa de tesis publicada en el diario Los Principios de Córdoba. (Legajo Personal).

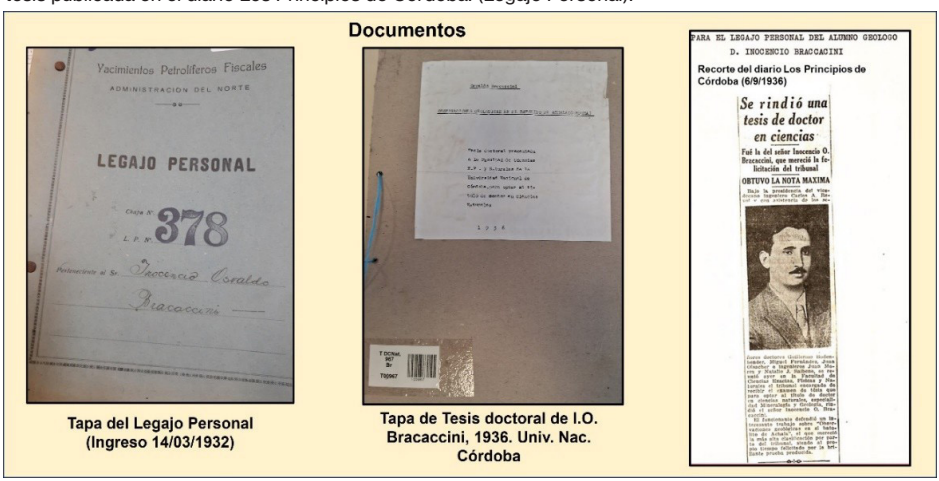

A los 25 años, y en reconocimiento a su desempeño, la Gerencia de Exploración lo seleccionó para participar de una capacitación internacional ofrecido por la Continental Oil Company, con sede en los yacimientos de la Costa del Golfo de México, West Texas y California (Legajo personal).

El 26 de noviembre de 1938 partió rumbo a Nueva York a bordo del navío Argentina, estrenando su nuevo cargo de Ayudante Mayor, con un salario equiparable al de un geólogo estadounidense en formación. Tras más de un año de trabajo y aprendizaje en el exterior, regresó a la Argentina el 16 de enero de 1940 a bordo del navío Uruguay,

habiendo adquirido una valiosa experiencia que aplicaría en su futura labor dentro de YPF (Family Search; CEMLA).

4. DECADA DE 1940: CONSOLIDACION PROFESIONAL

4.1. PRIMEROS CARGOS DE GESTIÓN Y PADRE DE FAMILIA (1940–1945)

El año 1940 marcó un punto de inflexión en la trayectoria de Inocencio Osvaldo Bracaccini. Apenas regresado de su capacitación en los Estados Unidos, fue ascendido y designado jefe del Distrito Geológico Salta.

Este traslado al norte argentino coincidió con un importante cambio en su vida personal: el 28 de agosto de 1940 contrajo matrimonio en Córdoba, con Delia Judith Josefina Carena. La pareja se estableció en Salta en noviembre de ese año, donde Bracaccini asumió su nueva función.

Desde su posición técnica debió enfrentar las complejas estructuras geológicas del Noroeste Argentino (NOA), en especial en las zonas de Tranquitas, Peña Colorada y Río Pescado. Esos estudios, enfocados en formaciones de edad paleozoica y terciaria, se extendieron a las provincias de Jujuy y Tucumán (Bracaccini, 1943a).

En mayo de 1942, la Gerencia de Exploración lo trasladó a la sede central en Buenos Aires, como Asistente del jefe del Servicio Geológico de Exploración. Este puesto le permitió participar simultáneamente en múltiples proyectos en distintas regiones del país, consolidando su experiencia técnica y su conocimiento de las diversas cuencas sedimentarias argentinas.

De manera paralela, integró el plantel docente del Instituto Argentino del Petróleo, donde se desempeñó como profesor titular de Geología Estructural hasta 1948. Su labor académica contribuyó a la formación de nuevas generaciones de geólogos en el país, fortaleciendo el vínculo entre la industria y la universidad (Ramos, 1979).

En ese mismo período, y como parte de las tareas exploratorias de YPF en la provincia de San Juan, Bracaccini encabezó nuevos estudios geológicos sobre la continuidad de los depósitos triásicos. Aunque sus conclusiones coincidieron con las de sus predecesores, al señalar las limitadas posibilidades petroleras de la región, identificó zonas de interés en el sureste provincial (límite con Mendoza) y al noroeste de la Sierra Pie de Palo, recomendando continuar los estudios (Bracaccini, 1943b). La catástrofe provocada por el terremoto del 15 de enero de 1944 retrasó la ejecución del proyecto en la provincia.

Durante 1943, propuso la perforación del pozo Santiago Temple–1, el primer sondeo en la provincia de Córdoba, ubicado en el sector occidental de la Cuenca

Chacoparana. Este pozo alcanzó 1040 metros de profundidad, atravesando sedimentos terciarios y paleozoicos hasta interceptar el basamento cristalino, sin manifestaciones de hidrocarburos (Bracaccini, 1943c).

Ese mismo año, nació en Buenos Aires su primera hija, Cristina Josefina, quien porta los nombres de sus dos abuelas. (ver Fig.1).

El mapa de la figura n° 3, ilustra la ubicación, por cuenca, de los principales proyectos de exploración y desarrollo en los que estuvo involucrado, muchos de los cuales, son mencionados a lo largo del trabajo.

Entre 1943 y 1944, publicó dos trabajos fundamentales sobre la metodología y el razonamiento estructural en la exploración petrolera, ambos textos consolidaron su prestigio como uno de los geólogos más sólidos y proactivos de YPF. (Bracaccini, 1943d, 1944a).

En paralelo, en 1944 lideró el proyecto San Cristóbal–2 (1909 m de profundidad), en la provincia de Santa Fe. Si bien el resultado fue negativo en términos de hidrocarburos, los datos permitieron ajustar el conocimiento de la Cuenca Chacoparaná, en ese sector (Calegari y Reinante, 2016).

La vida lo premió con la llegada de su segunda hija, Silvia Adriana.

Figura 3: Izquierda: mapa con las cuencas sedimentarias de Argentina y la ubicación esquemática de los principales proyectos y descubrimientos, mencionados en el listado de la derecha.

4.3. NUEVOS DESAFÍOS Y APORTES INTERDISCIPLINARIOS (1945–1949)

A comienzos de 1945, con solo 32 años, Bracaccini fue nombrado jefe del Servicio Geológico de Exploración. Ese mismo año presentó su trabajo “La problemática de los movimientos Intertriásicos del norte mendocino” ante el Instituto Panamericano de

Ingeniería de Minas y Geología (IPIMIGEO), donde formuló hipótesis originales sobre la evolución tectónica del continente Gondwana (Bracaccini, 1945a).

El crecimiento del sector científico argentino lo llevó a participar como vicepresidente de la primera comisión de la Sociedad Geológica Argentina, fundada junto con destacados colegas como los doctores Storni, Petersen, González Bonorino, Leanza, Angelelli y De Ferraris. (Ramos, 1979).

Entre 1945 y 1946, participó activamente en las campañas de exploración de las cuencas del Salado y del Colorado, interpretando datos geofísicos junto a los ingenieros Martínez y Rey. Estas tareas culminaron en la perforación de los pozos General Belgrano–1(4012 metros), Pedro Luro–1 (3278 m) y Ombucta–1(1836 m) (Bracaccini, 1945b, 1946a). Si bien no documentaron manifestaciones de hidrocarburos, aportaron importante información sobre la estratigrafía de ambas cuencas.

En febrero de 1946 nació su tercera hija, Graciela Delia, y Bracaccini fue ascendido a Segundo jefe de Exploración. Durante ese mismo año, represento a la empresa en el 1er. Congreso Sudamericano del Petróleo (Lima, Perú), con su trabajo "Bosquejo Geológico de la Argentina", una de las síntesis geológicas más completas del período (Bracaccini, 1946b).

En 1947, la Administración del ente nacional de Agua y Energía Eléctrica, lo convocó para evaluar los aspectos geológicos del proyecto Dique El Cadillal (Tucumán), que presentaba problemas técnicos significativos en su construcción. Sus conclusiones, elaboradas tras dos años de trabajo, motivaron el cambio de emplazamiento de la obra, demostrando su solvencia técnica en el ámbito de la Geotecnia (Bracaccini, 1947). (Fig. 4)

Figura 4: Composición realizada por el autor en base a una imagen satelital actual tomada de Google Earth y mapa geológico y fotografía de la base abandonada, extraídos del informe de Bracaccini de 1947.

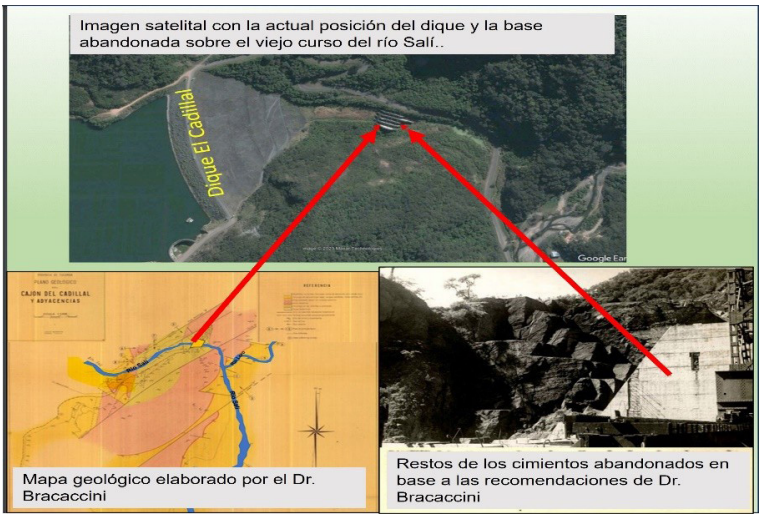

Ese año, también fue reactivada la exploración en San Juan, con la perforación del pozo Niquivil Viejo-1(2092 m). El sondeo, confirmo la existencia de impregnaciones de petróleo oxidado en areniscas terciarias, al igual que las observadas en superficie, por Bracaccini. Estas impregnaciones fueron analizadas posteriormente y los resultados permitieron correlacionar ese petróleo, con los niveles de pelitas y calizas generadoras de la Fm. Gualcamayo de edad Ordovícica (Calegari, 2020, 2023). A mediados de ese mismo año, nació en Buenos Aires su cuarta hija, Susana Eugenia.

En 1948, propuso el sondeo Tierra del Fuego-1(2071 m), perforado en 1949, siendo el primer descubrimiento de gas en la Formación Springhill en el sector argentino de la Cuenca Austral (Bracaccini, 1948; Calegari, 2023;).

En 1949, fue nuevamente convocado para analizar la zona del Dique Puntas Negras (San Juan), donde aplicó criterios estructurales innovadores. Sus conclusiones fueron publicadas en el año 1950 (Bracaccini, 1950). Los resultados del esfuerzo realizado, tuvo como recompensa, la designación de jefe del Departamento de Geología.

5. DECADA DE 1950- ALTOS CARGOS Y SU ALEJAMIENTO DE YPF

5.1. ASCENSOS Y ALEJAMIENTO DE YPF (1950–1955)

A fines de 1949, tras la renuncia del ingeniero Pedro Rey, Bracaccini fue designado director interino de Exploración de YPF. Su nombramiento se formalizó en octubre de 1950, consolidando así una trayectoria de casi dos décadas en la empresa.

Coincidiendo con esta nueva responsabilidad profesional, el 8 de enero de 1950, nació su hijo Alfredo Osvaldo, el esperado heredero varón, el cual lleva el nombre de su abuelo paterno (ver Fig. 1).

Desde su cargo de director, impulsó la elaboración de un plan que orientó las políticas exploratorias de YPF durante la primera mitad de la década. Su liderazgo combinó una sólida formación técnica con una visión estratégica de largo plazo, integrando geología, geofísica y perforación.

Los resultados de este período fueron notables: en cuenca Austral se produjo el primer descubrimiento de petróleo, con el pozo Palermo Aike–1(1874 m). Mientras que en el sector norte de Tierra del Fuego hubo nuevos descubrimientos, confirmando el potencial gasífero de la Formación Springhill.

En la Cuenca Cuyana, se incorporaron nuevas reservas con los campos Lunlunta Carrizal y Piedras Coloradas. En la Cuenca Golfo San Jorge, se intensificaron las campañas de exploración en el flanco sur. En Cuenca Neuquina, se incorporaron los

campos Cutral Co y Cerro Bandera. En el NOA, se produjeron los descubrimientos de los yacimientos Campo Durán–Madrejones (Calegari, 2023) (ver Fig.3).

En julio de 1952, fue promovido a Sub Administrador General de YPF, posición que le permitió participar en misiones técnicas en América Latina y Europa, y además fortalecer el programa de formación de jóvenes profesionales.

Los profundos cambios políticos ocurridos en 1955 con el derrocamiento del gobierno de Juan D. Perón implicaron una renovación general del personal directivo, y Bracaccini, como otros altos funcionarios, fue separado de su cargo. Su alejamiento marcó el cierre de más de veinte años de servicio en YPF, etapa en la que dejó una huella indeleble por sus aportes técnicos, su capacidad de liderazgo y su compromiso con el desarrollo de la exploración nacional.

Lejos de significar un retiro, esta nueva etapa representó una oportunidad para reorientar su actividad profesional hacia el ámbito privado realizando consultorías y asesorías geológicas en distintos puntos del país, aplicando la vasta experiencia acumulada durante su carrera pública (Ramos 1979).

6. CONCLUSIONES

El recorrido profesional del Dr. Bracaccini refleja con claridad el proceso de consolidación de la exploración de hidrocarburos en la Argentina del siglo XX. Desde sus primeros pasos en la década de 1930, como becario, hasta su desempeño como Sub Administrador General en los años cincuenta, su trayectoria, fue una síntesis de rigor científico, compromiso institucional y vocación de servicio público, como lo fueron entre otras, sus recomendaciones técnicas en la construcción de represas.

Su formación técnica y su capacidad de observación lo convirtieron en un geólogo de campo excepcional. Las numerosas campañas que lideró a lo largo del país dieron lugar a descubrimientos y publicaciones que aún hoy constituyen referencias históricas y científicas de valor incalculable.

Fue socio fundador de la Sociedad Geológica Argentina, entidad que se transformaría con el tiempo en la actual Asociación Geológica Argentina (AGA).

Su legado técnico, quedó plasmado en los más de 70 informes y publicaciones, muchos de ellos inéditos y dirigió las tesis doctorales de Eugenio Viloni (1947) y Armando Massabie (1975).

El 23 de mayo de 1979, a los 66 años, falleció en la ciudad de Buenos Aires, dejando un legado profesional y humano que trascendió su tiempo. Tal como destacó el Dr. Víctor Ramos en la nota necrológica publicada ese mismo año, Bracaccini fue “un apasionado de

su profesión, que compartió sin egoísmos su vasta experiencia y conocimientos". Su vida laboral en YPF representó una etapa importante de la exploración hidrocarburífera. Su figura permanece como ejemplo de ética, curiosidad intelectual y dedicación a la ciencia.

REFERENCIAS BIBLIOGRÁFICAS

Bracaccini, I. O. (1936). *Observaciones geológicas del Batolito de Achala, en la provincia de Córdoba.* [Tesis de maestría, inédita Univ. Nac. Córdoba].

Bracaccini, I. O. (1943a). *Problemas estructurales del norte argentino.* Boletín Informaciones Petroleras 222: 43-44.

Bracaccini, I. O. (1943b). *Una gira por San Juan.* Informe inédito Archivo YPF.

Bracaccini, I. O. (1943c). *Propuesta de perforación pozo Santiago Temple-1, Cuenca Chacoparana (Prov. de Córdoba).* Informe inédito Archivo YPF.

Bracaccini, I. O. (1943d). *El problema de la exploración petrolera en la República Argentina*. Sociedad Nacional de Estudios Geográficos 6: 3-6.

Bracaccini, I. O. (1944). *El factor estructural en las acumulaciones petrolíferas del país.* Sociedad Científica Argentina. Anales CXXXVIII: 191-192.

Bracaccini, I. O. (1945a). *La problemática de los movimientos Intertriásicos del norte mendocino.* IPIMIGEO Sec. Argentina, I Reunión de comisión: 1-26.

Bracaccini, I. O. (1945b). *Propuestas de perforación pozos General Belgrano-1, Cuenca del Salado y Pedro Luro-1, Cuenca del Colorado (Prov. de Buenos Aires).* Informes inéditos, Archivo YPF.

Bracaccini, I. O. (1946a). *Propuesta de perforación pozo Ombucta-1, Cuenca del Colorado (Prov. de Buenos Aires).* Informe inédito, Archivo YPF.

Bracaccini, I. O. (1946b). *Bosquejo geológico de la Argentina*. Primer Congreso Sudamericano del Petróleo Lima, Perú.

Bracaccini, I. O. (1947). *Informe geológico sobre la zona del Dique El Cadillal (Tucumán)*. Informe inédito, Archivo YPF.

Bracaccini, I. O. (1948). *Propuesta de perforación pozo Tierra del Fuego-1, Cuenca Austral (Prov. Tierra del Fuego).* Informe inédito, Archivo YPF.

Bracaccini, I. O. (1950). *Investigaciones Tectónicas en la Precordillera sanjuanina.* Boletín Informaciones Petroleras 301: 1-34.

Calegari, R.J. y Reinante, S. (2016) *El Petróleo en San Cristóbal ¿Realidad o Leyenda?* Revista Museo de La Plata edición especial 1:44-54.

Calegari, R. J. (2020). *Historia de la Exploración de Petróleo en la Provincia de San Juan.* Fac. Cs. E. F. y Naturales Univ. Nac. Córdoba 7(1): 163-172.

Calegari, R. J. (2022). *Fossa Mancini, Impulsor de la Exploración en la Argentina.* XXI Cong. Geológico Argentino I: 851-854.

Calegari, R. J. (2023). *El Dr. Bracaccini, de alumno-geólogo a Sub Administrador General de YPF (1932-1955).* VI Cong. Argentino y I Latinoamericano de Historia de la Geología I:61-69.

Fossa Mancini, E., Feruglio, E y Yussen, J.C. (1938). *Una reunión de geólogos de YPF.* Boletín Informaciones Petroleras 171:31-95.

Ramos, V. (1979). *Nota necrológica: Dr. Inocencio Osvaldo Bracaccini (1913–1979)*. Asociación Geológica Argentina, 34(3): 415-417.

Centro de Estudios Migratorios Latinoamericanos (CEMLA). (s.f.). *Registros de inmigración en Argentina (1880–1930)*. https://cemla.com/buscador/

Centro de Gestión Documental Archivo Histórico de RRHH YPF (s.f.).

Family Search. (s.f.). *Base de datos genealógica de la familia Bracaccini*. https://www.familysearch.org/es/tree/pedigree/landscape/G25M-JWP

My Heritage, (s.f.) *Tradiciones Italianas y españolas.* https://blog.myheritage.es/2016/07/costumbres-de-poner-nombres-a-los-ninos/

CAPÍTULO 10

DEVELOPMENT OF AGRICULTURAL LAND CONSOLIDATION IN RUSSIA ON THE PLATFORM OF LAND MARKET

Data de submissão: 03/11/2025
Data de aceite: 28/11/2025

Alexander Sagaydak
State University of Land Use Planning
Professor, Director of Department of Agricultural Economics and Farm Management
Moscow, Russia
https://orcid.org/0000-0002-6316-6134

Anna Sagaydak
State University of Land Use Planning
Professor of Department of Agricultural Economics and Farm Management
Moscow, Russia
https://orcid.org/0000-0003-4389-8570

ABSTRACT: Addressing global hunger is directly linked to the need to increase food production in individual countries. Unfortunately, the potential for agricultural growth in most of them has long been exhausted. In this regard, Russia has unique opportunities, as its agricultural land is virtually unlimited. Therefore, increasing the efficiency of the agricultural sector through land consolidation is particularly urgent. However, this process is currently being implemented haphazardly, often in violation of the rights of smallholders, which contradicts the fundamental principles of private property and a market economy. In this context, developing a land market and regulating agricultural production based on land rent determinism is crucial.
KEYWORDS: agricultural land; land rent determinism; agricultural land consolidation; agricultural land market; Oryol region; Russia.

DESENVOLVIMENTO DA CONSOLIDAÇÃO DE TERRAS AGRÍCOLAS NA RÚSSIA NA PLATAFORMA DO MERCADO DE TERRAS

RESUMO: Combater a fome global está diretamente ligado à necessidade de aumentar a produção de alimentos em cada país. Infelizmente, o potencial de crescimento agrícola na maioria deles já se esgotou há muito tempo. Nesse sentido, a Rússia possui oportunidades únicas, visto que suas terras agrícolas são praticamente ilimitadas. Portanto, aumentar a eficiência do setor agrícola por meio da consolidação fundiária é particularmente urgente. Contudo, esse processo está sendo implementado de forma desordenada, frequentemente violando os direitos dos pequenos agricultores, o que contradiz os princípios fundamentais da propriedade privada e da economia de mercado. Nesse contexto, o desenvolvimento de um mercado de terras e a regulação da produção agrícola com base no determinismo da renda da terra fundiária são cruciais.

PALAVRAS-CHAVE: terras agrícolas; determinismo da renda da terra; consolidação de terras agrícolas; mercado de terras agrícolas; região de Oryol; Rússia.

1. INTRODUCTION

Agricultural land consolidation is a merging, enlargement, eliminating of mosaic land ownership and improvement of configuration, as well as optimization of the size of land plots in order to increase the efficiency of agricultural production via rational use of scarce resources: land, labor, and capital based on reduction of transaction costs.

The specific objectives of agricultural land consolidation are the following: increasing the efficiency of agricultural production; providing sustainable development of the agrarian sector; rational use of land, labor, and capital in agriculture; optimization of agricultural production structures both in territorial and production aspects; increasing the competitiveness of agricultural producers in domestic, as well as foreign markets; environmental protection; development of production, as well as social infrastructure in agriculture. The main functions of agricultural land consolidation are the following: elimination of hunger and poverty, as well as reducing the gap in living conditions and incomes between urban and rural areas.

Agricultural land consolidation should be carried out based on the following principles: voluntariness; openness and transparency; financial and economic feasibility; considering the interests of the population groups involved, including women and youth, as well as indigenous people; step by step implementation; consideration of local conditions; state and NGO support.

In theory, agricultural land consolidation can be carried out as voluntary land consolidation and compulsory land consolidation. Both administrative and economic methods, for example, the development of the agricultural land market could be used for agricultural land consolidation. In our opinion, preference should be given to voluntary land consolidation. In that sense, the development of the agricultural land market is very important for the stimulation of agricultural land consolidation.

Agricultural land consolidation is a complex socio-economic phenomenon, which includes technical, institutional, financial, economic, environmental and social aspects, reflecting the methodology of project analysis in agriculture.

Due to it, the formulation of the main idea of the project on the consolidation of agricultural land involves the development of a methodology of implementation and evaluation of the projects on agricultural land consolidation, as well as carrying out summarize, scrutinize and analyze the domestic and international experience of agricultural land consolidation.

In this regard, the super goal of agricultural land consolidation projects is to implement and develop agricultural land consolidation in order to increase the efficiency of agricultural production to eliminate hunger and food shortages, as well as poverty due to the rapidly growing world population.

The technical aspect of agricultural land consolidation projects is the implementation of land use planning activities focused on the elimination of mosaic land ownership, improvement of configuration, and optimization of the size of land plots, as well as the development of the road network and production infrastructure in a rural area in order to increase the efficiency of agricultural production.

The institutional aspect of agricultural land consolidation projects involves the selection of a legal entity interested in the implementation of land consolidation projects in agriculture based on the criteria of financial and economic efficiency. The beneficiary may be private farms, agricultural holdings, as well as other legal entities.

The financial aspect of agricultural land consolidation projects is to determine the financial efficiency of land consolidation for legal entities directly involved in its implementation. It should be noted that with increasing the size of land plots used for agricultural production, the efficiency of farming is increasing due to the relative reduction of transaction costs per unit of land area. The maximum efficiency of agricultural production is achieved in the case when the level of transaction costs per unit of land is reduced to a minimum.

However, further increasing the size of land plots used in agriculture leads to a decrease in the efficiency of agricultural production due to the increase in transaction costs per unit of land area. In that sense, the major problem is to evaluate the effectiveness of projects related to the consolidation of agricultural lands. In our opinion, evaluation of the effectiveness of the above- mentioned projects should be carried out based on benefit-cost analysis.

The most important condition for the application of benefit-cost analysis for the evaluation of land consolidation projects is to ensure comparability of indicators of costs, benefits, as well as efficiency based on the international financial reporting system. It could create additional incentives to attract outside investors in agriculture.

Thus, the consolidation of agricultural land is the basis for the development of the investment process in agriculture, which allows increasing its efficiency by reducing transaction costs and attracting outside investors to allocate their capital in agriculture.

The economic aspect of agricultural land consolidation project is to determine the economic efficiency of land consolidation projects for society as a whole based

on the analysis of economic costs and benefits. It should be noted that the economic costs and benefits of the above- mentioned projects should be evaluated based on their "shadow" prices.

The environmental aspect of the agricultural land consolidation projects is the environmental assessment (EA) of its impact on the environment based on direct and indirect valuation methods.

The social aspect of the agricultural land consolidation projects is the assessment of its impact on the socio-cultural and demographic characteristics, a social organization of productive activities, cultural acceptability, as well as different groups of population such as women, indigenous people, youth and etc.

The life circle of the agricultural land consolidation project consists of creative design and implementation phases. In turn, the creative design phase consists of identification, feasibility study, preparation, detailed design, and appraisal stages. The implementation phase consists of negotiation, loan approval, implementation, supervision, and completion stages.

The goals and objectives of the agricultural land consolidation project are determined at the identification stage. Technical, institutional, financial, economic, environmental and social analysis of the agricultural land consolidation project is carried out at the feasibility stage.

A business plan for the agricultural land consolidation project is developed at the preparation stage. Clarification of the business plan of the project for the consolidation of agricultural land due to changes in the macroeconomic situation is carried out at the stage of detailed design. The external expertise of the agricultural land consolidation project is carried out at the appraisal stage.

Further, the business plan of the project on the consolidation of agricultural land is submitted to the bank to resolve the issue of allocation of loans for its financing. To this end, the owners and beneficiaries of the agricultural land consolidation project and the bank negotiate a loan to finance it. The signing of the loan agreement is carried out at the stage of approval of the loan to finance the project on the consolidation of agricultural land.

The agricultural land consolidation project starts at the stage of its direct implementation. Land use planning works focused on the consolidation of small parcels into larger land plots are carried out here. Monitoring the progress of the project on agricultural land consolidation in terms of cost and implementation time is carried out at the supervision stage using the PERT and GERT methodologies.

As a result of the agricultural land consolidation project, large land plots should be formed, allowing effective agricultural production, and using modern agricultural machinery and technologies. At the stage of completion of the project on the consolidation of agricultural land, a retrospective analysis of its implementation is also carried out, which allows identifying all the pros and cons of its implementation.

Training capabilities and public information programs should be included in the framework of the projects on the consolidation of agricultural land to support the implementation and developing of agricultural land consolidation.

The main take-offs of agricultural land consolidation projects should assist national and local officials and decision-makers involved with agricultural land consolidation to analyze policy and procedural constraints and opportunities to ensure that the above-mentioned process is a viable option and to strengthen movement towards eliminating hunger and food shortages, as well as poverty due to the rapidly growing the world's population.

Currently, to accelerate the process of consolidation of agricultural land and improve the efficiency of the agricultural sector of the national economy, it is necessary to develop a working digital model of the project on land consolidation in agriculture.

The present stage of agricultural land consolidation in Russia is featured by the development of agricultural holdings and the increasing size of private farms. After the implementation of land consolidation projects, agricultural producers are less sensitive to the disparity of prices for agricultural and industrial commodities, as well as can conduct their investment activities more efficiently based on self-financing.

In theory, as we mentioned before, agricultural land consolidation can be carried out as compulsory land consolidation and voluntary land consolidation. In that sense, the development of the agricultural land market is very important for the stimulation of agricultural land consolidation.

The objective of this paper is to analyze the current stage of agricultural land consolidation in Russia, evaluate its socio-economic, institutional, and environmental determinants, and assess the role of the land market in strengthening agricultural efficiency and sustainability.

2. METHODOLOGY

The methodology of the research presented in the article is based on the concept of land rent determinism, which presupposes the implementation of the following principles, which are theoretically, historically and logically interacted:

- land and mining rents generated in the agricultural sector and the fuel and energy complex directly correlate with the progressive reproduction of food and fuel, respectively, i.e. priority guidelines, trajectories and potentials of human activity;
- states seek to expand their territories in order to increase the appropriation of land rent;
- landlords try to increase the area of their agricultural land in order to generate higher land rent values;
- implementation of classical, neoclassical, and Keynesian theories to determine the paradigm of rent regulation of agribusiness;
- a dialectical synthesis of the classical and neoclassical theory of land rent, which is ultimately summarized in the economic rent arising in the process of rent formation as a result of the convergence of absolute, differential and monopoly land rents, reflecting the scarcity of agricultural land, especially arable land, which, of course, are the most important components of the country's land fund, since they serve as a starting point for the generation of food and the escalation of the value added of agricultural raw materials;
- economic rent is a platform for establishing land tax in agriculture, determining the collateral value of agricultural land, and paying compensation to agricultural producers for the illegal seizure of their land for non-core commercial purposes, as well as for environmental pollution;
- step by step transition of taxation of agricultural producers to a single agricultural land tax;
- development of auction and exchange trade in agricultural land;
- analysis of the effectiveness of the investment application, as well as an assessment of its static and dynamic effects based on the platform of rent dominants of agricultural sector.

3. RESULTS

As we mentioned before, the present stage of the development of agricultural land consolidation in Russia is featured by the further development of agricultural holdings and the increasing size of private farms.

The consolidation of agricultural land by legal entities, in essence, manifests itself as a modified form of integration of agricultural land, since the average size of agricultural land ownership in agricultural holdings in April 2025 compared to July 2022 progressed

by 19.2%, and also by 30.3% compared to May 2021, reaching almost 770.2 K ha with volatility from 443 K ha to 1,380 K ha (3.1 times) [1] (Table 1). It is also characteristic that compared to July 2022, the differentiation of agricultural land ownership in the top ten agricultural holdings progressed by 20 p.p. from 290% to 310%.

Table 1. Agricultural land ownership of the top ten agricultural holdings, Russia, 2025[1].

#	Agricultural holding	Area, K ha	%
1	Miratorg	1,380	17.9
2	Agrokompleks	1,230	16.0
3	Prodimeks	900	11.7
4	Rusagro	815	10.6
5	GAP Resurs	680	8.8
6	GK EkoNiva	632	8.2
7	BIO-TON	600	7.8
8	Agroholding Step	578	7.5
9	Agroinvest Group	444	5.8
10	Avangard-Agro	443	5.7
	Total	7,702	100.0

In 2023, the number of private farm decreased by 8.0% compared to 1995, while the total area of agricultural land occupied by private farm increased by 72.8% during this period. The average area of agricultural land occupied by a private farm increased due to agricultural land consolidation in 2023, compared to 1995.In 2023, it was estimated at 80.6 ha and increased by 87.9% compared to 1995 (Table 2)[2].

Table 2. Private farms, Russia, 1995-2023[2].

Item	1995	2010	2015	2020	2023	2023/1995,%
Number,K	279.1	261.7	261.6	262.0	256.9	92.0
Area,K ha	11,982.1	16,284.1	18,130.4	20,107.5	20,699.3	172.8
Average size,ha	42.9	62.2	69.3	76.7	80.6	187.9

In the Oryol region in 2024, the area of agricultural land was 2,034.9 K ha, which constituted 82.5% of its territory. Compared to 1990, the size of agricultural land regressed by 261.4 K ha - from 2,296.6 K ha to 2,035.2 K ha, which is equivalent to a reduction of 11.4%.

In 2022, the percentage of agricultural land in the total territory of the region regressed by 10.7 p.p., comparable to 1990, from 93.2% to 82.5%. In 2024, the distribution of land in the region was as follows: state and municipal - 965.0 K ha (39.2%), private - 1,161.3 K ha (47.1%), legal entities - 338.9 K ha (13.7%).

In 2024, state and municipal land decreased by 2.8 K ha compared to 2020, when it amounted to 967.8 K ha, i.e. regressed to 965 K ha, which is equivalent to a reduction of .3%.

Private agricultural land regressed by 8.5 K ha, from 1,169.8 K ha to 1,161.3 K ha, which is .7%. In 2024, the land of legal entities increased from 327.5 K ha by 11.4 K ha to 338.9 K ha (3.5%).

Compared to 2023, in 2024, state and municipal land decreased slightly from 965.5 K ha to 965 K ha by .5 K ha, private land – from 1,161.9 K h to 1,161.3 K ha by .6 K ha, and land of legal entities, on the contrary, increased – from 337.8 to 338.9 K ha by 1.1 K ha (.3%).[3]

In 2022, compared to 1994, the number of private farms in the region decreased by 25.7%, while the average area of a private farm increased by 3.4 times, indicating positive dynamics in the consolidation of agricultural land (Table 3).

Table 3. Private farms, Oryol region, 1994-2022[4],[5].

Item	1994	2000	2010	2015	2020	2021	2022	2022/1994,%
Number,K	1,754	1,420	1,247	1,292	1,297	1,303	1,303	74.3
Area,K ha	89.2	124.6	177.5	201.0	221.9	222.5	224,5	2.5 times
Average size,ha	50.8	87.7	142.3	155.6	171.1	170.8	172.3	3.4 times

To encourage land consolidation, it is necessary to develop the agricultural land market based on land auctions and exchange trade of agricultural land plots. In turn, the market price of land is the basis for agricultural land taxation and agricultural land mortgage transactions.

The share of agricultural land market transactions, which legal entities acted as participants, was calculated on average in 2020-2021 as 74.7% of their number. The share of agricultural land that was the object of land market transactions in 2023 amounted to 99.8% of all land transactions executed by legal entities in the region (Table 4). The average share of agricultural land value in the total land value that was the object of market transactions by legal entities in the region in 2023 was 73.0%. The average share of agricultural land leased in 2023 was 99.0% of all land leased in the region by legal entities. Legal entities entered into agricultural land lease agreements in 2023, accounting for an average of 71.6% of all lease agreements in the region. The share of agricultural land used as the object of land market transactions by legal entities increased from 97.8% to 99.8% (2.0 p.p.). During the same period, the value of agricultural land transactions increased from 67.5% to 73.0% (5.5 p.p.).

Table 4. Land Market, Oryol Region, 2023.

Transactions	Total		Including agricultural land		%	
	Private	Legal Entities	Private	Legal Entities	Private	Legal Entities
1. Buying and selling:	-	-	-	-	-	-
Number	7,665	846	1,232	644	16.1	76.1
Area, ha	8,154	184,466	6,815	184,015	83.6	99.8
Value, K rubles	5,184,153	3,932,008	2,175,220	2,871,802	42.0	73.0
2. Lease	-	-	-	-	-	-
Number	2,140	1,805	854	1,293	39.9	71.6
Area, ha	17197	83355	15608	82,509	90.8	99.0
3. Average Value, rubles/ha	635,780	21,316	319,181	15,606	-	-

In 2023, compared to 2020-2021, the share of legal entities' agricultural land leasing agreements increased to 71.6% from 63.6% (8.0 p.p.) of the total their lease agreements in the region. The price of agricultural land in land market transactions in 2023, compared to 2020-2021, increased by 6.9 times for individuals, while for legal entities, it decreased by 61.1%, indicating an increase in its purchases by them.

4. CONCLUSION

1. In the Russian agricultural sector, the process of concentration of agricultural land ownership and, accordingly, agricultural land rent on the platform of consolidation of agricultural lands by agricultural holdings, as well as private farms, continues.
2. This serves as a foundation for increasing the efficiency of agricultural production in Russia, the development of country's agricultural and food sovereignty, the generation of export potential for agribusiness, and the transfer from import substitution to the export of agricultural products abroad.
3. The share of state and municipal owned land and private land is decreasing, while corporate land of legal entities is growing now.
4. In the agricultural land use of parastatals, a trend has been identified of an increase in the share of agricultural holdings due to a reduction in the share of agricultural coops.
5. The trend of expansion of the average size of private farms continues, with an increase in their agricultural area, as well as a reduction in the number of them.

6. Due to the vastness of the country's territory and the differentiation of agricultural production potential in natural, soil, climatic, technical, financial, institutional, economic, ecological, and social, as well as other aspects, the above-mentioned trends in agricultural land consolidation are sometimes expressed in modified or unique ways, like, for example, in the Republic of Kalmykia.
7. Land consolidation serves as the foundation for the effective functioning of the agricultural sector, which creates the potential for increasing its efficiency via the reduction of transaction costs.

Due to it the following measures must be implemented to strengthen the organizational, as well as institutional sustainability of agricultural land market and agricultural land consolidation development in Russia:

- agricultural land consolidation legislation must be revised and improved both at the federal, as well as regional level based on the principles of land rent determinism.
- It is necessary to introduce legal regulation of the optimal size of agricultural land ownership and land use at the regional level.
- the institutional framework for implementation of agricultural land market, as well as agricultural land consolidation must be improved both at the federal, as well as regional level.
- it is necessary to make a transition to the assessment of agricultural land as a real estate in the agricultural sector.
- the agricultural land auctions and exchange trade of agricultural land plots must be introduced to stimulate the development of the agricultural land market and agricultural land consolidation.
- a reasonable and gradual legislative liberalization of the agricultural land market legislation should be carried out in order to ensure the formation of equilibrium prices for agricultural land plots.
- the establishment of land tax, the determination of the collateral value of agricultural land, and compensation to agricultural producers for the illegal seizure of their land for non-core commercial purposes, as well as for environmental pollution should be carried out based on economic rent, since it underlies these regulators.
- the training and retraining programs related to agricultural land market and agricultural land consolidation development issues must be introduced.

- the public relation campaign to strengthen people's ability to understand the role and importance of agricultural land market and agricultural land consolidation development must be initiated.
- The pilot projects focused on agricultural land market, as well as agricultural land consolidation development should be launched in some of the regions to make a demonstration effect.
- The domestic and international agricultural land market, as well as agricultural land consolidation development experience should be collected, scrutinized and disseminated.

REFERENCES

1. Top 64 owners of agricultural land-2025 (Топ-64 владельцев сельскохозяйственной земли-2025). URL:http://zol.ru.

2. The State (National) report on the status and use of lands in the Russian Federation in 2023, Rosreestr, 2024 (Государственный (национальный) доклад о состоянии и использовании земель в Российской Федерации в 2023 году. — Москва: Росреестр, 2024). URL:http://rosreestr.ru.

3. Regional report on the status and use of land in the Oryol region for 2023, Oryol: Department of State Registration, Cadastre and Cartography for the Oryol Region, 2024. (Региональный доклад о состоянии и использовании земель в Орловской области за 2023 г., Орел: Управление государственной регистрации, кадастра и картографии по Орловской области, 2024). URL:http://rosreestr.ru.

4. Regional report on the status and use of land in the Oryol region for 2022, Oryol: Department of State Registration, Cadastre and Cartography for the Oryol Region, 2023. (Региональный доклад о состоянии и использовании земель в Орловской области за 2022 г., Орел: Управление государственной регистрации, кадастра и картографии по Орловской области, 2023). URL:http://rosreestr.ru.

5. Regional report on the status and use of land in the Oryol region for 2021, Oryol: Department of State Registration, Cadastre and Cartography for the Oryol Region, 2022. (Региональный доклад о состоянии и использовании земель в Орловской области за 2021 г., Орел: Управление государственной регистрации, кадастра и картографии по Орловской области, 2022). URL:http://rosreestr.ru.

SOBRE O ORGANIZADOR

Alireza Mohebi Ashtiani possui graduação em bacharelado em Matemática, Matemática Aplicada, pela Amirkabir University of Technology (Polytechnic of Tehran), Teerã/Irã (2003), mestrado em Matemática Aplicada pelo Institute for Advanced Studies in Basic Siences (IASBS), Zanjan/Irã (2005) e doutorado em Engenharia Elétrica pela Universidade Estadual de Campinas (UNICAMP) na área de Automação (2012). Foi bolsista de Pós-doutorado Júnior do CNPq no Instituto de Matemática, Estatística e Computação Científica (IMECC/UNICAMP) e bolsista de Pós-doutorado da Fundação de Amparo à Pesquisa do Estado de São Paulo (FAPESP) na Faculdade de Ciências Aplicadas da Universidade Estadual de Campinas (FCA/UNICAMP). Desde 2013 é docente vinculado ao Departamento Acadêmico de Matemática do Campus Londrina da Universidade Tecnológica Federal do Paraná (UTFPR), e atualmente, docente permanente do Programa de Pós-Graduação em Matemática em Rede Nacional (PROFMAT) da UTFPR, Campus Cornélio Procópio.

Alireza Mohebi Ashtiani
http://lattes.cnpq.br/5025709771742662

ÍNDICE REMISSIVO

X

Y


EDITORA
ARTEMIS
2025